Morphological and Mechanical Analysis of the Glenoid Trabecular Bone

Raghad Mi'mar, MSc.

Submitted in accordance with the requirements for the degree of
Doctor of Philosophy

The University of Leeds
School of Mechanical Engineering

March, 2007

The candidate confirms that the work submitted is his/her own and that appropriate credit has been given where reference has been made to the work of others.

To:

my loving Husband,

my dearest Family,

my Friends,

and the Orthopaedic community.

Acknowledgements

The work on this thesis has been an inspiring, often exciting, sometimes challenging, but always interesting experience. It has been made possible by many other people, who have supported me.

I am deeply indebted to my supervisor, Dr. Richard Hall for his constant support. Without his help, this work would not be possible. Many thanks to my other supervisor Mr. David Limb, for all the help and advices in the surgical and clinical procedures of this work. And many thanks go to Dr. Roger Soames for his first year support in this project.

I also would like to thanks Dr. Ruth Wilcox for her help with the uCT and supporting my work throughout these years. And many thanks to Mr. Devon Darby for his design advices and manufacturing effort and all the other laboratory technicians who have been immensely helpful.

I would like to acknowledge the Iranian ministry of science which has funded this project and provided me with the financial support.

Also would like to thank all my colleagues in the department. It has been a pleasure to meet and work with such a great people who provided both excellent work advices and fun at the same time. Can't name you all...I'm sure I'll miss some. I would also like to thank Mr. Ted Allowed and Dr. Blyth for all their help and Dr. Maheshwaran Kollukattuvalas for all his support throughout my work.

Many thanks goes to my friends I have made in Leeds who have been of great support and provided me with an enjoyable time throughout my work.

Lastly, special thanks go to my family for their support. I am greatly indebted to my mother and grandmother, whom supported me throughout my life. My two sisters, my brother, and my in-laws, which were of great support and encouragements.

Special thanks to my loving husband Ehsan, for his support, understanding, and his outstanding help throughout my research. Without him this work would not be possible.

I dedicate this thesis to my father, which his memory will always inspire me...

Abstract

Bone quality is an important factor in glenoid component fixation and ultimately the long-term outcome of shoulder replacement. The aims of this study were to explore the relationship between bone morphology and mechanical properties, to develop an experimental fixation model to explore the properties of cemented glenoid fixation, and to investigate the strength of the bone anchors as a function of bone density. Nineteen embalmed and six fresh frozen human glenoids were acquired for testing. In order to determine basic morphological and mechanical properties, specimens were tested using a flat cylindrical indentor at eleven pre-selected grid points from which the strength and elastic modulus were acquired from the resulting load-deformation output. The subchondral thickness and bone volume to total volume ratio (BV/TV) were determined by scanning the whole glenoid using a MicroCT in the vicinity of the indentations. The thickness measurements were validated by sectioning the specimens post scanning. Multiple regression analysis found a significant correlation between strength and both BV/TV and subchondral thickness data derived across all of the indentation sites. Similar results were found for the elastic modulus. MicroCT provided to be a powerful tool for elucidating these relationships. Several previous studies have been undertaken on component fixation, but there are none that have investigated the differences between the peg and keel design, the cement mantle thickness and initial fixation strength. In this study Sawbones (open cell foam) were used to represent cancellous bone and these enabled the cement to flow within the surrogate bone structure and provide a more suitable morphological model. From this study, it was clear that open cell Sawbones are not applicable for mechanical testing of glenoid fixation. They may, however, be useful for looking at different cementing techniques and the interdigitation of cement for different cement formulations, designs of prostheses or surgical procedures. This study investigated the relationship between pullout strength and BMD when using suture anchors loaded with Orthocord™ (Depuy, USA) sutures. It is likely that the rank order and, therefore, the correlation between BMD and strength remain valid and that tissue quality is an important determinant of anchor strength.

TABLE OF CONTENTS

LIST OF FIGURES

LIST OF TABLES

KEY PUBLICATIONS

1. R. Mimar, D. Limb, R.M. Hall. Evaluation of the Mechanical and Architectural Properties of Glenoid Bone. Journal of shoulder and elbow surgery. Accepted subject to minor revisions
2. R. Mimar, D. Limb, R. W. Soames, R. M. Hall. Morphological and mechanical analysis of the glenoid trabecular bone; ISTA Annual Symposium of the international society for technology in Arthroplasty. Rome, Italy Sept. 23-25 2004. (Podium presentation)
3. R. Mimar, D. Limb, R.M. Hall. Glenoid microstructure and mechanical properties; EORS, Lisbon, Portugal, 4-7 June 2005. (Poster)
4. R. Mimar, D. Limb, R.M. Hall. Investigation of the Microstructure and mechanical properties of the glenoid; BORS, Stanmore, UK 4^{th} – 5^{th} July. (Poster)
5. R. Mimar, D. Limb, R.M. Hall, The relative importance of the subchondral plate and bone porosity on the mechanical properties of glenoid bone; European Society for Surgery of the Shoulder and the Elbow , Rome, Italy Sept., 21-24 2005. (Poster)
6. R. Mimar, D. Limb, R.M. Hall, Correlation of BMD of the glenoid bone with the pullout strength of Mitek GII anchors loaded with Orthocord TM suture; 5^{th} Congress of World Biomechanics, Munich, Germany, July 29^{th}-August 4^{th} 2006. (Poster)
7. R. Mimar, D. Limb, R.M. Hall, Influence of architecture on the structural properties of the glenoid surface and underlying bone; 5^{th} Congress of World Biomechanics. Munich, Germany, July 29^{th}-August 4^{th} 2006. (Podium presentation)

1 INTRODUCTIONS AND LITERATURE REVEIW

1.1 INTRODUCTION

This chapter reviews the literature relevant to the work reported in terms of both clinical background and the extent of previous experimental and theoretical work. The first section examines the literature relating to the anatomy and stability of the shoulder joint, along with the mechanical approach to shoulder arthroplasty and suture anchoring. This is followed by a review of the experimental work that has been undertaken to analyse the characteristics of the glenoid trabecular bone. The final section discusses the mechanical properties and the design consideration of the glenoid components, upon which the quality for prosthetic fixation will depend. At the end of the chapter, a summary of the literature is presented, preceding the research hypothesis and objectives.

1.2 BACKGROUND

1.2.1 Introduction

Several anatomic studies have provided general descriptions of the glenoid fossa of the scapula and its underlying cancellous bone structure [1-3]. Like other joints, the mechanical stress and adaptation conditions of the minimally constrained glenohumeral joint are reflected in the architecture of the subchondral plate and the cancellous bone. Variations in the subchondral bone architecture have important implications in artificial joint replacement. At present, loosening of the glenoid component is the most common long-term problem of total shoulder arthroplasty [4],

and loosening has been assigned to failure at the cancellous-cement interface [5]. This loosening rate was higher (39%) in keel components and lower (5%) in peg components [6]. Advances in shoulder joint arthroplasty, therefore, have necessitated research to characterize the mechanical and architectural properties of the glenoid cancellous bone stock. Total shoulder prostheses are less frequently implanted than total hip or knee prostheses [7-10]. Nevertheless, they have been widely and increasingly used since Neer published his first cases. The growing population of elderly patients may increase the number of these prostheses [11]. Many researchers have tried to find different anchoring techniques of the glenoid component in the scapular bone, either with or without cement in order to obtain better results on long term fixation of the glenoid component [12, 13]. No current implant design has succeeded in proving its superiority.

1.2.2 Current controversies and problems

Since the advent of unconstrained prostheses satisfactory results have been obtained both for pain relief and restoration of function [14, 15]. There are two basic issues when considering shoulder replacement for uncomplicated osteoarthritis. Firstly, the use of a cemented or uncemented humeral stem and secondly, whether to resurface the glenoid. The choice of stem fixation is easier to answer, as there is considerable experience with cemented implants. Given the satisfactory performance of the stem, the choice of implant is no longer between constrained and unconstrained devices, but rather between hemiarthroplasty and total joint replacement. It is often suggested that the results of joint replacement improve dramatically with the introduction of glenoid replacement [4]. A number of papers are quoted in this regard, but careful analysis demonstrates that there are many variables

[16-18], however, since fewer shoulders are included in the hemiarthroplasty group, at present the decision whether to replace the glenoid is based on relative merits [19, 20]. The potential advantages of total shoulder replacement are reduction in pain, treatment of instability due to wear and the mechanical advantage of lateralisation with restoration of the anatomical centre of rotation. Kelly and co-workers suggested that hemiarthroplasty gave incomplete pain relief in rheumatoid patients [20]. Neer introduced the glenoid component for very difficult technical problems encountered in cases of erosion. In rheumatoid arthritis, prosthetic replacement is impossible in approximately 15% of cases due to destruction of the glenoid [20]. Replacing the glenoid to allow lateralization and restoration of the axis of rotation may offer a theoretical mechanical advantage to deltoid and the rotator cuff. It is well recognized that even with an intact rotator cuff there is often failure of the muscles to centralize the prosthesis resulting in postoperative proximal migration [21]. Glenoid resurfacing increases the operation time considerably. It is technically difficult and a source of potential complications, such as glenoid fracture and sometimes the need for complex bone grafting. These factors have popularised hemiarthroplasty. There are disadvantages in hemiarthroplasty, such as the theoretical risk of articular wear and bone erosion particularly in cases of fracture and osteonecrosis. However, articular cartilage is not required for successful prosthetic replacement and stability can be enhanced by bone erosion creating conformity to the prosthesis [22, 23]. Another more technical disadvantage in total shoulder replacement is the difficulty associated with re-operating to replace the glenoid if it is a source of pain particularly in well-fixed non-modular prostheses. As noted previously, the main concern is the longevity of the glenoid component. The cause of radiolucent lines is poorly understood; it has been observed that some are seen on immediate post operative films and are ascribed

to poor cementing technique [18]. Furthermore, shift in position is more important than the width of the radiolucent line [24]. The association between loosening and poor clinical result has been particularly obvious in patients with massive tears and deficiency of the rotator cuff [5]. Undoubtedly, an intact rotator cuff improves the functional result and outcome. It should be considered how many of these repaired cuffs are truly functional and are able to prevent upward migration creating shear stresses and the "rocking horse" phenomenon that may be important in loosening. It is conceivable that this is a major cause of failure.

Improvements in the outcomes of shoulder arthroplasty, particularly in the field of glenoid component design, will come from increased understanding of the anatomy and biomechanics, and improvements in biomaterials as well as improvements in surgical technique and training. The glenoid articular surface is pear shaped and is flatter in the transverse than in the coronal plane. The normal glenoid consists of heavy plate-like trabeculae oriented perpendicular to the joint surface. The centre of the glenoid appears to be unique in terms of a cancellous structure transmitting pressure from the glenoid cavity towards the posterior cortical vault. In some cases, subchondral plate erosion, low density trabecular bone and a destroyed internal architecture are seen in the glenoid, making prosthetic fixation difficult [1, 25, 26].

The glenohumeral joint demonstrates certain biomechanical features, which cope with the unexpectedly high loads yet preserve the remarkable range of movement. Firstly, because the scapula rotates as the arm is raised, shear forces occur only during the initiation of elevation and compressive forces predominate throughout the remaining arc of arm elevation. Secondly, the scapular muscles act as shock absorbers for the energy dissipated. Thirdly, the small size and surface area of

the glenoid results in less constraint, since the glenoid fossa covers only 25% to 30% of the humeral head. Fourthly, the incongruence between radii of curvature of the glenoid and the humeral head also gives minimal constraint and minimal intrinsic stability [27]. Finally, the rotator cuff aims to keep the joint reaction force directed through the glenoid and hence prevent dislocation. Table 1.1 shows the glenohumeral contact forces in daily life activities [28]. In the absence of a rotator cuff the shear forces in a superior direction become even more significant and may be associated with progressive glenoid loosening [5]. The minimal volume of cancellous bone for fixation compounds the potential biomechanical problem of glenoid component loosening. The topographical distribution of glenoid trabecular bone and variation of bone strength decreases with distance from the subchondral plate [29, 30]. The current challenge of prosthetic design largely concerns the glenoid component. Little data exists on load transmission in the normal or pathological situation [31]. Friedman studied three aspects with finite element analysis; demonstrating the detrimental effect of subchondral plate resection [32], that angled humeral stem designs created high stresses at the inferior interface compared with the stem perpendicular to the surface and that high non-physiological stresses occurred with metal-backed components.

Table 1.1 Glenohumeral contact forces [28].

Study	Dimension	Task	Force (x BW)	Force (N)
Van der Helm,[33].	3D	Wheelchair propulsion	—	1900
Van der Helm[34].	3D	Abduction, straight arm, no load	—	370
Van der Helm [34]	3D	Abduction, straight arm, 0.75 kg load	—	600
Runciman [35]	3D	Push-ups	>7	—
Runciman[35]	3D	Chin-ups	>4	—
Runciman [35]	3D	Press-up*	>4	—
Runciman [35]	3D	Flexion, 2kg load	1.5	—
Karlsson and Peterson [36]	3D	Abduction, straight arm, 1 kg load	1.1	650
Karlsson [37]	3D	Hand drill use	1.4	995
Dul [38]	2D	Abduction, elbow flexed 90°, no load	0.4	—
Kessel and Bayley [39]	2D	Abduction, straight arm, no load	—	600
Post et al.[1]	2D	Abduction, straight-arm, no load.	—	600
Beuchel et al. [40]	2D	Abduction, straight arm, no load	—	420
Beuchel et al.[40]	2D	Abduction, straight arm, 110 N load	—	2070
Poppen and Walker [41]	2D	Abduction, straight arm, no load	0.9	—
Poppen and Walker [41]	2D	Abduction, straight arm, 1 kg load	1.4	—
Inman et al.[42]	2D	Abduction, straight arm, no load	0.9	—

* Subjects pushed themselves up from a chair with straightened leg.

1.3 ANATOMY OF THE SHOULDER JOINT

1.3.1 The joints

Normal shoulder function depends on four joints: the glenohumeral joint, the acromioclavicular joint, the sternoclavicular joint and the scapulothoracic joint (Figure 1.1). The scapulothoracic joint is not a true articular joint by definition, as it does not articulate with another bone via cartilage or fibrous tissue [43], but is instead considered a functional joint formed by the bursa between the scapula and the thoracic wall. Abnormality of any of these four joints may reduce the efficiency of the others, although functionally the deficit maybe taken up elsewhere. Certain authors consider shoulder function to also be reliant on a fifth joint, the acromiohumeral joint, which like the scapulothoracic joint is bursal [44].

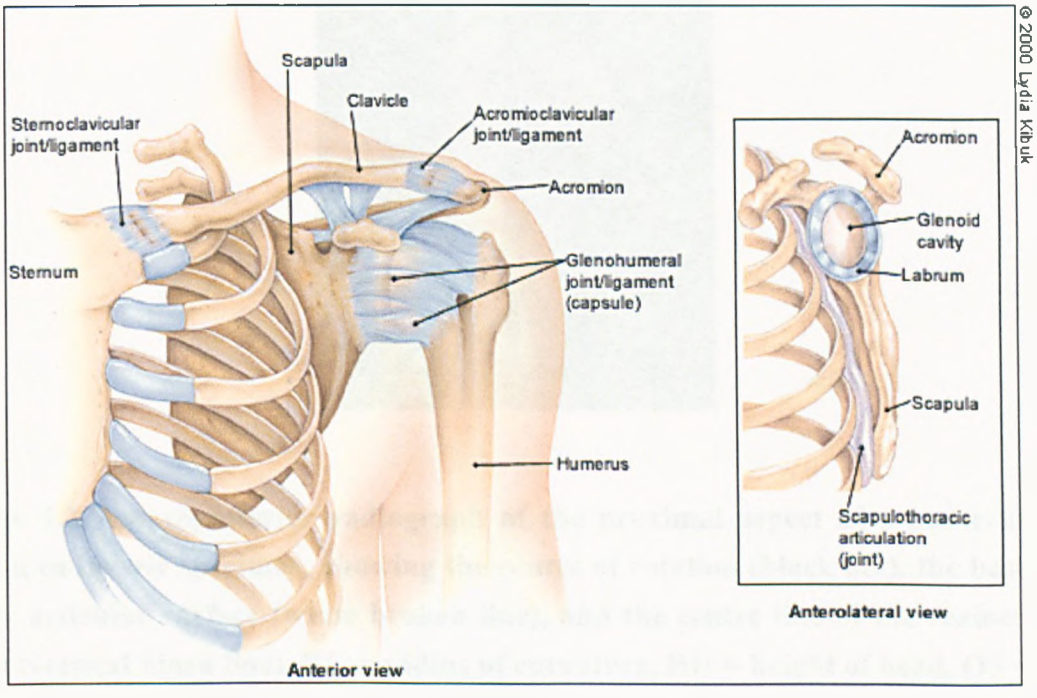

Figure 1.1 Anterior and anterolateral views of the shoulder joints. (From:www.stronghealth.com).

1.3.2 Glenohumeral joint

The glenohumeral joint has been described as a ball and socket joint [44]; however, Saha describes only 70% of glenohumeral joints as being of the ball and

socket variety [45]. In 30% of cases, the humeral articular surface is a segment of a sphere of larger radius than of the glenoid fossa. Even in the 70% of cases deemed to be of the ball and socket variety, the surfaces are not perfectly congruous.

1.3.3 Bony anatomy

In an erect posture, there is the relative flattening of the thorax anteroposteriorly, leaving the scapula lying at an angle of 30-45^0 to the coronal plane. With this scapula position, the glenoid fossa becomes reoriented to a more lateral position. The humeral head has undergone external rotation and the shaft internal rotation creating torsion in the humerus [46] (Figure 1.2).

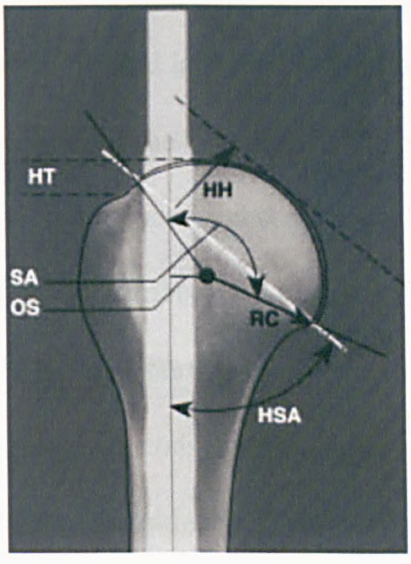

Figure 1.2 Anteroposterior radiograph of the proximal aspect of a humerus from a cadaveric specimen, showing the centre of rotation (black dot), the base of the articular surface (white broken line), and the centre line of the reamed canal (vertical black line). RC = radius of curvature, HH = height of head, OS = offset of humeral head, SA = arc of articular surface, HT = head-to-tuberosity height, and HSA = head-shaft angle [47].

The glenoid cavity is roughly pear-shaped having the appearance of an inverted comma: the superior portion being narrower than the inferior portion (Figure 1.3). The glenoid articular surface and glenoid labarum combine to create a socket that is approximately 9mm in depth in the supero- inferior direction and 5mm in depth transversely [48]. Based on a study of living and cadaver shoulders Iannotti et al reported the following measurements for the glenoid fossa: the average superoinferior dimension is 39±3.7mm, the broader lower half of the fossa is 29±3.1mm wide whilst the narrower upper half is 23±2.7mm at its mid-point [49]. Iannotti et al [49] also observed that the radius of curvature of the glenoid fossa in the coronal plane was greater than that of the humerus; however, it is deepened by the presence of the fibrocartilaginous glenoid labrum. For all positions of abduction the point of articulation is focused towards the bare area of the glenoid [48]. The bare area being an area of cartilage thinning and increased subchondral bone density. The bare spot of the glenoid cavity has been described as a central reference point to quantify the amount of bone loss of the inferior portion of the glenoid cavity [50]. Burkhart et al.[50] assumed that, the bare spot was a constant landmark within the glenoid cavity and that the inferior portion of the glenoid cavity had a circular shape with the bare spot as its centre. According to Burkhart et al.'s findings, the bare spot had a consistent localization and the measurements from the centre of the bare spot to the anterior, posterior and inferior rim of the inferior part of the glenoid cavity were approximately equal at 12 mm. The bare spot should, therefore, help the surgeon to determine the width of the inferior portion of the glenoid cavity arthroscopically in cases of glenoid bone loss. Warner studied the articular contact patterns of the glenohumeral joint at 0^0, 45^0 and 90^0 abduction with joint compression loads of 222N and 444N [51]. Their analysis revealed that articular congruence and the

percentage contact area increased with increasing abduction and was focused on the bare area. Although a previous study reported a slight upward tilt of the glenoid of about 5° relative to the medial border of the scapula [52], a more recent study suggests that the opposite may be the case [53]. The glenoid is retroverted approximately 6°. However, considerable individual variation in these measurements has been reported ranging from –13 to +8° (upward tilt) and from –2 to +13° (retroversion), respectively [53].

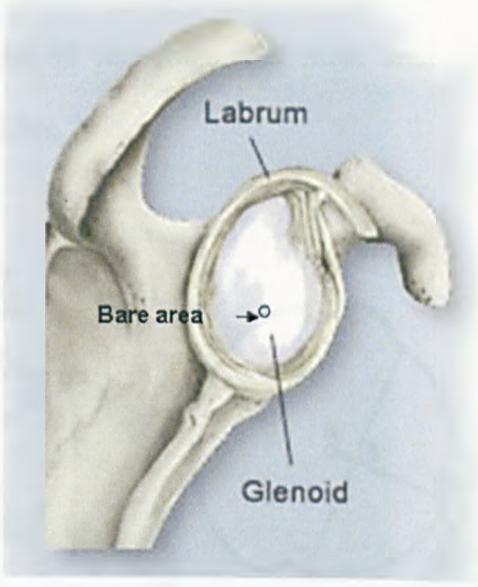

Figure 1.3 The glenoid cavity. (From: www.scoi.com)

The geometry of the humeral head can best be represented by a sphere [54]. The articular surface constitutes about a third of this sphere. The maximal diameter of the articular surface ranges from 37 to 58 mm, and the radius of curvature ranges from approximately 20 to 30mm, the height of the articular segment varies between 12 and 24 mm [49]. The inclination (neck shaft) angle can be defined as the angle subtended by the central intramedullary axis of the humeral shaft and the base of the articular segment (Figure 1.4): this angle varies between 30 and 55° [55]. The centre of

the humeral head does not coincide with the central intramedullary axis of the humeral shaft; this distance can be defined as the humeral head offset. In the coronal plane, the centre of the articular surface lies approximately 7mm (range, 3–11 mm) medial and in the axial plane approximately 2 mm (range –1 to 6 mm) posterior to the intramedullary canal [56]. The articular surface is retroverted approximately 18° with respect to the condylar line or 22° when measured in relation to a line tangential to the trochlea and the condyle of the distal humerus. However, a significant variation in retroversion angle ranging from –7 to 48° and –10 to 57° has been reported [57]. It is important to recognize that most anatomic parameters of the proximal humerus are variable.

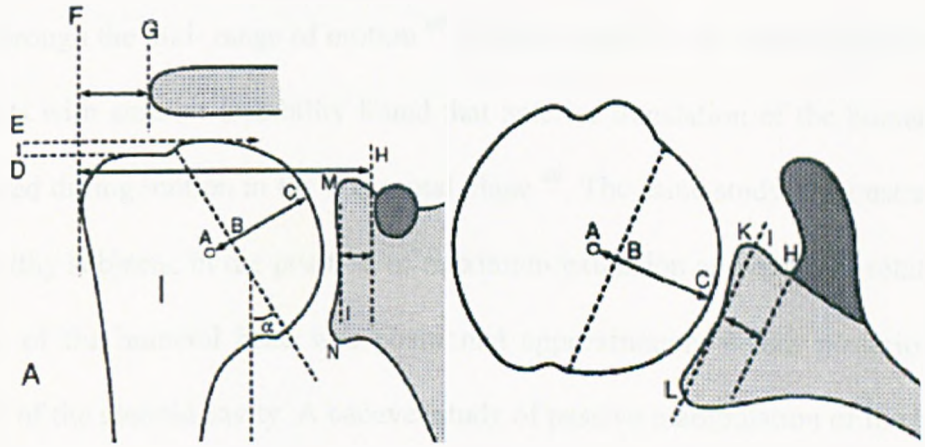

Figure 1.4 A–C, Radius of curvature; BC, Height of the articular surface, (α) Neck shaft angle. (With permission from JP Iannotti, *J Bone Joint Surg Am.* 1992;74:491-500.)

1.3.4 Glenohumeral mechanics

While recent studies have characterized the mechanical properties of articular cartilage and capsular ligaments [58]; differing opinions exist concerning normal or abnormal glenohumeral joint kinematics. Some researchers believe that the normal glenohumeral joint behaves as a "ball and socket," allowing only small

translations due to deformation of the articulating surfaces and small differences in their radii [59]. Others feel that the joint is relatively unconstrained, allowing larger translations through the range of motion [48]. This lack of consensus has motivated a number of differing approaches to the development and refinement of treatment interventions aimed at improving shoulder mechanics.

The earliest shoulder studies documented the motion of the clavicle, scapula, and upper portion of the sternum. Later, radiographic studies investigated glenohumeral motion in the frontal and scapular planes, as well as motion in normal and abnormal joints. Poppen and Walker reported that in normal shoulders, the geometric centre of the humeral head did not exhibit translations of more than 1 or 2 mm through the mid- range of motion [60]. A more recent *in vivo* radiographic study of patients with anterior instability found that anterior translation of the humeral head occurred during motion in the horizontal plane [49]. The same study demonstrated that in healthy subjects, in the position of maximum extension and external rotation, the centre of the humeral head was positioned approximately 4 mm posterior to the centre of the glenoid cavity. A cadaver study of passive manipulation of the humerus documented excessive translations of the humeral head on the glenoid at abduction and internal rotation of the arm [61]. Recently, a technique to reproduce the position of the humerus with respect to the glenoid in space was described in a study that demonstrated that the maximum humeral elevation occurred in a plane anterior to the scapular plane,[62].

1.3.5 Joint stability

Functional stability of diarthrodial joints is believed to be important in maintaining the health and longevity of their articular cartilage surfaces [27]. The glenohumeral joint has minimal bony constraint, allowing the largest range of motion of any major diarthrodial joint in the human body. It achieves a delicate balance between mobility and stability.

Glenohumeral stability is achieved through both passive (static) and active (dynamic) restraints [63]. Passive restraints include the capsule, ligaments, labarum, the geometry of the humeral and glenoid articular surfaces, compliance of the articular cartilage covering these surfaces, the phenomena of limited joint volume in adhesion-cohesion, and restraint provided by gross bony geometry. Active restraints (Musculature) includes; the rotator cuff and other shoulder musculature that exert forces on the glenohumeral joint.

The complex integration of these restraints is such that the glenohurneral joint has a high degree of mobility yet is stable during a wide spectrum of functional situations [64]. Alterations in either the anatomy of the joint or deficiencies in the biomechanical properties of the ligamentous and/or capsular components can cause motion abnormalities and focal contact stresses to develop [65]. These sites of high contact stresses may initiate focal lesions on the articulating surfaces and will tend to exacerbate the rate of cartilage degeneration leading osteoarthritis [65]. The orientation of the humeral head with the shaft is defined by the angle formed between a line drawn through the centre of the anatomic neck and a line drawn through the centre of the humeral head, this angle is about 30°- 55° [66]. An anatomic variant with significant deviation from these angles can lead to inherent instability. The articular surface area of the humeral head is larger than that of the glenoid, thus allowing for

large normal range of motion (ROM). The glenoid version is the angle that the glenoid centre line makes with the plane of the scapula, is also critically important for stability. In osteoarthritis (OA), the posterior glenoid wear is observed, leading to increased retroversion of the glenoid and predisposing to posterior instability. Coupled to these concepts of glenoid orientation are glenoid concavity and the possible effective arcs. The arc is defined by the maximal angle along which the joint reaction force can point outside which dislocation and/or subluxation may occur (Figure 1.5 and Figure 1.6). With glenoid rim wear or fracture, less effective arcs are possible (Figure 1.7). The deltoid and cuff muscle forces maintain the net humeral joint reaction force within the balance stability angles. The normally concave glenoid stabilizes the humeral head by the concavity compression mechanism in which the net force acting on the humeral head compresses it into the glenoid concavity [66]. The orientation of the glenoid in the space depends on the position of the scapula and the orientation of the articular surface in relation to the scapular body [66]. The horizontal (glenoid version) and vertical (glenoid inclination) orientation of the glenoid is not defined by a simple geometric relationship. The glenoid centre line can be related to scapular coordination and to the plane of the scapula, and to how the balance stability angle varies around the face of the glenoid cavity (Fig 1.5).

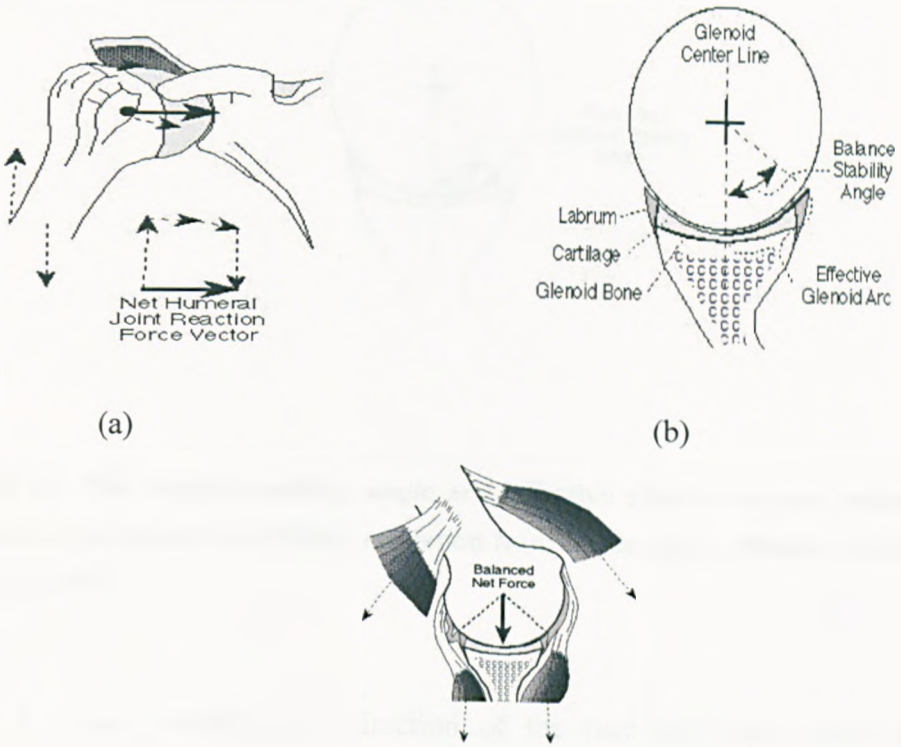

Figure 1.5 The glenoid: (a) The net humeral joint reaction force, (b) The effective glenoid Arc, and the (c) The deltoid and cuff muscle forces maintain the net humeral joint reaction force within the balance stability angles (With permission from Frederick A. Matsen, III, M.D: The shoulder, 1998).

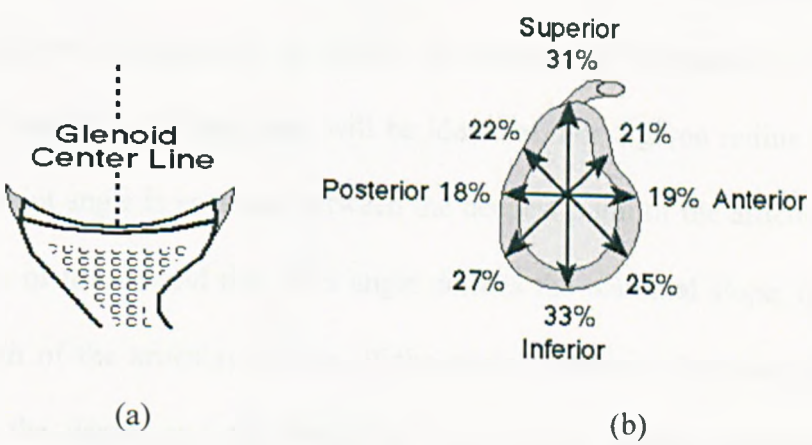

Figure 1.6 The glenoid centre: (a) The glenoid centre line can be related to scapular coordination and to the plane of the scapula; (b) The balance stability angle varies on the face of the glenoid (With permission from Frederick A. Matsen, III, M.D: The shoulder, 1998).

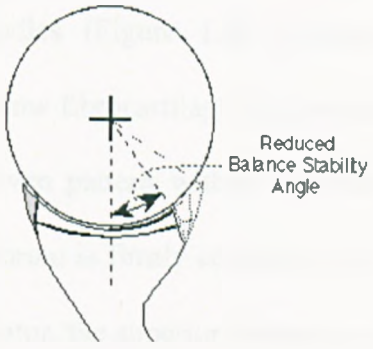

Figure 1.7 The balance stability angle and effective glenoid arc are reduced by a fracture of the glenoid rim (With permission from Frederick A. Matsen, III, M.D: The shoulder, 1998).

For joint stability, the direction of the resultant force vector must be constrained to remain within the balance stability angle (Figure 1.6). This angle represents the effective area into which the resultant reaction force vector can be directed in order to provide compression of the humeral head into the concave surface of the glenoid, and thus provide joint stability. A larger constraint angle means that the glenoid provides more bony stability to the joint. Assuming that the glenohumeral articulation is congruent; the radius of curvature of the glenoid and that of the humeral head in a defined plane will be identical. For a given radius of curvature, the constraint angle is enclosed between the deepest point of the articular surface and the edge of the glenoid rim. This angle defines the maximal slope, the depth, and the length of the articular surface. If the angle increases, the maximal slope at the edge, the depth, and the length of the articular surface increase. Consequently, the surface area increases and the joint become more constrained [66, 67].

The glenoid labrum is a wedge-shaped fibrous structure that consists of densely packed collagen bundles (Figure 1.8). Located between the articular cartilage and the labrum, a narrow fibrocartilaginous transition zone is composed of dense collagen fibres in a woven pattern within the hyaline cartilage. Below the glenoid equator, the inferior labrum is firmly continuous with the articular cartilage, whereas above the glenoid equator, the superior labrum is quite variable and is often loosely attached and more mobile. The labrum is vascularised throughout its peripheral attachment to the joint capsule and acts as an anchor for the glenohumeral ligaments and the biceps tendon [68].

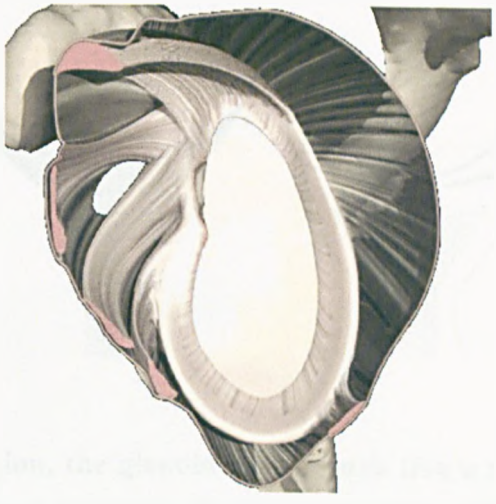

Figure 1.8 The glenoid labrum (From: www.shoulderdoc.co.uk).

The contribution of the labrum to glenohumeral stability has been clearly established; it acts as the anchor point for the capsuloligamentous structures, increases the depth of the glenoid socket, and facilitates the concavity-compression mechanism as the humeral head is compressed in the glenoid during rotator cuff contraction. The glenoid looks much like a rubber suction cup with respect to its feathered, compliant edges and a more rigid centre (Figure 1.9) [66]. The stabilizing

effect of intra-articular pressure is the result of the vacuum effect, which exists within a sealed joint compartment. The reduced pressure created within that compartment resists any force that tends to displace the articular surfaces. However, this effect has been shown to be minimal compared with the stabilizing effect of joint compression from dynamic muscle action. The glenohumeral joint contains a small amount of synovial fluid that provides cartilage nourishment. Viscous and intermolecular forces between the fluid and the joint surfaces create an adhesion-cohesion effect analogous to that seen when two glass plates are separates by a thin film of water: the plates side easily over one another but are difficult to separate.

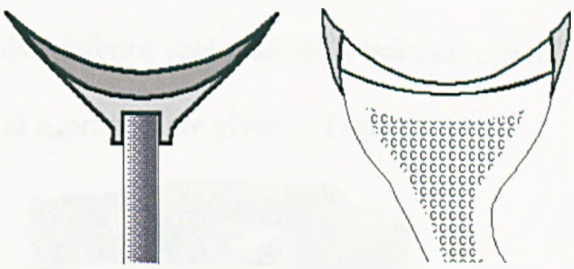

Figure 1.9 In cross-section, the glenoid looks much like a rubber suction cup. **(With permission from Frederick A. Matsen, III, M.D: The shoulder, 1998).**

The glenohumeral ligaments are discrete thickening of the joint capsule [69] (Figure 1.10). Since the advent of modern day shoulder arthroscopy the functional significance and variant anatomy of these ligaments has been more fully appreciated. The role of each ligament is complex and varies with the position of the arm, as well as the direction of the applied force. A summary of these roles, based on Levine and Flatow is outlined below [70] :-

i) The superior glenohumeral ligament (SGHL) resists inferior subluxation of the shoulder joint and provides anterior stability in the neural or adducted position.

ii) The middle glenohumeral ligament (MGHL) provides anterior stability in the mid-range of abduction.

iii) The inferior glenohumeral ligament (IGHL) is the most important anterior static stabiliser of the shoulder joint. It forms a complex of anterior and posterior bands with an intervening axillary pouch. The anterior band provides the greatest resistance to anterior translation with the arm in abduction and external rotation, while the posterior band provides resistance to posterior translation of the humeral head when the arm is abducted. When the arm is abducted, the inferior glenohumeral ligament resists inferior subluxation. A brief description of the role of the glenohumeral ligaments are given in Figure 1.11.

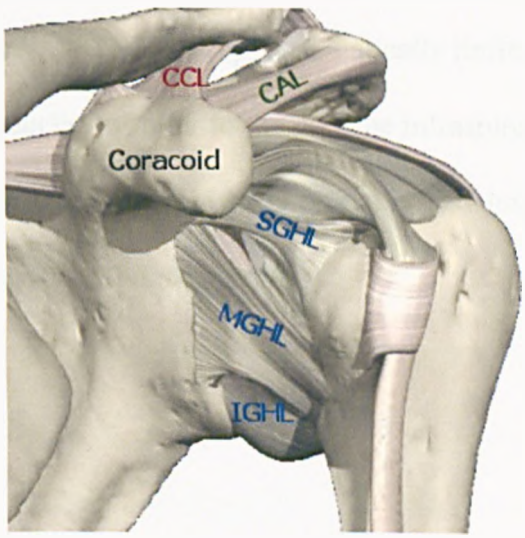

Figure 1.10 The glenohumeral ligaments. (From: www.shoulderdoc.co.uk).

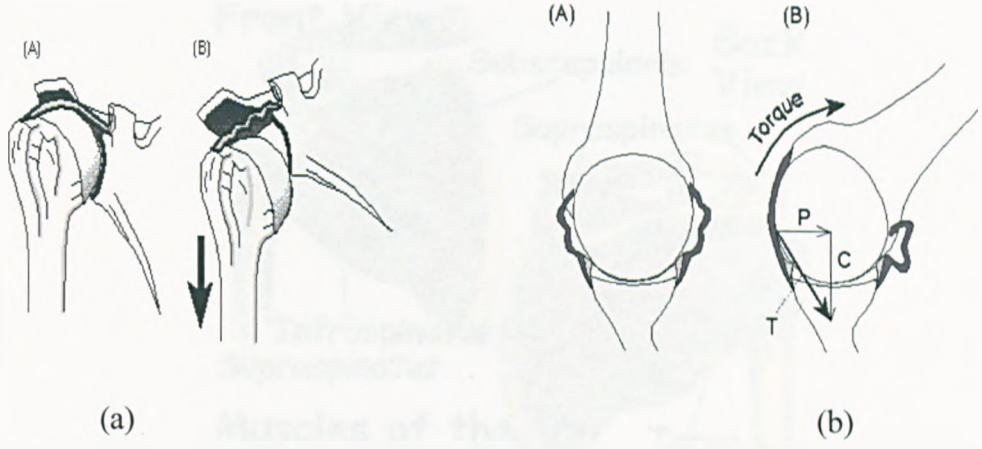

Figure 1.11 Capsule and Ligaments: (a) Scapular dumping. With the scapula in a neutral position (A), the superior capsular is tight, supporting the head in the glenoid. Depression of the lateral scapula (B) relaxes the superior capsular structures and rotates the glenoid and causes no support to the head of the humerus. (b) A, when the glenohumeral ligaments are loose, they apply no force. B, when torque is applied, the ligaments come under tension (T). This ligament tension apply a compressive force (C) directed into the glenoid and a displacing force (P) pushing the humeral head away from the tight ligament (With permission from Frederick A. Matsen, III, M.D: The shoulder, 1998).

Experimentally, the rotator cuff (Figure 1.12) has been shown to have a passive effect on stability [71, 72]. The subscapularis statically limits anterior translation in the lower ranges of abduction similar to the way the infraspinatus and teres minor limit posterior translation. This mechanism is probably less important *in vivo* than the contribution of the rotator cuff during activity.

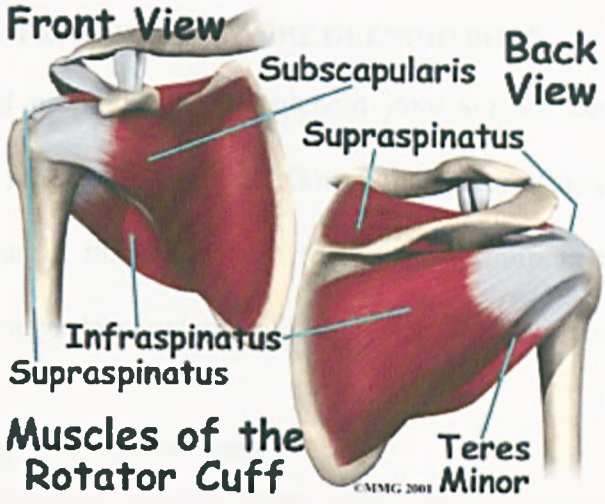

Figure 1.12 Muscles of the rotator cuff. (From: www.allaboutarthritis.com)

Several dynamic factors play important roles in enhancing glenohumeral stability. Active contraction of the rotator cuff contributes to stabilization by the joint compression mechanism from coordinated muscular activity and by secondary tightening of ligamentous constrains through direct attachments to the rotator cuff muscles. This effect works in combination with the concavity-compression mechanism, the compression of nearly congruent articular surfaces into one another by muscle contraction [73]. It is thought that, contraction of the long head of the biceps, coordinated scapulothoracic rhythm, and the proprioceptive modulation of all dynamic factors also contribute to dynamic stabilization of the glenohumeral joint [74]. In summary, any component design must mimic the function of the glenoid and aid the ancillary stabilising actions as well as provide good fixation. Indeed, it could be hypothesised that the poor design of the articulating surface may lead to instability which in itself exerts non-physiological stresses on the fixation interface.

1.4 MECHANICAL PROPERTIES OF THE GLENOID BONE

The mechanical properties of the glenoid joint surface dependents on the quantity and quality of the underlying cancellous bone and its structure. Bone quality is an important factor in the fixation of the glenoid component of a shoulder replacement and the longer-term outcomes in this arthroplasty procedure.

1.4.1 Mechanical properties of bone

From a morphological point of view, there are two types of bone: cortical (compact) and cancellous (spongy). In cortical bone, densely packed collagen fibrils form concentric lamellae, and the fibrils in adjacent lamellae run in offset planes. Cancellous bone has a loosely organized, porous matrix (**Figure 1.13**). Differences in the structural arrangements of the two bone types are related to their primary functions; cortical bone provides mechanical and protective functions and cancellous bone provides additional metabolic, as well as structural, functions. In the entire skeleton mass 80% of bone is composed of cortical bone and only 20% is cancellous bone [75-77]. The surface-volume relationships are much greater in the cancellous bone. Thus, it is metabolically more active. This is the usual explanation for differences between remodelling activities in the two types of bone. Cortical bone and cancellous bone share many features of remodelling, particularly in the sequences of origination, activation, resorption, formation, and mineralization. Bone remodelling is a renewal process, which involves the continuous removal of bone in packets by osteoclastic resorption followed by synthesis of new bone matrix by osteoblasts and its subsequent mineralization. The process serves to preserve the mechanical integrity of the skeleton.

Figure 1.13 Porous structure of the trabecular bone (From: www.hull.ac.uk/cmet/osteoporosis.htm).

Biological structures generally have orderly structural elements that give them very different material and mechanical properties under different conditions. Thus, the mechanical response of bone varies not only according to the magnitude of the applied force, but also to its direction, a phenomenon known as anisotropy. Anisotropy is a parameter that defines the direction of preferred orientation of trabeculae and is important for directionally dependent mechanical properties. The anisotropic nature of bone is shown by data for the material properties of cortical and trabecular bone in several loading directions (Table 1.2). Cortical bone is stronger in compression than in tension [78], and after maturation the tensile strength and the modulus of elasticity of femoral cortical bone decline by approximately 2% per decade [78]. The ultimate compressive strength of trabecular bone is related to the square of its apparent density so that a decline in the latter due to aging or metabolic bone disease is associated with a more rapid reduction in compressive strength [79].

Table 1.2 Mean values for human bone material parameters [78].

Type of bone	Direction and type of load	Apparent Density (g/cm^3)	Ultimate Strength (MPa)	Modulus of elasticity (MPa)
Cortical (mid femur)	Longitudinal Tension	1.85	133	17,000
	Longitudinal Compression	1.85	193	17,000
	Longitudinal Shear	1.85	68	3,000
	Transverse Tension	1.85	51	11,500
	Transverse Compression	1.85	33	11,500
Trabecular (vertebral body)	Compression	0.31	6	76

Trabecular bone has a lower modulus of elasticity than cortical bone due to its greater porosity. However, although less stiff, trabecular bone can undergo greater strains, fracturing at deformations of approximately 7%, while cortical bone will fail at strains of only 2% [80].

The mechanical behaviour of bone may be studied at two levels: material and structural. The material or tissue level properties of bone are evaluated by performing standardised mechanical tests on uniform bone tissue samples. Depending on the level of resolution, tissue level testing is relatively independent of bone structure or geometry. Second, by examining the behaviour of bones as completely anatomical units, the contributions of structural properties can be determined. Taken together, these two levels of properties represent the way bones respond to forces *in vivo* and can be observed by means of experiments on sections of bones or on intact bones with normal geometry.

Assessments of bone structure and/or geometry maybe made using micro-computed tomography (μCT), magnetic resonance imaging (MRI), and peripheral quantitative CT (pQCT). In addition, these techniques may also be able to provide

information on the bone mineral density, and thus some indication of the bone strength and/or modulus.

However, when performing mechanical tests on bone, it is important to know that the differences between tissue level and structural level properties are not always clear. If one considers a small cube of vertebral trabecular bone as a tissue section, then trabecular element preferred orientation may influence what is assumed to be a material property, when in fact it is largely influenced by structural configuration [81]. Likewise, both material and structural properties of bones can change with the level of resolution.

With the progress in Micro-computed tomography (μCT), it is now possible to measure the 3D structures non-destructively (Figure 1.14). In bone research, μCT is used to image and quantify trabecular bone. It has also been used to aid the investigation of the relationship between the trabecular architecture and the mechanical properties of the bone. From the bone images, the μCT scanner measures and calculates several trabecular bone parameters, which are important in determining a bone's condition, and it's response to different loading. These include the bone volume to total volume ratio (BV/TV), the trabecular spacing and thickness as well as the anisotropy of the trabecular structure.

Figure 1.14 MicroCT scanner (SCANCO Medical AG, Switzerland).

1.4.2 Mechanical properties of the glenoid bone.

Mechanical and geometric information on the glenoid is important for a number of reasons including providing the base information for finite element modelling and assessing those areas of the underlying bone that may provide best fixation in cemented glenoid components. To achieve this, imaging technique can be used to measure the bone mineral density and other morphological parameters. Mechanical testing is used to obtain the elastic modulus and the strength of bone directly. CT scans have been used as an imaging method to visualize bone structure and to analyze morphological factors whilst an indentation techniques can be applied to obtain the mechanical properties of the glenoid bone. Regional variations in bone properties have been observed from both the above-mentioned methods. These differences in the regional properties emphasize the importance of identifying the regions of bone of sufficient quality for adequate fixation during prosthetic replacement. Table 1.3 outlines the relationship of bone quality to mechanical properties previously been determined for the glenoid component [30]. Frich et al. [82]

used a form of penetration test, perforating a needle into trabecular bone to obtain a plot of penetration force versus penetration depth. The needle had a 90-degree conical profile with a base diameter of 2.5 mm and the needle shaft was milled to 2.3 mm diameter. They obtained fresh bone blocks, machined with an Exact grinding cutting device from different regions of the glenoid. Oxland and Grant et al. [83] used indentation tests on the lower lumbar vertebral endplates. A 3mm diameter hemispherical indenter was pressed into the bone at 0.2mm/s to a depth of 3 mm by a stepper motor-controlled electromechanical linear actuator.

A successful total shoulder arthroplasty is highly dependent on the quality of the glenoid bone. The amount of cancellous bone available for fixation of the glenoid prosthesis is small [4]. Knowing the quality of the cancellous bone stock is important to understand the load transmission through the glenoid. Whilst there is some information on the glenoid structural properties (Anglin et al [30] and Frich et al [82]) little is known of its relationship to the underlying bone. A variation in the subchondral bone architecture has important implications in artificial joint replacement since this may help to define the loosening process in glenoid components. Indeed the mechanical strength of the glenoid joint surface is dependent on the amount and mineralization of the underlying cancellous bone and its architecture [30].

Table 1.3 Glenoid properties in the literature [30].

Study and method used	Mean values	Number of specimens and age	Regional properties
Anglin C. et all (1999)	σ = 6.7 to 17 MPa E = 67 to 171 MPa ρ = 0.25	10 embalmed ; age 81	The postero-superior edge highest values. Posterior much stronger than the anterior and central column.
Mansat et al Baréa (1998); Baréa et al (1997): Ultrasound, CT; cubes core	E1b= 372 MPa E2b= 222 MPa E3b= 198 MPa ρ = 0.27 g/cm3	6 spec. (3pairs); 80 ± 9 yr	Central and posterior moduli highest, inferior weaker decrease with depth; anisotropic
Frich et al. (1997,1998); Frich and Odgaard (1995); Frich (1994): CT, MRI (a) Penetrometer, (b) Cylinders (central) (c) Cubes (sup. & inf.)	σ ac =37 MPa E b = 105 MPa E c = 411 MPa ρ b = 0.34 g/cm3 ρ c = 0.38 g/cm3 ν c = 0.26	20 healthy Spec. (10 pairs); 31-74 yr (mean 57); 6 (RA) spec.; 45-75 (mean 56)	Posterior-superior strongest; posterior> anterior; anisotropic close to surface, isotropic deeper; RA bone volume fractions half that of healthy
Battle et al. (1996); Batte (1996): CT, indentation; slices	K d ≈ 370 MPa ρ = high volume fraction of bone	8 spec (0 pairs); 55-74 yr, plus one in early 40s	Superior stiffest; ant.-post. Trends varied; weaker below 6mm
Manson et al. (1994): CT	ρ = 0.37 g/cm3	16 spec (6 pairs); age not specified	Superior densest; central column weaker than post. or ant.; deepest portion inf. To Ant- superior.
Müller- Gerbl et al. (1992): CT (*in vivo*) (a) healthy, (b) gymnasts, (c) patient with dislocation	-	(a) 20 spec. (22 -86) (b) 11 (16-29) (c) 1 (45)	Higher anterior and posterior density in young; more central in elderly

[a] E = modulus, ρ = density, σ = strength, ν = Poisson's ratio, K = indentation modulus [d], [b] E_1= is latero-medial, E_2 is anterior-posterior, E_3 is superio-inferior, [c] penetrometer strength of 37 MPa ≈ 14 MPa ultimate strength [d] Indentation modulus, K, is the stress/strain from indentor, which is higher than the elastic modulus.

The load- bearing function of the cortical vault has been investigated by compression tests before and after removal of the cortical bone [82]. Using harvested cubes of bone, Mansat et al [84] showed that the average values of the mechanical properties of seventy-four specimens had higher elastic modulus at the lateromedial zone, whereas anteroposterior modulus had an intermediate value, and superoposterior modulus had the lowest value [85]. According to the atlas of the mechanical properties of human cancellous bone [86], the axial elastic modulus of the glenoid cancellous bone has been found to be lower than the axial modulus for all the other bones (humerus, vertebra, femur, tibia, patella). From Manset et al. [84] findings, the glenoid cancellous bone is stiffer at the centre of the glenoid and near its posterior edge. The forces across the glenohumeral joint varying not only with the load applied but also with the position of the arm [84, 87]. To keep the humeral head in the glenoid cavity during abduction, the vector of the resultant force must stay within the glenoid arc [41]. This may explain the high values for stiffness found in the central-posterior region. Further, Mansat et al showed that the glenoid has anisotropic material properties [85]. A study by Frich et al. [82] suggested that the correlation between the elastic modulus and the apparent density of the glenoid subchonral region was poor (r=0.55). The data provided from this study indicate that the glenoid consists of medium-density, highly anisotropic cancellous bone with a pronounced variation in topographic strength. It also demonstrated a major contribution to strength from the cortical shell. Average elastic modulus at the bare area was found to be approximated 100MPa, whereas the elastic modulus superior to the bare area was increased fourfold [88]. The differences of the mechanical properties of the glenoid regions could be explained by the differences in the trabecular microstructure. The highest strength values were found at the proximal subchondral

region immediately posterior, superior, and anterior to the glenoid bare area [88]. This off-centre increase in bone strength of the normal glenoid is the physiologic off-centre loading or shear-stress loading according to theory of Wolff [89]. The volume fraction of trabecular bone varied from 11% to 45%, with peak values at the posterior glenoid vault. The density ratio from posterior to anterior was 2:1 [90]. The middle portion of the glenoid appeared as transverse, isotropic, plate like trabecular, radially oriented perpendicular to the subchondral plate, whereas the peripheral zones tended to be more anisotropic [90] and higher density was observed in the posterior third of the glenoid vault and this explain the structural adaptation to functional stresses. Hayes et al found that the cancellous bone is more dense in regions of high shear stresses [91]. The upper extremity is usually positioned anterior to the body during activity, adding a transverse contact pressure on the posterior part of the joint surface. In the study on shoulder muscle forces, it was shown that the strength of the anterior short rotator muscles exceeds the strength of the posterior rotator muscles [91]. The stronger anterior rotator muscles may cause an increased posterior stress on the underlying subchondral bone, which, however, is balanced by the retroverted humeral head and the slightly anteverted glenoid neck [92]. Frich et al. [93] found the thickness of the subchondral plate was on average 1.9mm, whereas Simkin et al. [94] reported a thickness of the glenoid subchondral plate of 2.3mm obtained by microradiography. The glenoid is usually considered to be a low-density cancellous structure [1, 5, 94], but Frich et al. [93] strongly indicated that the glenoid cancellous bone should no longer be considered as low density bone.

1.5 SHOULDER ARTHROPLASTY

1.5.1 Introduction

Total shoulder replacement is a successful treatment for the painful, arthritic glenohumeral joint. The principle long term concern is the mechanical loosening of the glenoid component [95]. Loosening is confirmed on sequential X-rays by a positional shift or rotation of a component. These changes are often seen in long term follow up, although the components may have been loose for a considerable period of time before becoming symptomatic. Early loosening is often defined as the presence of radiolucent lines. For glenoid components the overall prevalence of these radiolucent lines is reported to range from 22% to 95% [24, 95-97]. The indications for hemi- or total shoulder arthroplasty is pain and the associated patology include degenerative joint problems; i.e., rheumatoid arthritis, degenerative arthritis, and avascular necrosis; and for post traumatic problems; i.e., severe, unreconstructable fractures of the proximal humerus, fracture-dislocations of the humeral head; (dysplastic problems – very difficult as anatomy completely abnormal – rarely done) and tumour replacement of the proximal humerus [98].

1.5.2 Prosthetic design

As constrained prosthetic designs were developed to compensate for absent dynamic stabilizers of the shoulder joint, high loosening rates for the glenoid component have been observed. For this reason unconstrained designs are generally preferred [4]. Several approaches to prosthetic replacement of the original anatomy of the proximal humerus and glenoid have been attempted. The so-called first generation of shoulder arthroplasty, originally developed by Neer, is based on one radius of curvature for the humeral head with a choice of different sizes [99]. The

second generation of shoulder prosthesis is modular, offering a greater choice for both the prosthetic head and stem. To allow more natural translations of the humeral head on the glenoid, non-conforming articulations have been created. In order to restore the variable three-dimensional geometry of the proximal humerus and the geometric centre of rotation, a new type of humeral component which is not only modular, but can also be adapted to the variable inclination angle and medial and lateral offset has been recently developed (third-generation design) [100].

1.5.2.1 Humeral head component

The size and placement of the humeral head are both important factors that may have an effect on eccentric glenoid loading and subsequent component loosening. As the anatomy of the proximal humerus has been studied, the understanding of the posterior and medial offset position of the humeral head in relation to the shaft has aided in the design of the third-generation humeral implants [101] (Figure 1.15). It has been believed that an increase in subacromial contact could lead to pain, decreased motion, and rotator cuff degeneration after total shoulder arthroplasty [102]. Harryman et al. [103] thought that subacromial impingement could also potentially lead to eccentric loading of the glenoid component and subsequent early glenoid component loosening. Thus, an incorrect humeral head offset can lead to capsular tightening and subsequent glenohumeral translation and component wear [103, 104]. Replacement with an anatomic head size may also reduce eccentric glenoid loading. The humeral head size should always be as anatomically correct as possible. Soft tissues should be balanced around an anatomic implant, rather than changing the head size to make up for soft-tissue imbalances. Harryman et al [103] showed that when a large, nonanatomic humeral head was used, all motions were diminished.

Thus, using an oversized head will over tighten the soft tissues, causing pain. Likewise, capsular laxity can significantly increase asymmetric load stresses of the glenoid, which can compromise glenoid fixation as well [103].

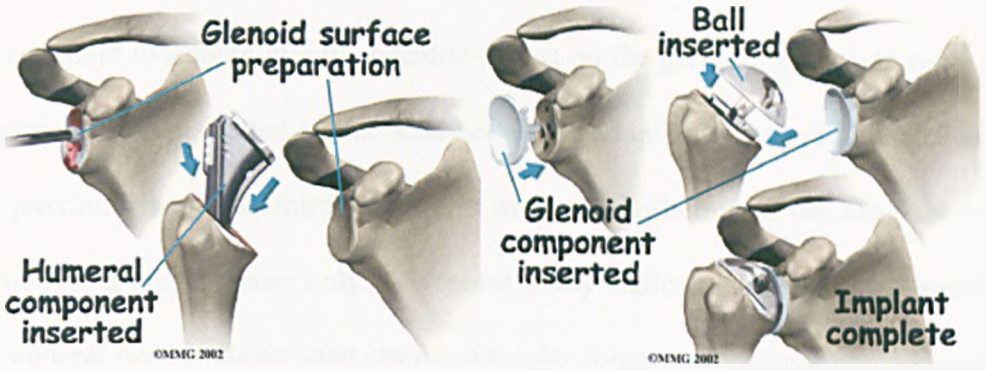

Figure 1.15 Humeral head component (Depuy, USA, (www.depuy.com)).

If the prosthetic components fail to reproduce the natural anatomic parameters, changes in the geometric centre of rotation and in the soft tissue balance of the shoulder joint may result. Furthermore, impingement of the prosthetic components may lead to pain and limited range of motion. Increasing the height of the humeral head component in comparison to the natural head may decrease range of motion by placing excessive tension on the soft tissues, predisposing them to rupture [105], (Figure 1.16).

Failure to respect the natural neck shaft angle or the medial offset of the humeral head (coronal plane) may result in subacromial (if the prosthetic head is too high) or glenoid impingement (if the prosthetic head is too low). Failure to respect the natural retroversion angle or the posterior offset of the humeral head (axial plane) can lead to impingement of the uncovered metaphysis against the glenoid [106] or to glenohumeral instability. Although malalignment of the humeral head and

changes in the soft tissue balance may theoretically lead to changes in the joint reaction forces and to changes in the joint articulating pressure distribution, there is still a lack of biomechanical studies in this field. The tendency of prosthetic systems to displace the centre of rotation superiorly and laterally in the coronal plane was observed by Pearl et al.[107]. This, in turn, might increase the chances of polyethylene wear or glenoid loosening due to eccentric forces on the glenoid. However, none of the prosthetic systems tested in that study could be adapted to the variable anatomy of the proximal humerus (third-generation design). Furthermore, the analysis was performed in a single plane only. A recent study indicates that an anatomically based humeral head induces bone stress, muscular forces and contact pressures that may be more similar to the values of an original humeral head [100].

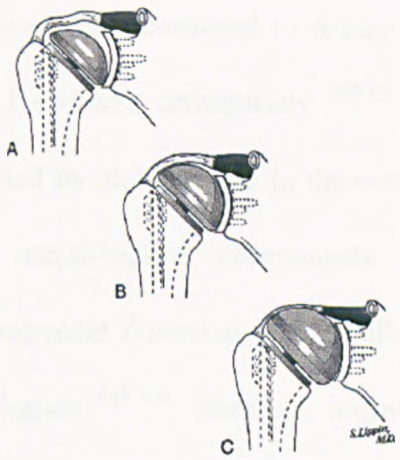

Figure 1.16 a–c A smaller head makes soft tissues less tight and may lead to increased translation, instability, internal impingement, and decreased range of motion. B. Correct size of the humeral head component. C. A large humeral head size will increase tension in the soft tissues, as lateralization of the centre of rotation takes place. This may lead to eccentric glenoid loading and may put too much tension on the soft tissues, which could lead to a decrease in glenohumeral motion and translation and rupture of the soft tissues (With permission from Frederick A. Matsen, III, M.D: The shoulder, 1998).

The optimal length of the humeral stem has been suggested as six times the diameter of the humerus [108]. This length should allow for diffusion of stresses over a broad surface while permitting the exchange of bone resorption and formation at the bone–prosthesis interface. The benefit of some degree of micromotion at the fibrous interface of a press fit or the cement mantle has been emphasized, as this should compensate for the differences in the rigidity between the implant and the bone [108].

1.5.2.2 Glenoid component

The stresses generated in the polyethylene were of low level for all of the glenoid component designs. Numerous different all-polyethylene or metal-backed glenoid component designs, with keel- or peg- shaped backings, fixated either with or without cement, have been introduced to reduce the high glenoid component's loosening rate in total shoulder arthroplasty [109-111]. However, cemented glenoid components are restricted by high stresses in the cement layer [112] and osteolysis [113], whereas cementless metal-backed components show problems with rapid polyethylene wear, component dissociation and pullout of the screws used in some designs for implant fixation [114-116], therefore, improvement of glenoid component design is still an important task. Many glenoid component fixation methods are available; they may be broadly classified as keeled, pegged, and uncemented. Keeled designs have tapered fin of approximately rectangular cross section, whereas pegged designs have several circular pegs of various lengths and configurations that insert into the glenoid. Both designs are intended for cemented fixation. Figure 1.17 shows the three types of glenoid components.

Reducing the glenoid component loosening still remains a significant challenge in the design of prosthetic components. Specific issues need to be considered in glenoid component design, include materials, geometry: including radius of curvature, surface area of articulation, component thickness and fixation. The main reason for total shoulder arthroplasties are performed to relieve pain caused by the various causes of arthritis. The diseases cause extensive changes in bone shape and material properties. Since the stresses that occur at the cement/bone interface and the strength of this interface itself, depend on the properties of the underlying bone, it can be argued that different prosthesis designs should be used for different disease states depending on bone quality [117]. However, Gupta et al [109] analysed both cemented and uncemented designs by FEM and found that, because cemented prostheses have high cement fixation stresses, cementless prostheses were predicted to have better outcome than cemented prosthesis. Three studies analysed the consequences of reduced bone quality for prosthesis fixation, and predicted that pegged prostheses are best in normal bone while keeled prostheses are best in rheumatoid arthritis bone [109, 118]. This may be attributed to the material property distribution within the glenoid vault in relation to the anchorage type and position. More specifically, the positioning of the pegs compared with the centre keel may result in each design deriving its support from different regions of glenoid bone, resulting in alternative levels of stability (ie, different levels of "warp" or "wobble" of the component)[119].

(a)

(b)

Figure 1.17 (a) Keel and peg components. (b) The Copeland Mark-2 cementless surface replacement; humeral and glenoid components,[120].

The optimal keel design would use a large portion of the glenoid fossa to achieve stability through increased cancellous bone contact. The strength and rigidity of this cancellous bone increase laterally, within 2 to 5 mm of the cortical wall [94]. In addition, a substantial load-bearing function of the surrounding cortical bone of the glenoid fossa has been recommended [88, 121], therefore, fixation extending near or to the cortical wall should be advantageous. Increasing the depth of the keel does not result in improved stability when relying on cancellous bone support only. Cement also offers improved fixation by integrating the keel into the dense cancellous bone within several millimetres of the cortex and allowing a more even distribution of stresses at the interface. Screw fixation may be more reliable in the short term with regard to minimizing implant micromotion [11].

The peg-shaped anchorage systems provide greater stability against shear forces. Anglin et al [111] showed better loosening performance in pegged versus keeled

designs. Lazarus et al [122] evaluated the radiographic outcomes of cemented pegged versus cemented keeled glenoid components in total shoulder arthroplasty. They concluded that radiolucencies at the cement-bone interface and incomplete component seating occurred more frequently with keeled components than pegged components. Wirth et al [123] compared a pegged component with a central specialized cementless peg versus cemented keeled components in a canine model. They found the histology and radiographs for the keeled design supported the conclusion that the implant was not well integrated into the bone. The pegged design allowed a more "biologic" fixation between the implant's central peg and bone. The pegged glenoids demonstrated excellent osseous integration and adaptation and increased bone density [122]. Qualitative studies have evaluated the influence of fixation peg design on implant stability [123]. The parameters included the number and size of the fixation pegs, as well as the aspect ratio (length/diameter). Five peg geometries of various shapes and sizes were tested for shear stability. The results suggested that components with multiple small pegs create a homogeneous stress distribution in the anchoring material and provide more shear stability per unit volume than implants with fewer but larger pegs [124]. Fixation of the glenoid component is an important issue in the outcome of the total shoulder arthroplasty. The main reason of the glenoid component failure is the off-centre loading known as the rocking-horse phenomenon. The articular shapes of the humeral and glenoid components in total shoulder arthroplasty affect the loading, translation, and contact stresses in the joint, thereby affecting stability, glenoid loosening, and wear. The main complications after this treatment are shoulder subluxation and dislocation, these complications are influenced by patient characteristics, design of the prostheses, and surgical factors [125].The rocking was tested by loading the superior

and inferior rim of the glenoid cyclically. This was tested using a bi-axial apparatus: the humeral head was compressed horizontally in to the glenoid at a constant load, 750±5 N [111]. To reduce the glenoid loosening a non-constrained, non-conforming, pegged design with a macrostructure on the cemented surface would be an advantage [111]. The tilting moment of the glenoid component is a result of humeral head translations in the superior and lateral direction causing eccentric joint-contact forces acting on the glenoid component. This tilting damages the underlying bone and cement structure, which leads to component loosening,[126]. Non-conformity leads to increased stresses at the glenoid component-cement interface [127]. This may lead to strain that are greater than the yield strength of the polyethylene, resulting in a higher risk of wear and subsurface cracks leading to fatigue [128] and subsequent radiolucent lines. Two significant problems of total shoulder replacements are loosening of cemented glenoid components and wear of polyethylene inlays of uncemented, metal-backed glenoid components [129].

Many studied have investigated the effect of glenoid component design on its fixation by cyclic loading. The component was fixed in to bone substitutes compressed against the humeral head. In these studies, humeral head displacements were applied [28, 126]. Oosterom et al.[126] found higher articular conformity (smaller glenoid component radius of curvature) decreased glenoid component tilting, which might be an advantage for component fixation.

A glenoid component inserted with an increased inclination angle, leading to a more upward facing glenoid component, has shown increased values of the positive superior and negative inferior glenoid rim-displacement [128]. This might influence component fixation, and may increase the chance of early component loosening. However, decreasing glenoid component inclination angles, leading to

more downward facing glenoid components, allows for higher superior subluxation forces relative to the joint compression force, which increase superior shoulder stability. Therefore, a more downward facing glenoid component is preferable [129]. On the basis of the results of Walch.[130] it appears that prosthetic radius mismatch influences the glenoid radiolucency score. Theoretical advantages of peg implants over keels include less bone removal during bone preparation, greater surface area for cement contact, and a smaller volume of cement required for fixation [131]. Figure 1.18 shows two types of peg and one keel glenoid components used in shoulder arthroplasty.

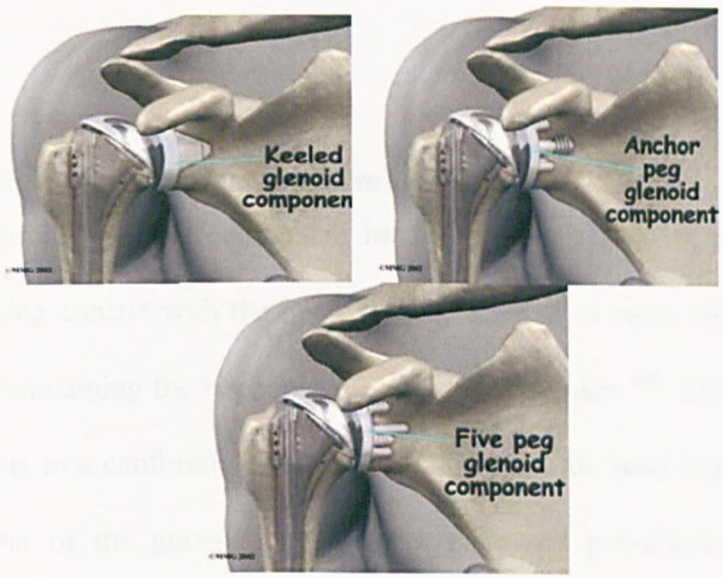

Figure 1.18 Keeled and two types of pegged glenoid components (Depuy, USA. (From: www.depuy.com)).

Collins et al. [132] demonstrated the importance of complete seating and support of the glenoid prosthesis on subchondral bone. Failure to achieve complete osseous backing for the glenoid component was associated with deforming and rocking forces at the component edge. In Lazarus et al.[113] review of the in-vivo

changes of the glenoid components; they found better component implantation was associated with both prosthesis-related and surgeon-related variables. They observed a clear trend toward improved technical outcomes for pegged components compared with keeled components. The pegged component had a more fixed geometry than a keel one, that resulted in a more precise fit to bone. In addition, the instrumentation used for the implantation of a pegged component is more exact. Finally, the smaller cement volume contained within a peg compared with a keel may cause less heat during cementing and a less risk of bone necrosis. They concluded radiolucencies at the glenoid bone-cement interface and incomplete component seating was an extremely common observation on initial postoperative radiographs.

1.5.3 Conforming versus non-conforming glenoid

A conforming glenoid component has been associated with a more stable joint by increasing contact with the head, thereby leading to more uniform contact pressures and maintaining the head in the centre of the socket [133]. However, if any translation occurs in a conforming shoulder replacement, the head immediately tips up onto the rim of the glenoid, resulting in increased polyethylene wear and deformation and inducing a "rocking horse phenomenon" (Figure 1.19) [5]. This rocking horse effect can occur in the vertical plane (in the case of cuff deficiency) and/or in the horizontal plane (in the case of anterosuperior instability). This off-centre loading is caused by migration of the humeral head, particularly superiorly, usually as a result of rotator cuff muscle tears [5, 134, 135]. Inferior migration [136] and posterior and anterior wear [134, 135] have also been associated with loosening. In some cases this has resulted in a noticeable tilt of the glenoid component [24]. A non-conforming prosthetic articulation may, on the other hand, lead to increase contact

stresses, which may exceed the material failure limit [137]. A 3mm to 4mm radial mismatch in the prosthetic shoulder has been shown to reasonably recreate normal humeral head translations [24].

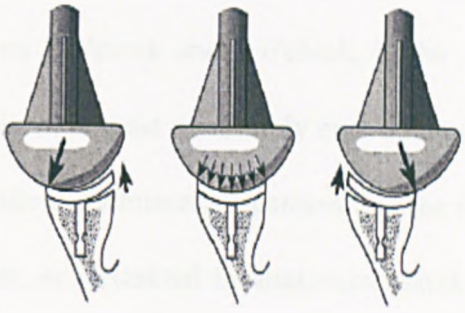

Figure 1.19 If translation occurs in a conforming shoulder replacement, the head immediately tips up onto the rim of the glenoid, causing polyethylene wear and deformation and inducing a "rocking horse phenomenon." (With permission from Frederick A. Matsen, III, M.D: The shoulder, 1998).

1.5.4 Kinematics following shoulder replacement

Prosthetic components frequently display abnormal glenohumeral kinematics [138]. This may be due to the underlying pathology (cuff-deficient shoulder), consequences in surgical technique, and to limitations imposed by the design of the prosthesis itself. In some patients, a reversed scapulo-humeral rhythm with a reduction of movement between the prosthetic components and unchanged scapulothoracic movements has even been observed [139].

1.5.5 Conclusions

Precise reconstruction of the three-dimensional structure of the proximal humerus may lead to an improved functional outcome. However, there is still a lack of biomechanical data to support this concept. The optimal design of the glenoid component remains a challenge for future research.

1.6 SOFT TISSUE RECONSTRUCTION

A sheet of fibrous tissue, which includes both the capsule and the ligaments, encloses the shoulder joint. This sheet surrounds the glenoid, except for the rotator interval, and the humerus. The inferior glenohumeral ligamentous structure inserted on the glenoid between 2 o'clock and 6 o'clock, is the zone primarily involved in anteroinferior instability, the most commonly encountered clinical problem [140]. This zone includes the middle glenohumeral ligament and the anterior band of the inferior glenohumeral ligament, as described in anatomical studies of the shoulder [27]. The kinematics analysis of the joint is made more difficult by the fact that no one ligament is taut in all positions. In the past the rotator cuff was considered the only significant stabilizer of the shoulder [66]. Research has redressed the balance by showing the importance of the ligaments [141] between the resting position (with the arm hanging at the side) and maximum scapular-plane abduction. The ligaments around the joint go from complete relaxation to a state of uniform tension [142]. Thus, the contribution to stabilization of the joint by the ligaments gradually increases throughout abduction. The rotator cuff, in turn, has a very important role to play at the start of elevation, becoming progressively less important as the movement continues [142]. Conversely, destabilization of the humeral head in rotator cuff lesions occurs chiefly at the start of abduction. In order to understand the mechanisms of instability, it is useful to consider the findings at surgery using the Bankart technique, i.e. with separation of the subscapularis from the capsule, to provide a detailed and comprehensive picture of the ligamentous lesions. This can be seen better at arthroscopy than in open bankart repair [143]. In the overwhelming majority of cases, the ligamentous apparatus will be continuous, and inserted on, or at a distance of less than 1 cm medial to, the glenoid rim. The labral lesion will vary from a

complete disappearance of the structure and bone wear, through greater or lesser detachment, to discreet surface damage. In some patients, there will be evidence of a glenoid rim fracture [144]. Lesion types were classified by different authors, and it's beyond the scope of this thesis [145-147]. In order to dislocate a shoulder, at least the anteroinferior portion of the capsuloligamentous apparatus must be rendered incompetent – they are not usually divided. In the right shoulder, the division should extend from 3 o'clock to 6 o'clock. The injury to the capsuloligamentous apparatus is not enough to cause dislocation and the rotator cuff are hardly damaged. Some authors have obtained dislocation following division of the supraspinatus tendon [148, 149]. The creation of an isolated Bankart lesion is nowadays accepted as the typical pattern in chronic instability of the shoulder. This lesion combines damage to the glenoid labrum, which may be worn, avulsed, or almost entirely destroyed, and anterior soft-tissue stripping, of varying extent (Figure 1.20). This anterior detachment has been to be usually very limited. It is doubtful that the labral lesion will lead to a major loss of stability. It is also now known that anterior lesions tend to get worse with recurrences [150]. Thus, the importance of the initial lesion may not be as great as assumed; and the real question is whether the Bankart lesion as such can account for chronic instability, has also been found to be insufficient alone for the production of shoulder instability [151]. The lesion is visible on plain radiographs but a more detailed view can be obtained through multiplanar reconstruction using CT arthrography. The bony Bankart's lesion is usually seen as a small fracture or an osteophitic deposit probably due to micro fractures, there is often a corresponding Bankart's fracture of the inferior margin of the glenoid fossa [152]. The treatment of this condition depends upon the age, sex and occupation of the patient and the disability due to the frequency of the dislocation.

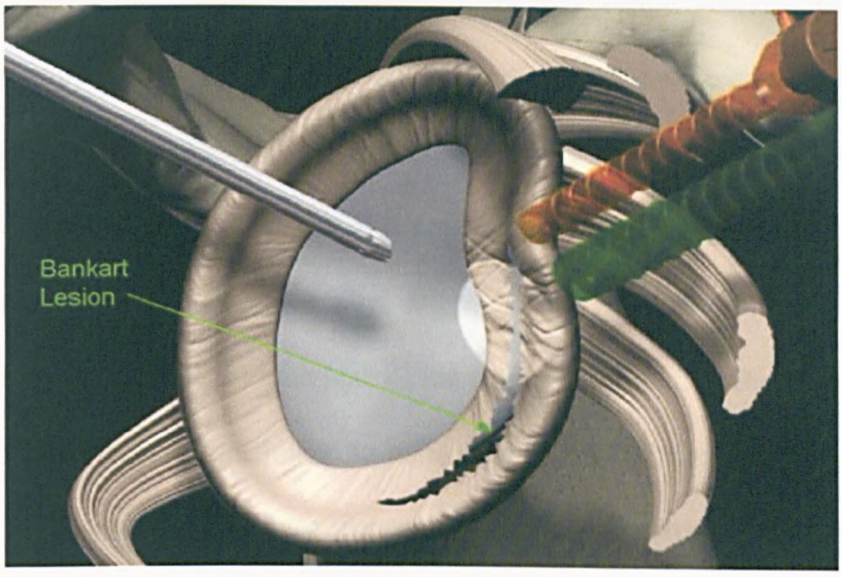

Figure 1.20 The Bankart Lesion: The anterior labrums rupture (www.shoulderdoc.co.uk)

Suture anchors are used for the reattachment of soft tissue to bone. This is especially popular in the shoulder, where the use of suture anchors has improved and simplified Bankart repairs (Figure 1.21).

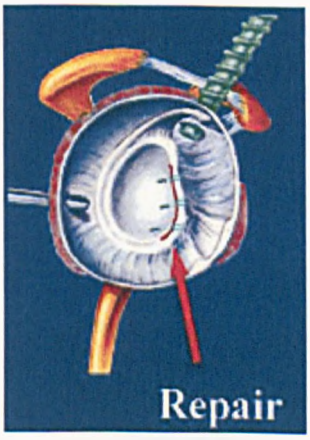

Figure 1.21 Bankart lesion repair (www.shoulderdoc.co.uk)

A number of studies have been performed to test the security of the suture anchor to bone interface by testing the anchor's pull-out strength [153-155]. These

provided information on the performance of various suture anchors at the bone interface. Suture failure has been reported to be the main source of failure in many such studies [154-159]. Abrasion of the suture during intra-operative and post-operative cyclic loading may be an important cause of suture weakening and breakage. This situation may be made worse by angulations of the rotational orientation of the anchor's eyelet with respect to the plan of the suture [160]. Suture anchors are effective implants for soft tissue reattachment to bone. The Mitek GII anchor has been widely studied in the context of shoulder surgery, being inserted through drill holes at the glenoid margin into underlying cancellous bone (Figure 1.22). Clinical studies have shown it to be effective for instability repairs whilst in vitro pull out tests have shown that it is often the suture material that fails under extreme loading conditions and this could be the weakest link in the system [160, 161]. The strength of the cancellous bone of the glenoid is an important factor in Mitek GII suture anchor failure because the anchor is inserted deeply in the bone for fixation. There has been substantial experience in the implantation of two or more anchors in the middle and inferior anterior glenoid as a method for reattachment of the labrum to the bone [162]. Movement of the anchor within the cancellous bone, after insertion, may affect the tension of the repair [163].

Figure 1.22 Mitek GII™ anchor (Depuy, USA. (From:www.depuy.com)).

Avulsion of the anteroinferior capsulolaberal complex of the shoulder from the anterior rim of the glenoid is referred to as a Bankart lesion. Bankart is the essential lesion of recurrent shoulder instability [164]. The use of suture anchors in the repair of Bankart lesions in shoulder joint instability is widespread. Techniques for both open [164] and arthroscopic repairs [165] have been described using suture anchors. The suture anchors have the ability to secure the labrum and capsule to the glenoid after anatomical reduction, and eliminating the need to drill tunnels through the glenoid. The barbs of the GII lock the anchors within the bone. According to the manufacturer (Depuy, USA), pulling the GII anchor back after insertion with a load of about 40 N is recommended to set the anchor and to lock the barbs.

Clinical studies have shown it to be effective for instability repairs, whilst in vitro pull out tests have shown that it is often the suture material that fails under extreme loading conditions and this could be the weakest link in the system. The cancellous bone of the glenoid is an important consideration in Mitek GII™ suture anchor failure because the anchor is inserted deeply in the bone for fixation. There has been substantial experience in the implantation of two or more anchors in the middle and inferior anterior glenoid as a method for reattachment of the labrum to the bone [165]. In successful shoulder reconstruction, the relationship of anatomic factors to anchor placement determines the anchor's failure properties to a high degree [166]. Fatigue properties of suture anchors must also be considered when assessing the minimum number of anchors required. During postoperative exercises, the suture anchor is subjected to repeated submaximal loads. Thus, the load needed to failure is lower after cyclical use, and may eventually lead to anchor failure or pullout [166]. Attempts to measure the pullout strength under laboratory conditions have been slightly limited by the fact that often the suture material used with the

anchor fails before pullout occurs. The pullout strengths of several soft tissue devices (suture anchors) have been examined in surrogate shoulder models [167] or in a cadaveric proximal tibia model. These models, however, do not accurately represent the clinical context of these devices. In successful shoulder reconstruction, the relationship of anatomic factors to anchor placement determines the anchor's failure properties to a high degree [164]. Fatigue properties of suture anchors must also be considered when assessing the minimum number of anchors required. During postoperative exercises, the suture anchor is subjected to repeated submaximal loads. This load reduces the fixation strength of the anchors and may eventually lead to anchor failure [164]. Attempts to measure the pullout strength under laboratory conditions have been limited by the fact that often the suture material used with the anchor fails before pullout occurs.

1.7 BONE SUBSTITUTE FOR PROSTHESIS FIXATION

Trabecular bone analogues have been used for shoulder arthroplasty simulation. This novel method is presented as a bone substitute called sawbones (Sawbones, Sweden). Sawbones is used to simulate the mechanical properties of the glenoid bone [168-170]. These material properties are similar to the strength and elastic modulus of human glenoid cancellous bone and considered to be an appropriate model of the bone stock. Figure 1.23 shows the microscopic image of an open-cell sawbones structure.

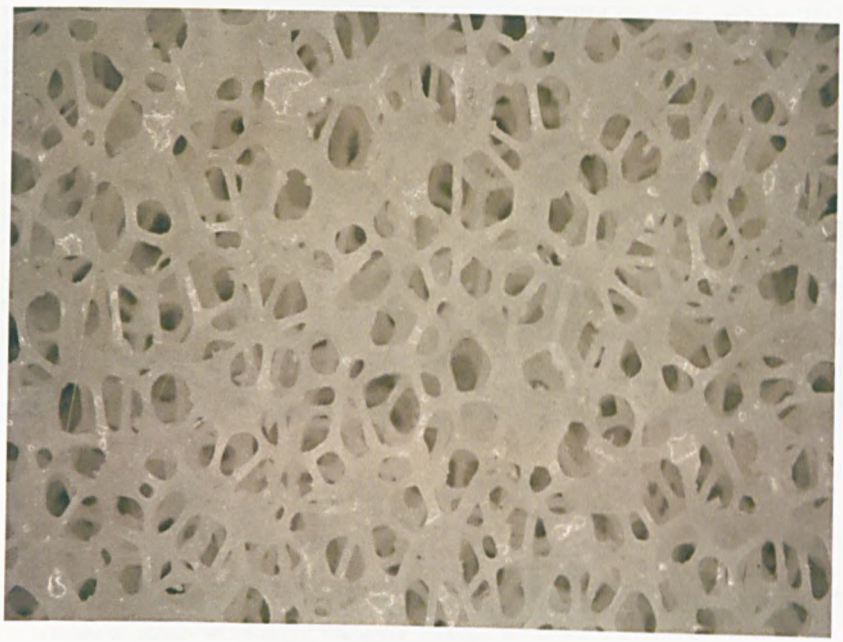

Figure 1.23 The open-cell foam sawbones microscopic image.

Different studies have investigated the effect of glenoid component designs upon the forces required to generate complete subluxation of the humeral head. The prostheses were mounted within close cell polyurethane block (Figure 1.24), which had similar material properties to those of the glenoid cancellouse bone [139, 169, 170]. Limitations of these in vitro studies include the use of polyurethane foam to simulate the morphological characteristics (closed pore) of the glenoid bone and the application of relatively few loading cycles to simulate shoulder mechanics during activity. The cement penetration could not be tested with close cell foam. The foam was selected, in accordance with ASTM standards [171], to represent glenoid bone quality. However, there is wide variation in the mechanical properties of human glenoid bone and these *in vitro* test results may not fully reflect base plate fixation in all shoulder arthroplasty patients.

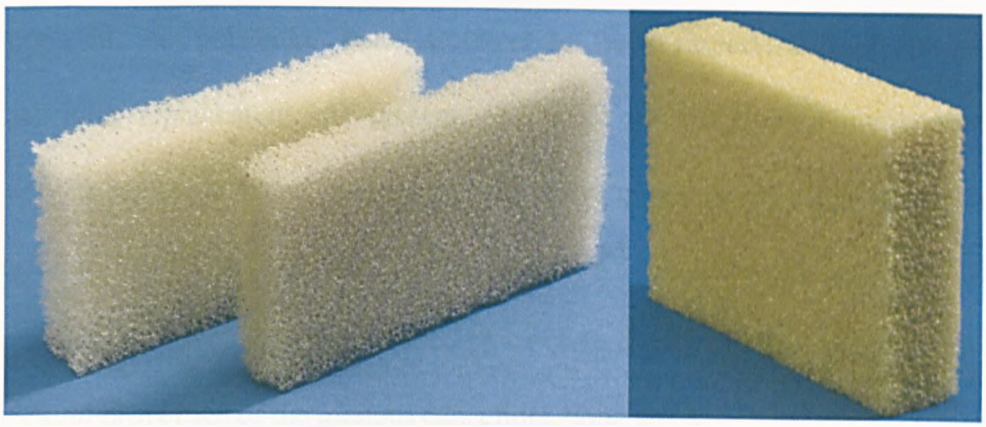

(a) (b)

Figure 1.24 (a). Open cell foam block. (b) Close cell polyurethane block. (Sawbones, Sweden. (From: www.sawbones.com))

1.8 SUMMARY

Prosthetic replacement arthroplasty for the glenohumeral joint is a well-developed and well-described technique with good to excellent results. The surgeon is faced with many decisions to make, however, regarding choice of implant, implant fixation, soft tissue management, and options for glenoid resurfacing. In general, when the precise cause of the arthritic condition is identified, the choices become more straightforward. Similarly, for advanced rheumatoid arthritis in patients with an intact rotator cuff, a total shoulder arthroplasty results in the best pain relief. If the rotator cuff is deficient and irreparable, an anatomically sized humeral head replacement is appropriate, taking care to preserve the coracoacromial arch. Acute, nonreconstructible fractures of the proximal humerus are treated best with a humeral head replacement. The anatomic studies have provided general descriptions of the glenoid and its cancellous bone structure. Like other joints, the mechanical stress and adaptional conditions of the minimally constrained glenohumeral joint are reflected in the architecture of the subchondral plate and the cancellous bone.

Variations in the trabecular bone architecture have important implications in artificial joint replacement. At present, loosening of the glenoid component is potentially a major problem in total shoulder arthroplasty and loosening has been assigned to failure at the cancellous interface. Advances in shoulder joint replacement, therefore, have necessitated research to characterise the mechanical and architectural properties of the glenoid cancellous bone stock.

Restoring the anatomic position and securing a torn superior labrum or Bankart lesion to its bony bed on the superior or anterior glenoid is the objective in surgical repair. The mechanical performance of bone anchors depends on the loading mode. Although most studies use a single pull to ultimate load at failure, cyclic loading more closely duplicates the submaximal loading activities of post-surgical rehabilitation. Cadavers of different ages would likely have different holding strengths. Furthermore, there would also be expected differences in holding strength depending on location within specific bone.

1.9 AIM AND OBJECTIVES

The aim of this research is to study the mechanical properties of cancellous bone throughout the glenoid and to determine its effect on the fixation of the glenoid component. The motivation was to select an appropriate cadaveric bone to determine the regions of the stronger and deeper bone location for prosthetic fixation. The objective of this study was to investigate the relationship between the mechanical properties of the glenoid surface and both the trabecular bone volume fraction of underlying bone and the subchondral thickness of the glenoid surface. Both of these factors are predicted to affect the local strength and stiffness of the bone in the glenoid fossa. MicroCT technology is used in 3D imaging the glenoid. A computing

environment (IDL) for the interactive analysis and visualization the 3D data is used to determine the glenoid subchondral thickness.

The second objective was to simulate the glenoid fixation prostheses in a bone substitute (sawbones) to investigate the component loosening and failure.

The third objective of this study was to investigate the pullout strength and the fatigue properties of Mitek GII™ anchors when loaded with Orthocord™, a novel suture material with greater reported tensile strength than suture material used in previous pullout studies. Additionally we aim to measure bone mineral density at the precise location of anchor insertion using microCT to determine if this affects the pattern of failure or ultimate pullout strength.

2 Materials and Methods

2.1 INTRODUCTION

Shoulder arthroplasty has been used as a successful surgical intervention in patients suffering from shoulder arthritis since the 1960s. It is designed to replace the diseased joint and provide enhanced functionality so as to improve the quality of life of the patient. Loosening of the glenoid component, however, is a significant long-term complication in total shoulder arthroplasty [172-174]. The loosening process is multifactorial, with a number of contributory factors that encompass both mechanical and biological attributes. These factors include the amount of cement used in glenoid fixation [175], the risk of thermal injury to bone [176], eccentric loading of the glenoid component due to translation of the humeral head [177] and poor cementing technique [178]. One of the critical parameters in successful glenoid component fixation, as well as tissue re-attachment is the quality of the underlying bone including both architecture and the degree of mineralization. Thus, knowledge of the bone properties together with their spatial variation are of great importance in deducing the most appropriate design that allows for effective fixation or re-attachment.

A number of methods are available for investigating the mechanical properties and bone architecture in the glenoid [82, 179-182]. In terms of the former, indentation testing has been used previously to determine regional changes in the mechanical properties of the glenoid surface [30], whilst histological or microCT techniques have been used to deduce bone morphology [183, 184]. However, there has

been little published material that relates mechanical properties to the quality or structure of the surrounding bone.

This chapter gives detailed descriptions of the materials and methods employed in the experimental part of the study. The first section describes the methods used to scan the cadaveric glenoid in the laboratory. The second section determines the mechanical properties of the glenoid, as acquired by tensile testing, followed by glenoid component simulation. The tools developed for data acquisition and analysis of the results, including the statistical methods employed, are described. The final section outlines the tool developed to test the pullout strength of the suture anchors used clinically to reattach labral tissue to the glenoid.

2.1.1 Preparation of the specimens

19 embalmed and 6 fresh scapulae were harvested from cadavers that were donated to the Department of Anatomy, which were embalmed, or from the newly formed GIFT tissue bank at the University of Leeds that were fresh but stored frozen. An ethical approval was obtatined for testing the cadaveric bones. In the case of the embalmed specimens there was no macroscopic evidence of structural or degenerative change in the rotator cuff or articular surfaces of the shoulder. In all specimens soft tissues and muscle attachments were removed from the acromion and coracoid processes by sharp dissection, as was the glenoid labrum, to leave the bony glenoid fossa with its articular cartilage intact. Embalming was achieved by the arterial method, using pre-embalming fluid with blood clot disperser and cell conditioner to remove blood clots and allow complete drainage of blood. The articular cartilage was carefully removed by immersing the glenoid fossa in a

solution of Papain (crude dried papaya latex, Sigma-Aldrich, Stenheim Germany) at 40°C for 6 to 8 weeks: the cartilage surface was scored to facilitate penetration of the Papain and aid cartilage disintegration and removal. Anglin et al [30] have previously indicated that embalming had minimal impact on the mechanical properties of bone used for indentation testing [185].

Nineteen embalmed glenoids were tested including both the right and left shoulder, and both sex specimens (Table 2.1). The average age was 82 and the majority were female. The glenoid were resected from the scapula to fit in to a 76mm/74mm outer/inner diameter and 85mm height microCT holder for scanning (Figure 2.1). Six fresh frozen glenoids are also tested, including both right and left shoulders. The cadavers where defrosted at room temperature prior to any mechanical testing. The cartilage and the labrum were removed carefully using a surgical scalpel.

Table 2.1 Details of the embalmed glenoid specimens

Glenoid	Age	Sex	Shoulder
G03/02	69	F	R
G17/01	91	M	R
G7/02	63	F	L
G22/02	72	F	R
G32/02	70	F	L
G22/02	72	F	L
G24/02	80	F	L
G43/01	82	F	L
G7/02	63	F	R
G28/02	73	F	L
G47/01	82	F	L
G36/01	87	F	R
G43/01	82	F	R
G28/01	90	F	R
G1/02	90	F	L
G15/02	88	M	L
G24/02	80	F	R
GUNM4	80	F	R
GNO.NU	89	M	R

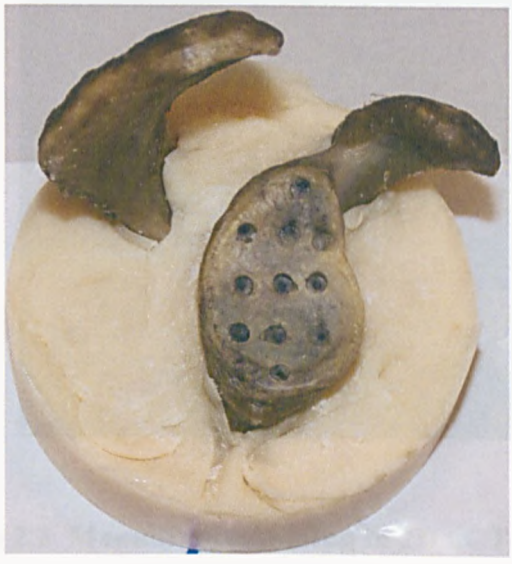

Figure 2.1 Glenoid resected to fit in the microCT holder

2.1.2 Scanning protocol

To determine the morphological characteristics of the specimens a microCT 80 scanner (Scanco Medical GmbH, Rassersdorf, Switzerland) was used. MicroCT allowed non-invasive glenoid scanning without damage to the specimen. Serial images were obtained along an axis orthogonal to the joint surface with an isotropic voxel. The Scanco software included with the MicroCT system was used to perform all subsequent image processing and analysis. A semi-automatic contouring method was used to select a volume of interest in the 2D image. The resulting image was then segmented using a low-pass Gaussian filter to remove noise, and a fixed threshold to extract the mineralized bone phase as described in previous studies [186, 187]. The threshold was often determined visually (Figure 2.2) [186]. The resolution used was 76 μm, allowing the observation of all but the most slender trabeculae.

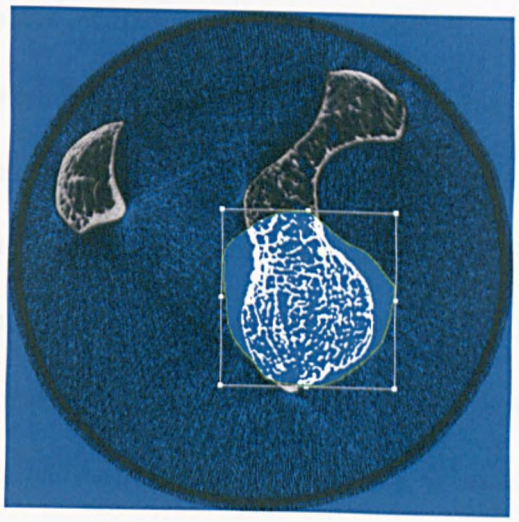

Figure 2.2 Manual thresholding in 2D uCT image.

The test profile used as follows: effective energy E (kVp) 70, intensity I (μA) 170, standard resolution (250 projections with 1024 samples each, 1024 x 1024 pixels). Figure 2.3 displays a section through a three dimensional representation of the glenoid bone architecture.

Figure 2.3 3D MicroCT image of the glenoid bone architecture.

The trabecular bone of the glenoid was digitally separated from its subchondral shell by manually outlining the contour of the cortical-cancellous boundary in each specimen. Morphological parameters of the cancellous bone could then be independently calculated using a cylindrical sub-volume of the original object imaged, referred as the volume of interest (VOI). Morphometric parameters are calculated by CT-analyser either in 3D based on a volume model, or in 2D from cross sectional images (individually or integrated over a volume-of-interest). Total volume of the volume-of-interest measured in 3D [188].

2.1.3 Subchondral bone thickness measurement

Clearly, subchondral bone thickness of the glenoid will have an impact on the biomechanical aspects of fixation as well load transfer. In the design of prostheses, the subchondral bone thickness profile is necessary for the optimization of the performance of these devices since load transfer should be through those sections that are thickest and presumably strongest. As an example, recent evidence from vertebral compression fractures in the elderly has noted that fractures occur in the cranial endplate more than the caudal one and that this maybe a result of the thinner subchondral bone in this region [189, 190]. Further, it has been suggested that the problem of mechanical loosening of the glenoid is related to a significant degree to geometrical factors of the prosthetic device and the bone structure. Such problems as mechanical loosening can be reduced significantly by optimizing the combined load carrying ability of bone and prosthesis by modifying the geometry of the device in conjunction with bone thickness in regions under consideration [191]. In addition, the diagnosis of advanced osteoporosis is partly based on changes in subchondral bone thickness [191]. Thus, an accurate measurement of subchondral bone thickness in

the human glenoid could be very important clinically. In this study, the subchondral bone thickness in nineteen embalmed human cadavers was measured after indentation test was performed, to enable identifying the exact indented zones.

Following the indentation test the specimens were scanned by a microCT and the 3D reconstructed images were used to measure the subchondral thickness. Three dimensional images in this plane allowed measurement of subchondral thickness at either side of the indentation site. By spinning this plane through ninety degrees around the axis of the indentation channel a second set of two measurements could be obtained so that the subchondral thickness adjacent to the hole at four equally separated points could be measured (Figure 2.4). The subchondral thickness was measured manually at each of these four points by converting the number of scaled pixels into millimetres using a high level image processing language IDL (RSI, USA) to reconstruct 3D visualization.

Figure 2.4 Subchondral thicknesses: measuring each hole in two planes.

This measurement was undertaken for each of the indentation holes. To validate our data from the microCT, we measured three of the specimens with two other techniques (digital callipers and shadowgraph instrument) by cutting the specimen in the middle of the indented holes (Figure 2.5).

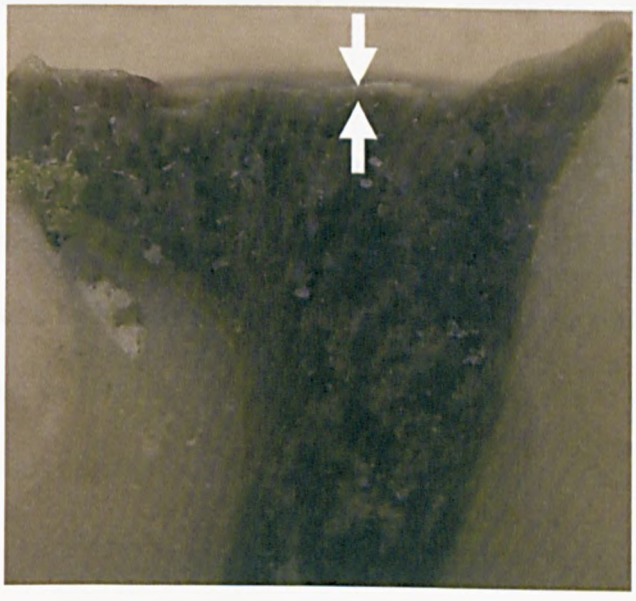

Figure 2.5 Glenoid cadaver's subchondral thickness.

2.1.4 Quantitative measurement

Bone mineral density, geometry of bone and microstructure of bone are the bone properties that determine bone quality, namely strength as defined by the bone's ability to withstand loading. Bone volume fraction is an important parameter that is often used to describe trabecular microstructure, and can be calculated from voxel based three-dimensional reconstructions of microCT images [192-194]. The variations in bone volume fraction can be used as a surrogate for the changes in apparent bone density if we assume the level of mineralisation is relatively constant. For each deformation zone which was generated during indentation (see page 58), a

volume of interest (VOI) was chosen immediately below this position with a volume of 63 mm^3, (Figure 2.6). For each VOI the bone volume fraction (BV/TV)was determined. Bone volume fraction has been shown a significant influence on the mechanical properties of bone [195, 196]. The degree of anisotropy for the same volume of interest was measured from the 3D reconstructed images of the microCT. Quantitative structural analysis has revealed different degrees of anisotropy within the glenoid cancellous bone [82].

The bone volume fraction, the bone mineral density, and the degree of anisotropy of the fresh bones were obtained from the microCT 3D reconstructed images, using the same technique used for the embalmed specimens. Bone mineral density was available for this part of the study due to an upgrade of the microCT during the course of this project.

Figure 2.6 VOI on a 2D microCT image of the glenoid bone.

After scanning, the 3D data sets were segmented by using one unique threshold throughout the test. The threshold of each data set was determined using a manual threshold and also compared to an adaptive threshold method, where the gray-level data set is segmented at different levels. The threshold where the volume fraction changes the least, the steepest gradient of gray levels, is chosen as the threshold for the data set [197]. After segmentation, the BV/TV and the DA (Degree of Anisotropy) measurements were carried using a cylindrical VOI. The mean threshold was chosen 90 and the BV/TV and the DA were calculated from the segmented 3D data [198, 199]. The degree to which the local properties of a material depend on its directional variation is referred to as structural anisotropy. Three-dimensional images enable the direct assessment of metric indices by actually measuring distances in the 3D space. All data were collected from nineteen scan and the mean values were used and correlated to the subchondral thickness and the mechanical properties of the glenoid surface. The same procedure was carried out for the six fresh glenoids too, but with the additional BMD values being determined for each VOI.

2.1.5 Summary

This section of this chapter has presented the scanning protocol and the specimen used for the morphological analysis and the technique to assess the bone volume fraction and the trabecular bone structure. MicroCT techniques have the potential to reveal greater detail about the functional structure of the trabecular bone than previously known. To our knowledge, high-resolution microCT images have not yet been used to demonstrate structural variations in trabecular bone architecture of the glenoid and using these data to correlate with the mechanical parameters.

2.2 DETERMINATION OF THE MECHANICAL PROPERTIES OF THE GLENOID

The shoulder arthroplasty function depends on some important factors, including; bone structural integrity, which is governed by tissue density, architecture, and mechanical properties. Although the mechanical properties of the glenoid cancellous bone have been studied [30], and uCT imaging has lately enabled investigation of the relationship between architecture and structural properties in cancellous bone in small samples [200, 201], little is known about the behaviour specific to the glenoid. Mechanical characterization of bone at a localized level can provide additional insights those regions that might provide the strongest bone for component fixation. This must be weighed against have a degree of porosity available to allow interdigitation. Several methods have been used in the literature for identifying the elastic modulus of bone, such as mechanical testing, combinations of CT-scan and finite element modelling, and ultrasonography [202, 203]. In this study we determined elastic moduli and strength of bone of the glenoid surface obtained from glenoid cadavers by indentation test. Indentation testing has increasingly being used to assess the mechanical properties of bone surfaces [30, 83].

2.2.1 Design of the equipment and specimen mounting

All 25 cadaveric glenoid were used of which 19 were embalmed and 6 were fresh frozen. These specimens were the same as those used for morphological analysis described in section 2.1. The structural properties of the glenoid surface were tested using an indentation technique based on that previously used by Anglin et al [30]. In our study a 2.95 mm a flat cylindrical indentor was attached to a tensile testing machine (Shimadzu Autograph, Tokyo, Japan) with 10 kN load cell, that

penetrated the glenoid bone at predetermined positions on a grid of 11 pre-selected points (Figure 2.7). The location of the test sites were mapped in relation to proportional positions along the glenoid width in order to standardize the results, by 15% of the superior–inferior (SI) length (approximately 5 mm). This ensured no effect between adjacent holes [30]. The specimens were mounted in a polymethylmethacrylate (PMMA) mould that itself was located on an angle jig that could be adjusted to ensure that the indentor was positioned normal to the surface for all test measurements, regardless of surface curvature (Figure 2.8).

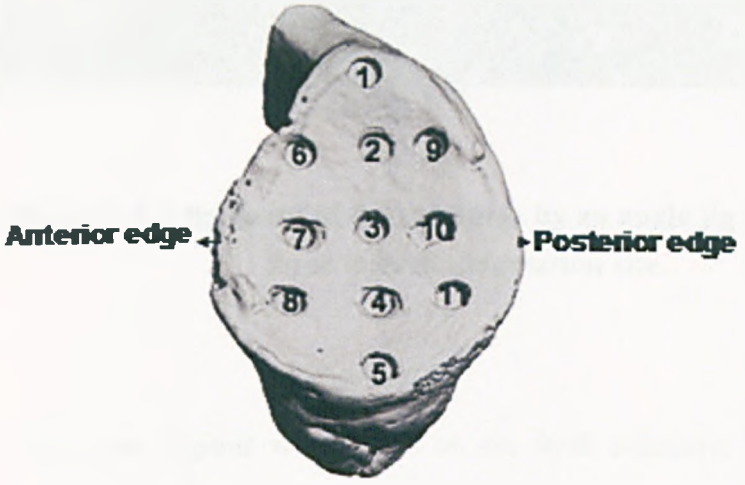

Figure 2.7 Pre-selected indentation points on the glenoid surface. Position of the points was selected relative to the maximum width and height of the glenoid.

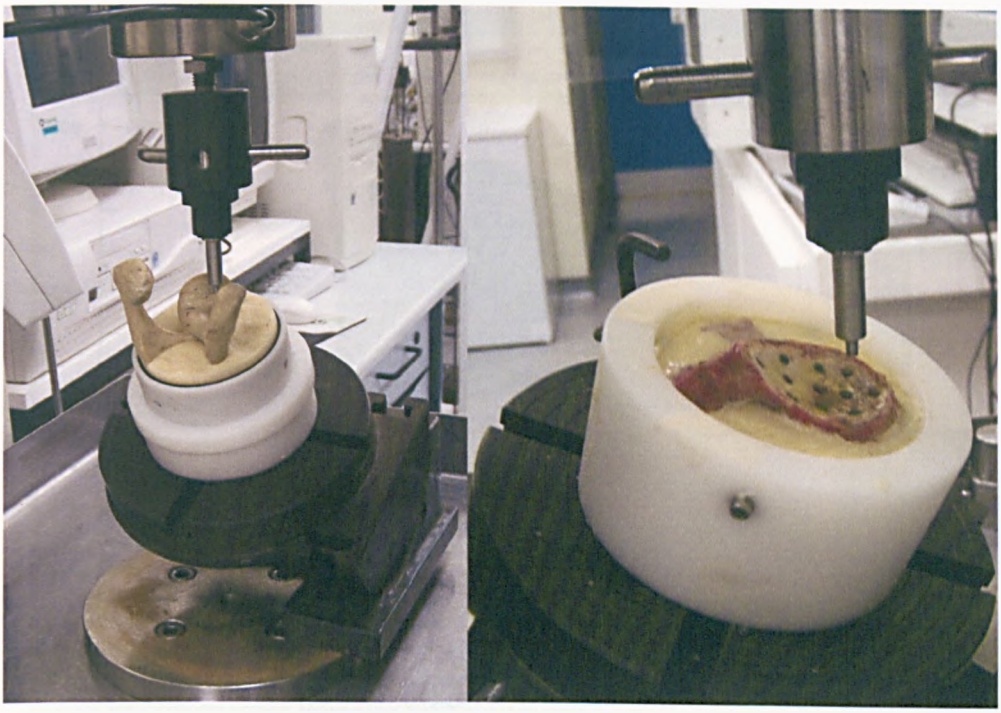

Figure 2.8 Alignment of the specimen by an angle jig to obtain a normal force to each indentation site.

The same regions were tested on six fresh cadaveric bones and the same alignment and angle jig was used to ensure the load was applied normal to each region. The subchondral thickness of the fresh bone was measured from the 3D reconstructed images of the microCT. This measurement was carried out using the same procedure for the embalmed bone, which was later compared to the subchondral thickness of the embalmed specimens (Figure 2.9).

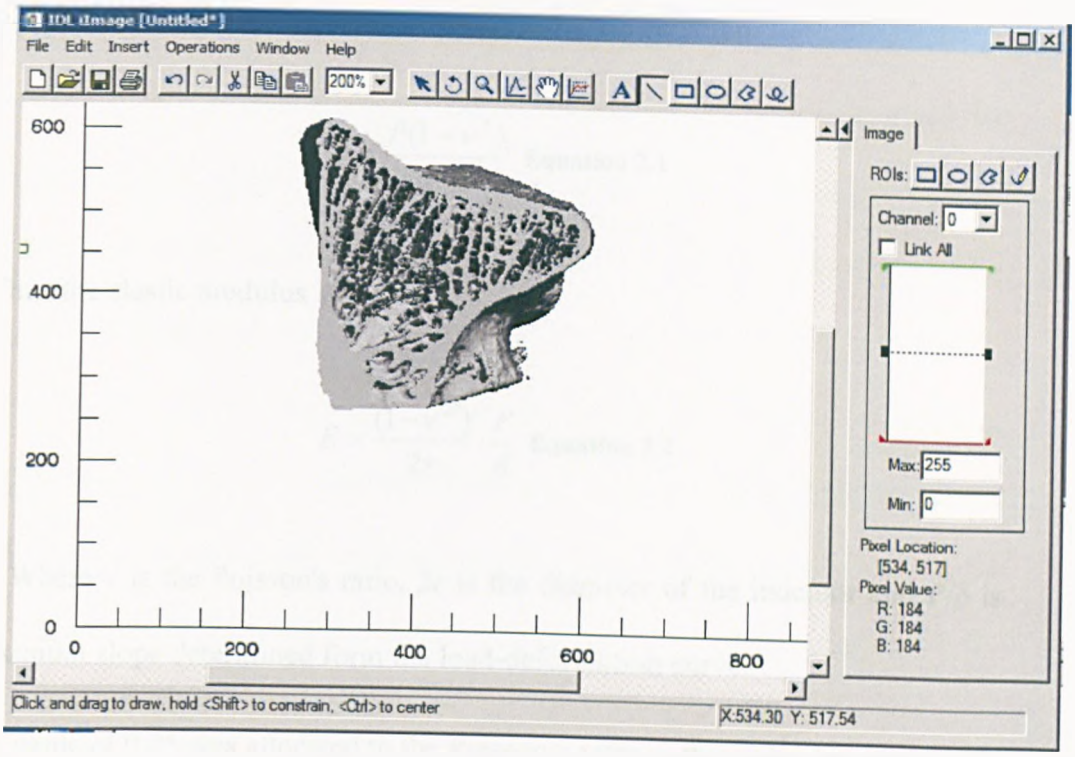

Figure 2.9 The subchondral thickness of the fresh bone measured by IDL.

2.2.2 Loading protocol

Indentation was performed at rate of 2mm/min in to a depth of 3mm from the initial point of the contact with the glenoid surface. The indentation process was continually monitored, allowing the derivation of a load-deformation curve. The strength of the bone for each indentation site was calculated as the failure load divided by the area of the indentor [30]. The failure load was chosen as the peak region on the load deformation curve, (Figure 2.10). The modulus was calculated using equation 1.4 [204], which has previously used in these types of experiment [30].

The displacement of the indentor is given by the equation:

$$\delta = \frac{P(1-\nu^2)}{2rE} \quad \textbf{Equation 2.1}$$

Thus the elastic modulus is:

$$E = \frac{(1-\nu^2)}{2r} \cdot \frac{P}{\delta} \quad \textbf{Equation 2.2}$$

Where ν is the Poisson's ratio, $2r$ is the diameter of the indentor and P/δ is the maximum slope determined form the load-deformation curve.

A value of 0.25 was allocated to the Poisson's ratio as this value has previously been used in this type of study [30, 205].

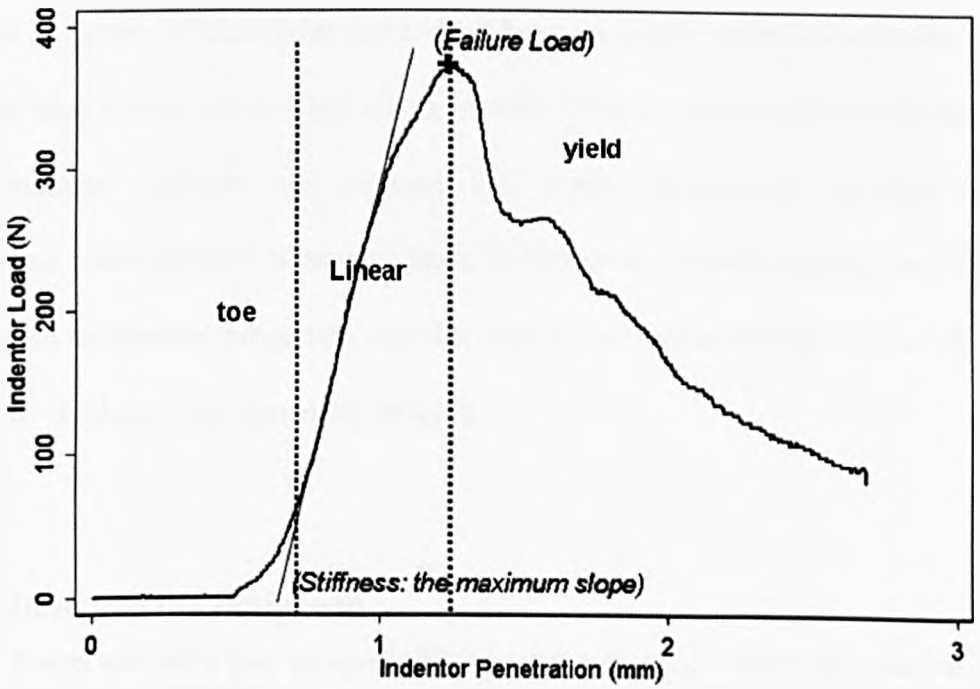

Figure 2.10 The load-deformation behaviour for a typical indentation test. The elastic modulus was determined from the steepest portion of the rising curve whilst the strength from the max load sustained by the bone.

2.3 GLENOID COMPONENT FIXATION SIMULATION

Loosening of the glenoid component is a common mode of failure in total shoulder arthroplasty. Clinical and radiographic observations show that loosening generally occurs at the bone-cement interface. The incidence of radiolucent lines surrounding the glenoid prosthesis has been reported in many studies. Loosening is characterized by bone resorption and interfacial micromotion, depends on the state of the underlying bone quality, the implant design, the surgical technique, as well as the condition of rotator cuff muscular system. The normal glenohumeral joint reaction force ranges from 370 to 2070N depending on daily activities [28, 206, 207]. Anterior or posterior eccentric loading of the glenoid component can contribute a "rocking horse" effect that may initiate component loosening. The following section will investigate component loosening simulation on a bone substitute material. The material properties of cancellous and cortical bone are highly variable, depending on both the bone mineral density and microstructure. To allow producible test results, a bone analogue material was selected that would demonstrate physical and mechanical characteristics similar to those of the bone, but with specific and low variance in mechanical properties, and that would allow investigation of fixation of polymeric implants with cementing process.

2.3.1 Design of the equipment

Trabecular bone has an open cell structure which provides a mechanism by which cement keys in the bone. Previous bone analogues have been closed cell and although used in previous testing of cement implants they do not provide a realistic environment for testing. In this investigation a newly marketed open cell structure was chosen to test whether it was suitable for the mechanical testing of the fixation

interface in the glenoid component. (Sawbones® Europe AB, Malmö, Sweden), (Figure 2.11a). Two blocks of open cell rigid foam were used to have sufficient thickness to implant the glenoid components. The Sawbones blocks were filled with water and frozen prior to cutting in to a pyramid shape, to eliminate the destruction of the block structure, and a silicone tape was rapped around the Sawbones prior to mounting in to a PMMA on the simulator testing machine (Figure 2.11b), to eliminate cement leakage. The pyramid shape was prepared to have similar shape to the glenoid bone. The Sawbones specimen was then mounted into PMMA, providing a 5 degree anterior-posterior tilt of the Sawbone.

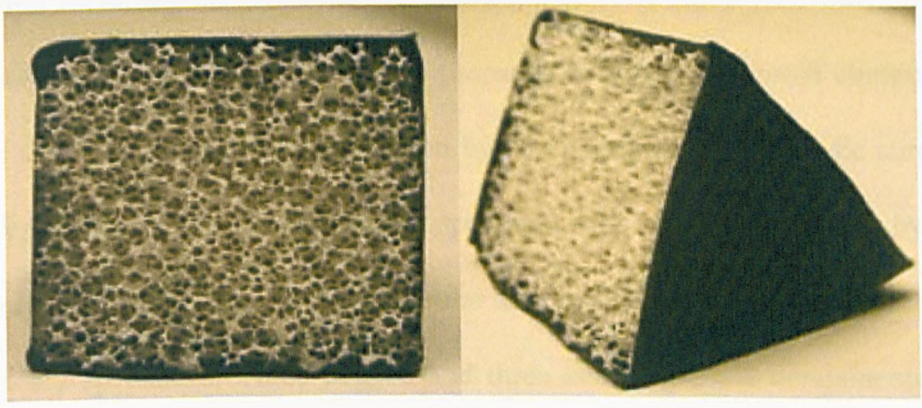

(a) (b)

Figure 2.11 (a). Open cell rigid foam, (b). Silicon tape wrapped around the Sawbones

2.3.1.1 Bone substitute fatigue testing

The properties of the open cell foam used in the component simulation are provided in Table 2.2. These material properties are similar to the average elastic

modulus of human cancellous bone. To validate the density value of the sawbones and the glenoid cancellous bone, the BV/TV was measured using the MicroCT.

Table 2.2 Open cell foam properties (from the manufacturer) and the osteoporotic bone.

	Density		Strength	Modulus
	(pcf)	(g/cc)	(MPa)	(MPa)
Open cell	5.5	0.09	0.11	6.2
Osteoporotic Bone	7.5	0.12	0.28	18.6

After mounting the Sawbones in PMMA, they were filled with water which was subsequently frozen. The block was prepared to accept a glenoid component using the standard surgical instrumentation by an experienced orthopaedic surgeon (DL). Preparation whilst the sawbones specimen was still impregnated by ice eliminated excessive damage to the trabecular structure that was observed on initial testing of dry specimens. Three pegged and three keeled glenoid components (all size 48) were cemented into the surrogate bone (Figure 2.12), the blocks were mounted in to the simulator plastic holder facing upwards. The humeral head was then mounted to articulate onto the glenoid within ±0.5mm of the central axis of the glenoid, this was to ensure the contact between the two components matched [169], and then were placed in a fatigue simulation machine.

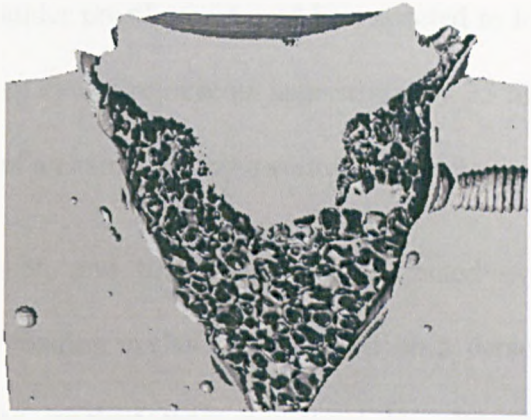

Figure 2.12 MicroCT image from the glenoid component mounted in PMMA in a bone substitute, which is fixed in PMMA to avoid any motion.

The simulator (Prosim, UK) used is a six-station pneumatically operated biomechanical fatigue-loading simulator. A station has two axes of motion, axial and rotation each of which may be programmed to operate in either load or displacement controlled mode. The axial load is applied to the glenoid component by a ball shaped humeral head. The machine is connected to a control PC. A rigid screw clamp was added to the testing apparatus to prevent motion of the specimen over the duration of the test. To obtain a loading demand of 400N t0 1000N, a cyclic, sinusoidal loading program was applied along the main axis of the humeral head for 100,000 cycles, at a frequency of 1Hz.

The polyethylene head applied an eccentric vertical force on the glenoid (Figure 2.13). Loading duration was 100,000 cycles to simulate 10 years of *in vivo* function and evaluate the fatigue behaviour of the cement interface during prolonged cyclic loading as well as the suitability of the model as a whole [111, 169] Although 100,000 cycles is low compared with hip and knee testing, this value is justifiable because the test does not investigate component strength, because high-load activities occur much less frequently at the shoulder than in the lower limb, and

because people with shoulder prostheses would be expected to load their arms even less often. This number of cycles represents approximately 25 high-load activities a day (such as getting out of a chair or lifting a suitcase) for 10 years [111].

Load, displacement, and time data were collected every few cycles at maxima and minima of loading cycles and recorded on a personal computer. The overall migration of the implant was monitored by observing the change in displacement of the component via the LVDTs while testing and also at the beginning and the end by using the microCT images, by scanning the specimen before and after the simulation. The cement thickness was also measured by using the microCT 3D images and using a threshold which only shows the cement blocks. (Figure 2.14). The same set of test was carried out with a higher range of loading (800N-1800N), to investigate the destruction rate of the sawbones.

The load applied was higher than the demand load (750N); this force is used in the ASTM standard [138, 139] in testing the glenoid component fixation. Prior to start the cyclic loading, the machine was calibrated using load control mode; the calibration procedure had to be undertaken for each station, and each specimen has been cast into the plastic holder. Dummies were tested prior to the main test to check the two sets of loading profile (Appendix B).

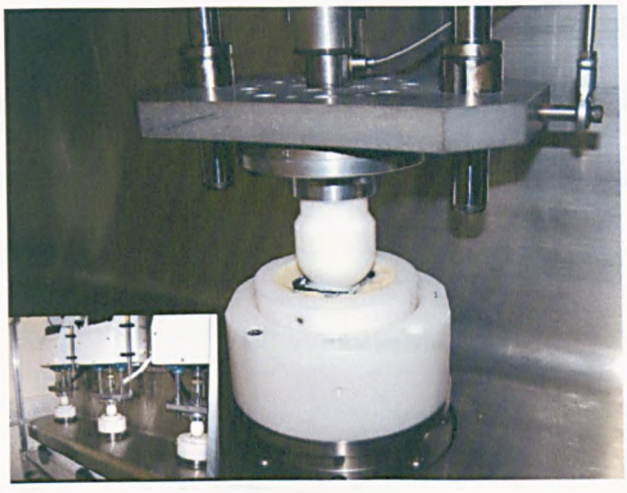

(a)

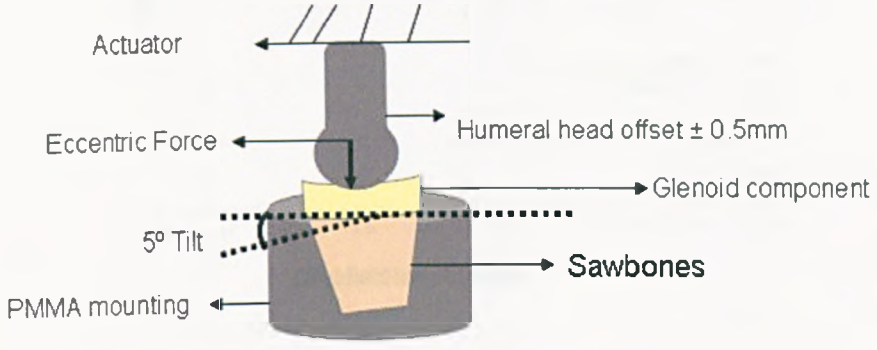

(b)

Figure 2.13 (a). The shoulder arthroplasty simulation procedure. (b) A schematic diagram of a vertical compressive force applied on the cemented glenoid component.

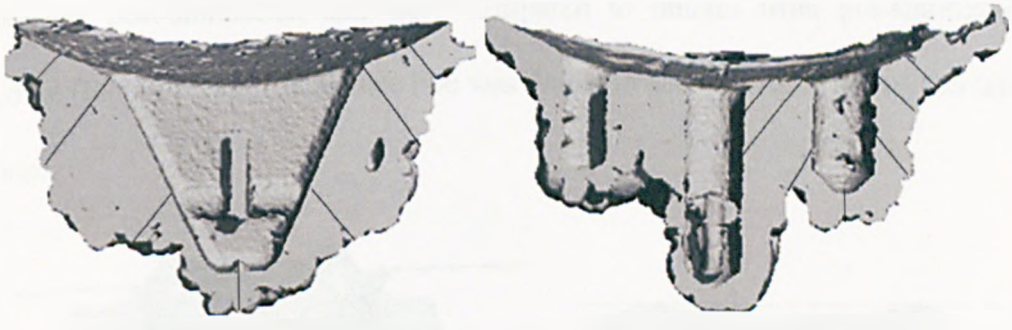

Figure 2.14 microCT images from keel and peg component cement thickness

Displacement and the stiffness of the each component were measured using the normalized average specimen displacement and the average gradient of the graphs for different cycles, (Figure 2.15). This was obtained from 12 cycles for the

400N-100N and 12 cycles for 800N-100N. The displacement of the glenoid component with respect to the sawbones deformation after cycling was measured using pre-and post-simulation microCT images, which was measured manually using IDL software.

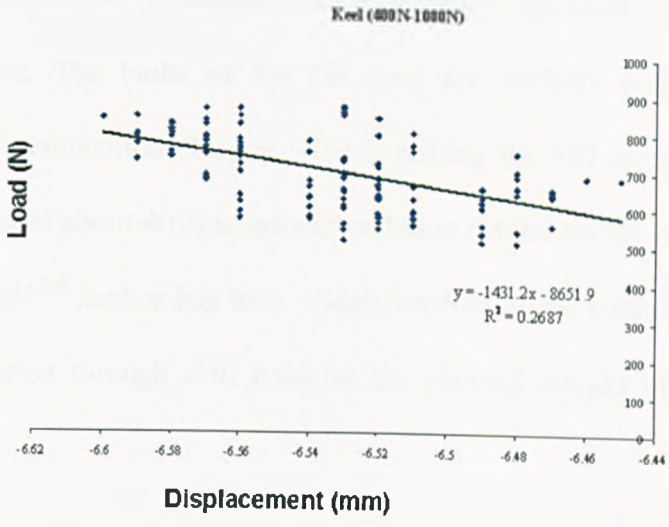

Figure 2.15 Load versus displacement graph for measuring stiffness.

3D images from the microCT were used to measure the displacement of the components post-simulation and were compared to images from pre-simulation procedure (Figure 2.16). A reference line was drawn in accordance to the silicon tape position.

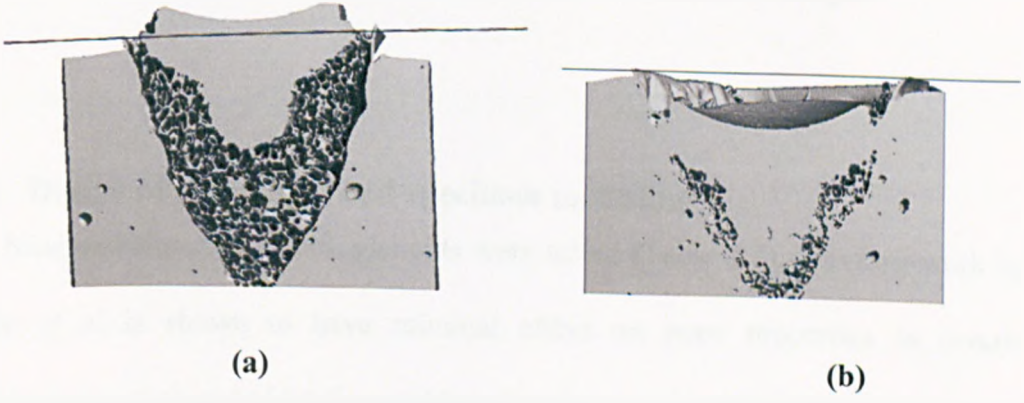

Figure 2.16 (a) The Sawbones structure prior to any fatigue test. (b) The sawbones structure post-fatigue test.

2.4 PULLOUT STRENGTH OF SUTURE ANCHORS

Bankart is the essential lesion of recurrent shoulder instability. The use of suture anchors in the repair of Bankart lesions in shoulder joint instability is widespread. The suture anchors have the ability to secure the labrum and capsule to the glenoid after anatomical reduction, and eliminating the need to drill tunnels through the glenoid. The barbs of the GII lock the anchors within the bone. According to the manufacturer (Depuy, USA), pulling the GII anchor back after insertion with a load of about 40 N is recommended to set the anchor and to lock the barbs. The Mitek GII^{TM} anchor has been widely studied in the context of shoulder surgery, being inserted through drill holes at the glenoid margin into underlying cancellous bone.

The purpose of this study was to develop a method of mechanical testing bankart lesion repairs in human glenoid cadaveric model. And to investigate the pullout strength and the fatigue properties of Mitek GII ^{TM} anchors when loaded with Orthocord^{TM}, a novel suture material with greater reported tensile strength than suture material used in previous pullout studies. Additionally we aim to measure bone mineral density at the precise location of anchor insertion using microCT to determine if this affects the pattern of failure or ultimate pullout strength.

2.4.1 Design of equipment and specimen mounting

Nine embalmed cadaveric glenoids were tested (Table 2.3). Previous work by Anglin et al is shown to have minimal effect on bone properties in certain circumstances, such as indentation test but the effect in the following tensile testing arrangement is unknown. Initial tests were undertaken using embalmed specimens

whilst later tests were undertaken using fresh frozen bone. The Mitek anchors are usually used in younger patients [155], but the reason more elderly cadaveric bone were tested, is the availability in comparison to the younger specimen. In addition the older bones allowed the BMD correlation to the pullout strength to be established.

Table 2.3 Details of the glenoid specimens

Glenoid	Gender	Age	Shoulder
G1/02	F	90	R
G32/02	F	70	R
G36/01	F	87	L
G6/02	M	66	L
GNoNu	M	?	L
GUNM5	F	?	L
GUNM6	F	?	L
GUNM2	F	?	R

The GII suture anchor consists of a titanium body with two nitenol arcs. Orthocord™ (Depuy, USA) suture is a new material that has been shown to have superior strength characteristics but as yet no clinical studies have confirmed that this has any *in vivo* advantage. Orthocord is a synthetic, sterile, braided composite suture composed of dyed (D&C Violet #2) absorbable polydioxanone (PDS) and un-dyed non-absorbable polyethylene. The partially absorbable suture is coated with a copolymer of 90% caprolactone and 10% glycolide (Depuy, USA). Orthocord™ is threaded onto the GII suture anchor, which is inserted into the bone through a 2.9mm diameter drill holes in the glenoid rim, (Figure 2.17). An axial alignment of the Mitek anchor to the drill hole should be established and inserted. No twisting or bending force should be applied to the inserter as either may damage the anchor or inserter tip (Manufacturer recommendation). Each anchor was inserted with their

barbs parallel to the articular surface to prevent migration of the barbs in to the joint surface. In this study, the anchors were placed in the posterior rim and three anteriorly. Anchors are used for anterior and posterior labral repairs, the former being the most commonly performed in the clinical context [210]. These drill holes were placed in locations commonly used in instability repairs, (1, 3, 5, and 9 O'clock on the right shoulder and 6, 8, 9, and 3 on the left shoulder). The glenoid was first divided in to 8 equal sections to have an accurate locations for each specimens, (Figure 2.18). It is important to direct the drill medially, away from the articular surface of the glenoid, by at least 15 degree angle to avoid damage to the articular surface. The drill was directed to bisect the cortical surface of the glenoid rim.

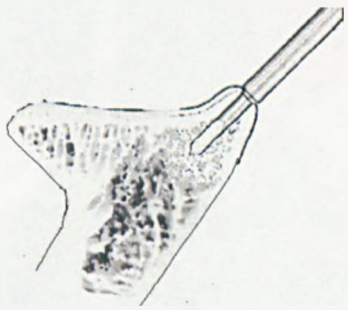

Figure 2.17 A 2.9mm drill used for glenoid suture anchoring holes.

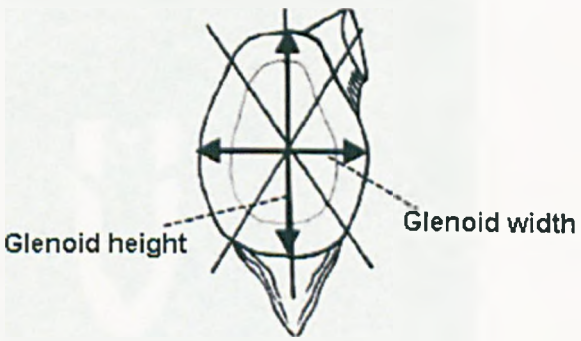

Figure 2.18 The eight divided sections on the glenoid surface.

The specimens were mounted in polymethylmethacrylate bone cement (PMMA) on an adjustable jig allowing pullout tests to be performed directly in line

with each anchor using a tensile testing machine (Shimatzu, Keyoto, Japan) with 1kN load cell (Figure 2.19). Two step loading conditions were applied: conditioning cycles of 20 cycles from 15N to 30N to detect any creep in the system on repetitive loading that was then followed by an increasing load until the point of failure. The displacement rate was 10 mm/min, and the mode of failure (Anchor pullout or suture breakage) was recorded for each test site.

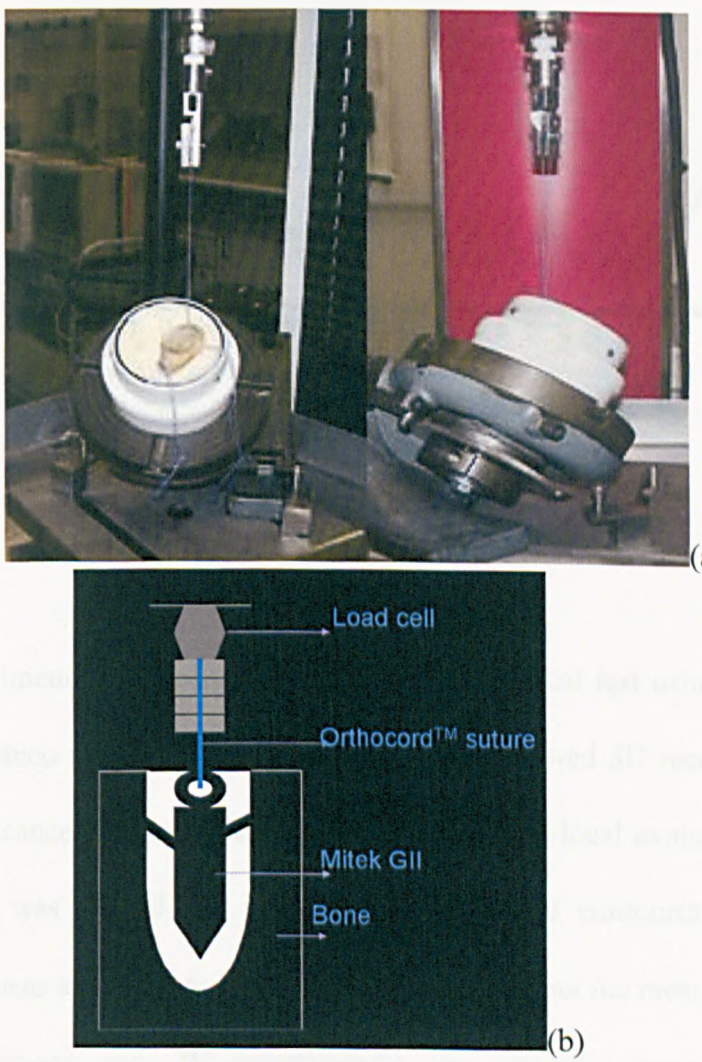

Figure 2.19 (a).The clamping of the suture on an angle jig. (b). A schematic diagram of the pullout procedure.

A sample of two steps, load profile curve is shown in Figure 2.20, which explains the pullout behavior of the specimens. As we can see from the graph, the load was applied from 0N to 30N initially, then 20 cycles between 15N to 30N, prior to pullout to failure of either the anchor or the suture.

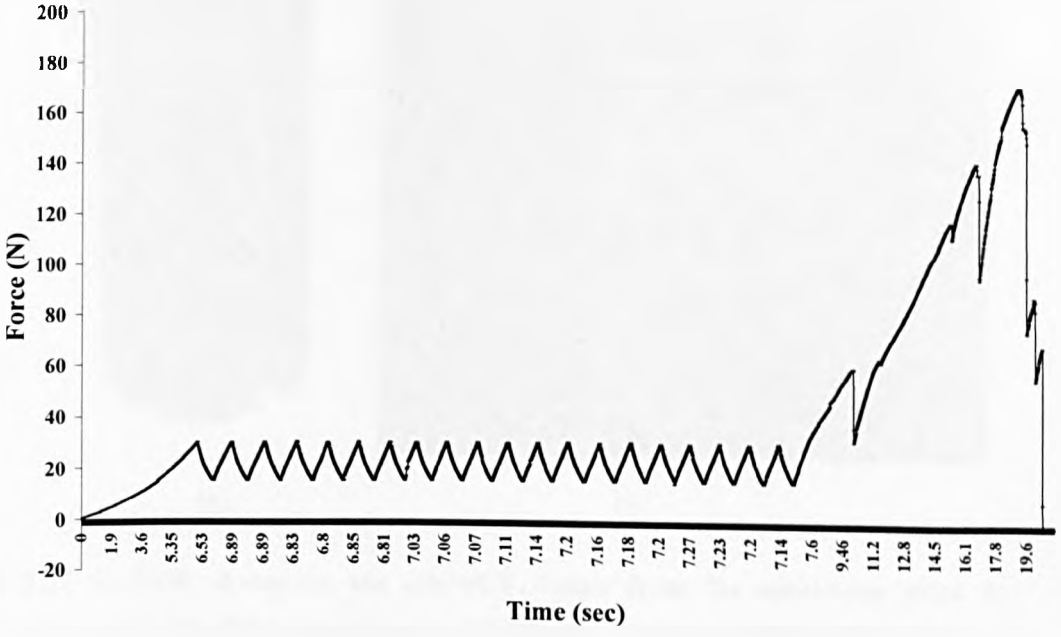

Figure 2.20 The load profile of pullout testing.

The specimens were scanned prior to the mechanical test using a MicroCT (microCT 80 Scanco medical AG, Switzerland). This allowed 3D reconstruction of the cortical and cancellous architecture of the glenoid and local evaluation of bone mineral density was carried out using a semi-automatic contouring method. A DEXA machine was also used to look at the BMD values, but the measurement were not analysed because only 2D measurement was available from this type of machines. The volume of interest in the microCT was chosen at each anchor site and was cylindrical with a 15mm length (the drill hole's depth) and 2.9 mm diameter (Figure 2.21). The QCT version of the Scanco software was used to measure the

BMD. The BMD measurement was measured beneath the cortical bone to include only the cancellous bone.

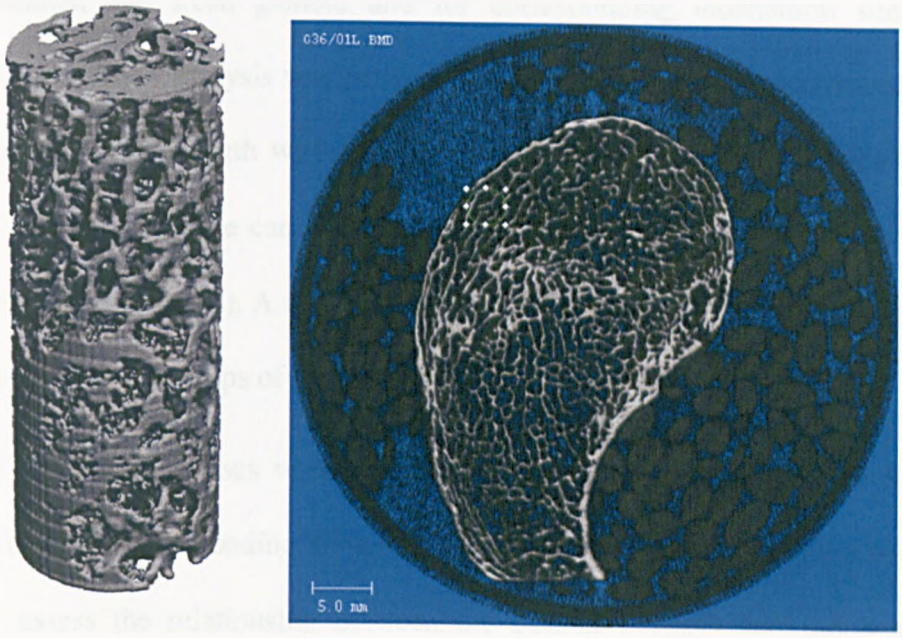

(a) (b)

Figure 2.21 (a).VOI chosen on the microCT, taken from the specimens prior to mechanical test. (b) The ROI chosen on the 2D images, just beneath the cortical shell.

The same pullout test protocol was carried out using fresh frozen cadaveric bones. Two specimens were available for testing and only the three anterior regions were anchored and tested for pullout. Orthocord™ suture material was not available, which instead green ETHIBOND® (size 2) braided polyester, non absorbable suture (ETHICON, Inc.; Somerville, NJ) was used. The pullout strength, displacement of the anchors prior to cycling and the BMD values was measured the same way as the embalmed specimens.

2.5 STATISTICAL ANALYSIS

Statistical analyses were determined for each of the parameters for the whole of each embalmed and fresh glenoid and for corresponding indentation sites. Multiple linear regression analysis was performed to assess the relationship between the elastic modulus and strength with the subchondral thickness and bone volume fraction. The calculations were carried out within a proprietary computer program (Stata 9, College Station, USA). A student's unpaired t-test was used to calculate the p-values between the two groups of specimens.

Again statistical analyses were determined for each of the parameters for each glenoid and for corresponding anchored sites. Linear regression analysis was performed to assess the relationship between the pullout strength and the bone mineral density and the anchor slippage.

3 Results

3.1 INTRODUCTION

This chapter presents the results and analysis of the series of interlinked experimental studies concerning the use of glenoid components and its fixation to the glenoid fossa. The first section shows the results obtained from the bone morphology, which focuses on the spatial distribution, as well as the average values of the glenoid bone. The next section examines the results obtained from the mechanical properties of the glenoid and its relationship to bone morphology. These two sections also compare the behaviour of fixed and cadaveric specimens in an attempt to validate Anglin's statement [30] concerning the usage of fixed tissues in indentation experiments provide *no meaningful difference in specimen observations.* The third portion of this chapter outlines the results of the glenoid components fixation using bone substitute. And the final section reports the results of pullout strength of the suture anchors.

3.2 BONE MORPHOLOGY RESULTS

3.2.1 Introduction

Analyses of the glenoid bone morphology were carried out using the microCT scanner to determine the bone volume fraction, degree of anisotropy, the bone mineral density, and the subchondral thickness of the glenoid. The motivation was to investigate the spatial variation of these parameters and their influence on the mechanical properties of the glenoid. These latter parameters can be used for finite

element analysis. The subchondral thickness measurements were validated using images from the shadow microscope.

3.2.2 Bone volume fraction (BV/TV) results

Visual examination of the specimens indicated no signs of joint disease and no signs of arthritis. Three-dimensional reconstructions and multiplanar image analysis of the different regions of all nineteen glenoid cadaveric specimens revealed a remarkable trabecular structure (Figure 3.1). The trabecular bone direction was almost perpendicular to the glenoid surface. The orientation of the trabecular structure is anisotropic arrangement, and the 3D image clearly depicted thick plate-like trabeculae interconnected by thin rod-like structures. The trabecular orientation is aligned to resist the major forces on the glenoid surface. This suggests that it is the micro-architecture of trabecular bone that attributes to its anisotropy and variations in apparent modulus at different anatomical location.

Figure 3.1 The three-dimensional reconstruction of the glenoid

The bone volume fraction (BV/TV) is a ratio of the volume of bone present (BV) to the total volume of interest (TV). TV is equal to the volume of the VOI in the present study. The evaluation of the bone architecture is of great importance for the understanding of the biomechanical behaviour of bone. The changes in the

internal structure of the trabecular bone and the BV/TV is used as a predictor for bone strength.

For the embalmed specimens large variations were observed in the mean value of BV/TV at each of the 11 glenoid positions and this varied from 0.14 to 0.41. Analysis of variance showed that the differences in bone volume fraction for approximately the same depth below different positions of the glenoid surface were found to be significant ($F = 14.5$, $P<0.001$). Table 3.1 provides the spatial distribution of the BV/TV values for the eleven selected regions in each specimen. The red dots in Figure 3.2 indicate the indentation sites in which the BV/TV was at the median value or higher. In general, there was a trend for the larger values of BV/TV to be found at the posterior margins of the glenoid whilst the more porous regions were observed near the anterior-inferior edge.

Table 3.1 The BV/TV of 11 zones of the embalmed glenoids.

Zone	BV/TV	SD
1	0.15 ±	0.08
2	0.24 ±	0.09
3	0.22 ±	0.11
4	0.14 ±	0.05
5	0.16 ±	0.07
6	0.24 ±	0.11
7	0.28 ±	0.07
8	0.19 ±	0.07
9	0.24 ±	0.10
10	0.41 ±	0.08
11	0.27 ±	0.08

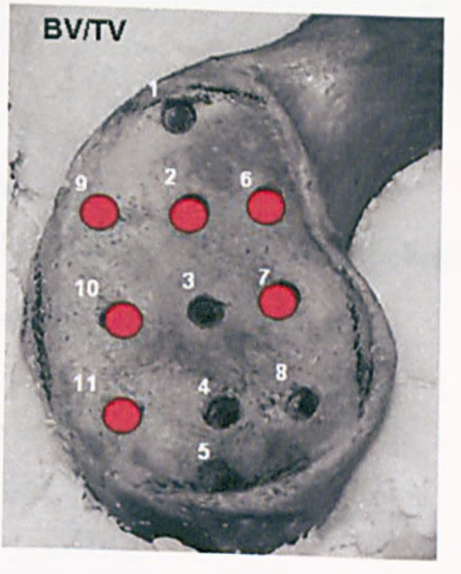

Figure 3.2 The red dot is the median values and higher of the BV/TV of the 11 pre-selected areas of the embalmed glenoid.

Figure 3.3 provides the mean BV/TV values of the individual glenoid with regards to their age. Mean values ranged from 0.35 to 0.15. The correlation in Table 3.2 shows that the association between BV/TV to the age of the specimens is ~38%. This can explain that as age goes higher the BV/TV of the bone decreases.

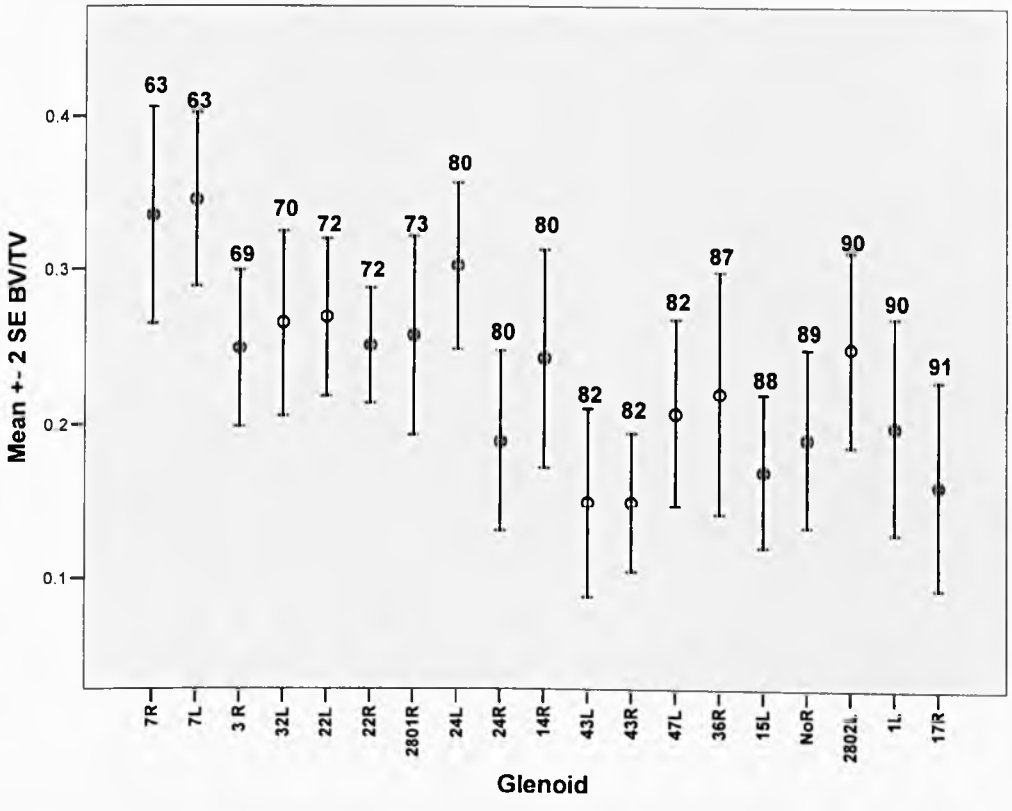

Figure 3.3 The mean values of the BV/TV of the <u>embalmed</u> glenoids labelled with regards to their age.

Table 3.2 The correlation of BV/TV to the age of the specimens.

		Glenoids age (y)	BV/TV
Glenoids age (y)	Pearson Correlation	1	-.375**
	Sig. (2-tailed)		.000
BV/TV	Pearson Correlation	-.375**	1
	Sig. (2-tailed)	.000	

**. Correlation is significant at the 0.01 level (2-tailed).

For the fresh specimens large variations were observed in the mean values of BV/TV at each of the 11 glenoid positions and this varied from 0.19 to 0.44. Table 3.3 provides the spatial distribution of BV/TV values for the eleven selected regions in each fresh specimen. The red dots in Figure 3.4 indicate the indentation sites in which the BV/TV was at the median values or higher in fresh glenoid. In general, there was a trend for the larger values of BV/TV to be found at the posterior margins of the glenoid whilst the more porous regions were observed near the anterior-inferior edge.

Table 3.3 The BV/TV of the fresh bone for the 11 zones.

Zone	BV/TV	SD
1	0.19 ±	0.08
2	0.24 ±	0.08
3	0.30 ±	0.11
4	0.21 ±	0.05
5	0.23 ±	0.09
6	0.24 ±	0.13
7	0.28 ±	0.08
8	0.21 ±	0.06
9	0.40 ±	0.14
10	0.44 ±	0.12
11	0.29 ±	0.08

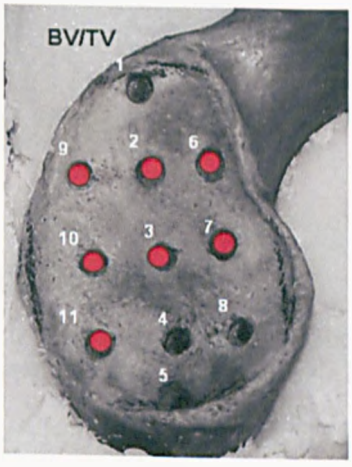

Figure 3.4 The red dot is the median and higher BV/TV values of the 11 regions of the fresh bone.

Figure 3.5 shows the BV/TV mean values of the six fresh specimens tested. This ranged from 0.17 to 0.35. The age of the fresh specimens was not available. The one way analysis of variance (ANOVA) for each of variable

across each of its zones for the fresh bone shows substantial significant differences. The one way analysis for the BV/TV is F=4.1, P<0.0003.

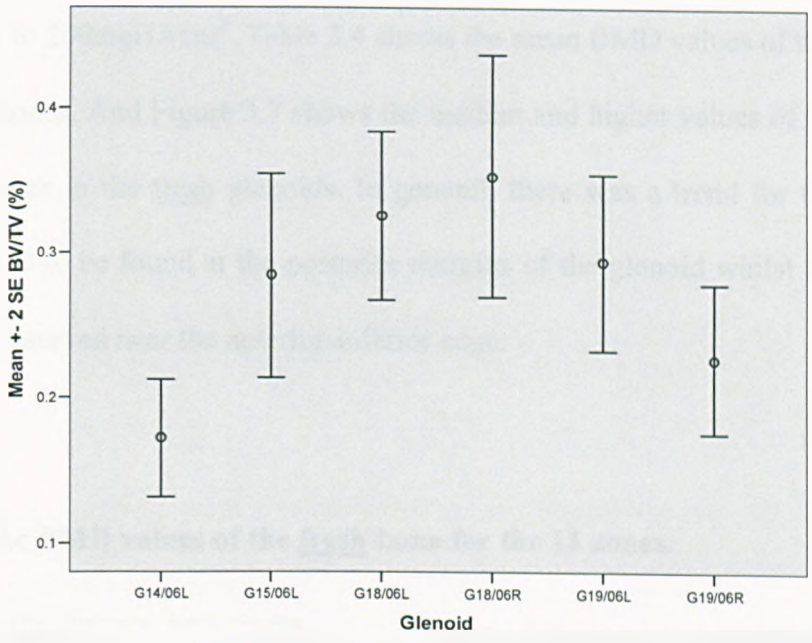

Figure 3.5 The BV/TV of the fresh specimens.

Figure 3.6 shows the BV/TV of the embalmed and the fresh specimens. The bone volume fraction was higher in the fresh specimens.

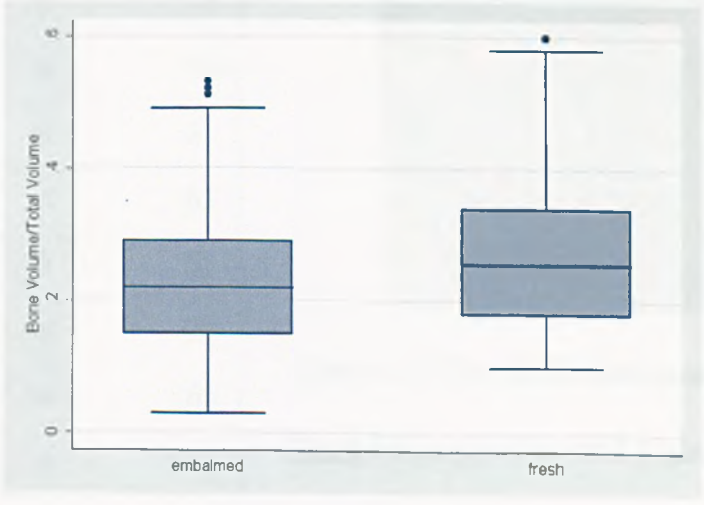

Figure 3.6 The BV/TV of the embalmed and the fresh specimens.

3.2.3 The bone mineral density

The BMD values of the fresh bone for the same volume of interest were obtained from the microCT 3D images. Large variations were observed in the mean values of the BMD at each of the 11 glenoid positions and this varied from 77mgHAcm^3 to 200mgHAcm^3. Table 3.4 shows the mean BMD values of the eleven pre-selected zones. And Figure 3.7 shows the median and higher values of the BMD for the 11 zones in the fresh glenoids. In general, there was a trend for the larger values of BMD to be found at the posterior margins of the glenoid whilst the lower values were observed near the anterior-inferior edge.

Table 3.4 The BMD values of the fresh bone for the 11 zones.

Zone	BMD mgHAcm^3		SD
1	83	±	45
2	92	±	51
3	121	±	62
4	77	±	72
5	92	±	76
6	105	±	61
7	111	±	63
8	90	±	55
9	182	±	73
10	200	±	66
11	133	±	32

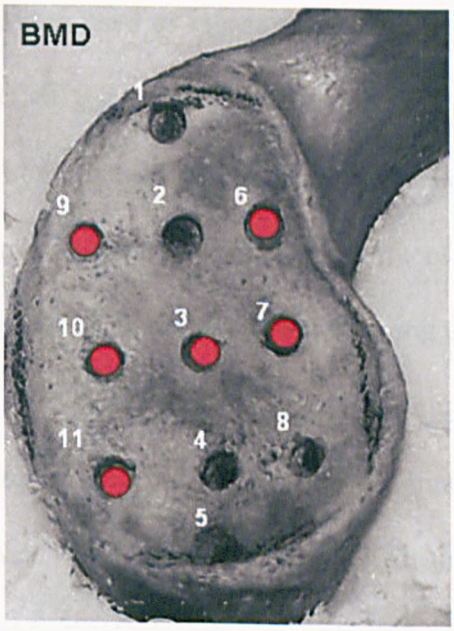

Figure 3.7 The BMD distribution of the fresh bone, (median and higher values).

Figure 3.8 shows the BMD of the six fresh glenoid and these values range from 26.40mgHAcm^3 to 167.60mgHAcm^3.

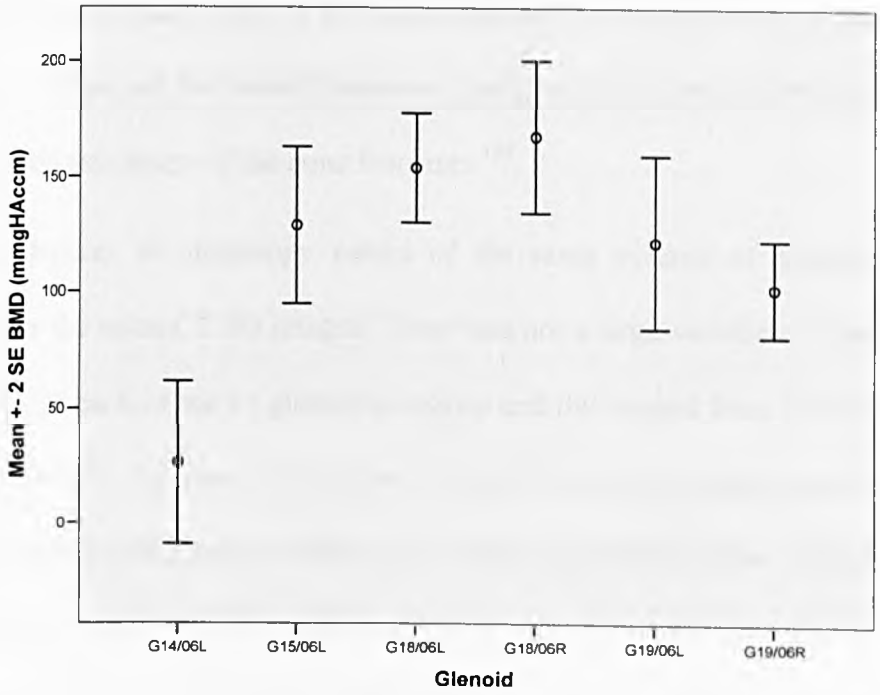

Figure 3.8 The BMD of the six fresh glenoids.

3.2.4 The degree of anisotropy

The mean intercept length (MIL) method was used to measure the anisotropy of the trabeculae in the VOI. To calculate the MIL, a circular grid of parallel test lines is superimposed on images of trabecular bone in each of the three image axes, x, y, and z. The average distance between bone-marrow cavity interfaces is calculated by counting the number of interfaces along the test lines and dividing that sum by the length of all lines in the test grid. This yields the mean intercept length. Subsequently, the grid is rotated 5° with respect to an arbitrary axis on the image, and the counts are repeated in angular increments of 5° through 180° for all three scan axes. These counts create a series of values in the form MIL (α_i), where α is the angle at which the count was taken (0°–180°) with respect to a reference axis, and i is the scan plane of the image (= x, y, or z scan planes which are orthogonal to each other). These MIL (α_i) data are fit to the function of an ellipsoid. The degree of anisotropy of the trabecular architecture (MIL-DA) is defined as the ratio of the

primary axis to the tertiary axis of the MIL ellipsoid. At ratios close to 1, the axes are of similar value and the bone structure is isotropic. As the ratio increases above 1, the degree of anisotropy of the bone increases [184].

The degrees of anisotropy values of the same volume of interest were obtained from the microCT 3D images. There was not a large variation in the mean values of DA at each of the 11 glenoid positions and this ranged from 1.43 to 1.97. Table 3.5 provides the mean DA values of the eleven pre-selected zones of the embalmed glenoids and Figure 3.9 shows the median and higher values of the DA of the pre-selected zones. The DA values show an anisotropy structure in the mid-superior region and posterior region of the glenoid and more isotropy at the superior and anterior regions of the glenoid.

Table 3.5 The DA values of the 11 zones of the embalmed glenoids.

Zone	DA	SD
1	1.43 ±	0.16
2	1.97 ±	0.41
3	1.56 ±	0.21
4	1.68 ±	0.35
5	1.78 ±	0.21
6	1.63 ±	0.25
7	1.59 ±	0.18
8	1.57 ±	0.25
9	1.86 ±	0.38
10	1.84 ±	0.34
11	1.67 ±	0.23

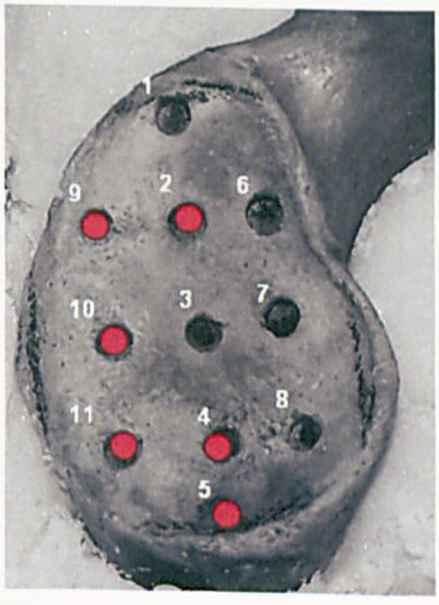

Figure 3.9 The DA median and higher values of 11 pre-selected zones of the embalmed glenoids.

The degree of anisotropy of the 19 embalmed glenoid is shown in Figure 3.10, which ranges from 1.5 to 2.1. The correlation in Table 3.6 shows that the association between DA and the glenoids age is ~19%. This explains that as age increase the DA of the bone increase and the bone structure become more anisotropic.

Table 3.6 The correlation of DA with glenoid age of the embalmed bone.

		Glenoids age (y)	DA
Glenoids age (y)	Pearson Correlation	1	.186**
	Sig. (2-tailed)		.007
DA	Pearson Correlation	.186**	1
	Sig. (2-tailed)	.007	

** Correlation is significant at 0.01 level (2-tailed).

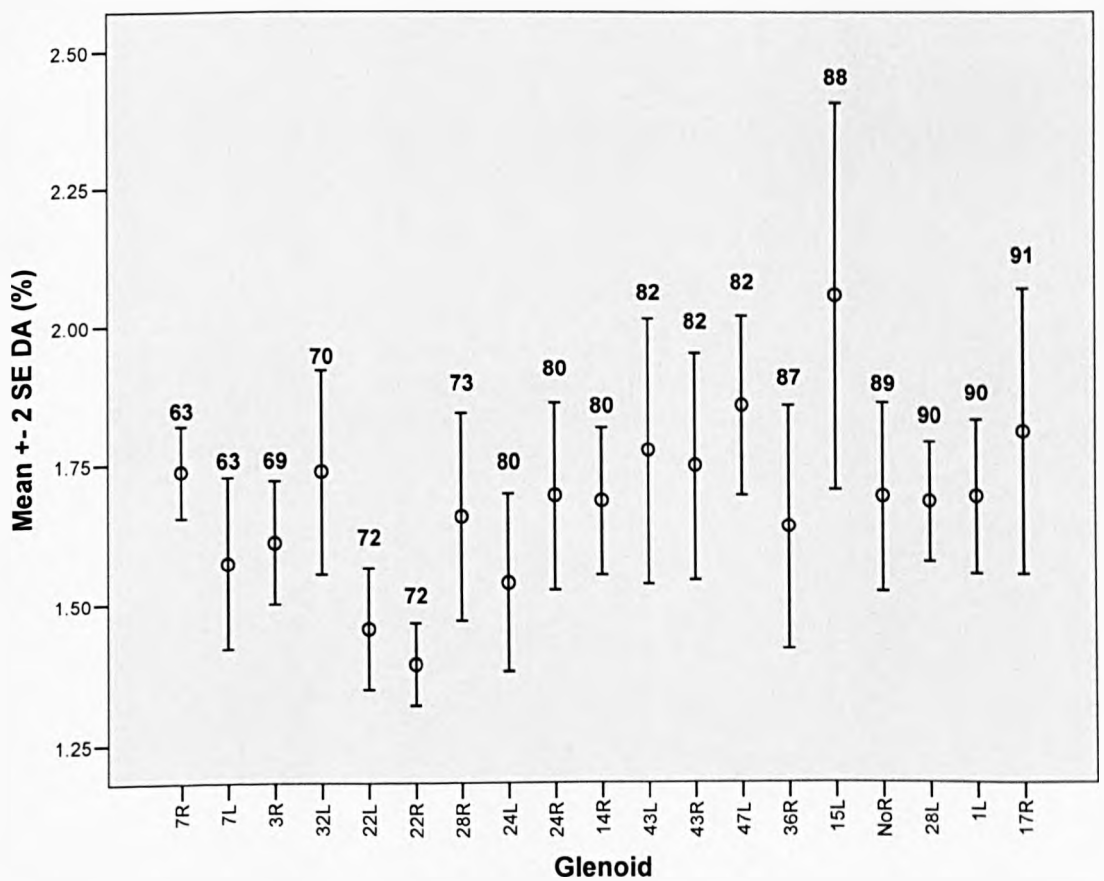

Figure 3.10 The DA of the embalmed glenoid labelled with regards to their age.

The degree of the anisotropy values of the 11 pre-selected zones of the fresh bone is given in Table 3.7 and the red dots in Figure 3.11 represents the median and higher value of the 11 areas. These values were higher at the posterior-inferior region and lower at the anterio-superior region. The DA of the fresh specimens approximately matches the embalmed specimens which is higher on the edges of the glenoid.

Table 3.7 The DA values of the fresh bone for 11 zones.

Zone	DA	SD
1	1.55 ±	0.25
2	1.85 ±	0.26
3	1.80 ±	0.12
4	1.70 ±	0.15
5	1.64 ±	0.35
6	1.50 ±	0.15
7	1.42 ±	0.27
8	1.80 ±	0.26
9	1.94 ±	0.45
10	1.90 ±	0.42
11	1.96 ±	0.19

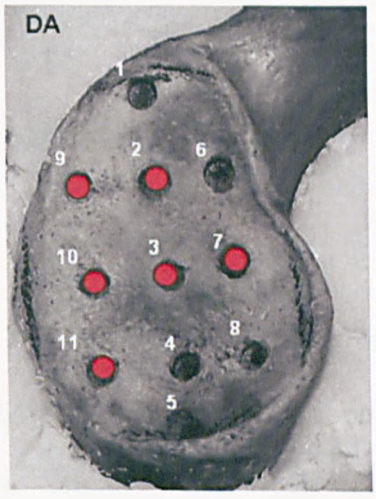

Figure 3.11 The DA of the fresh bone (median and higher values).

Figure 3.12 shows the DA values for the six fresh specimens, range from 1.73 to 1.96.

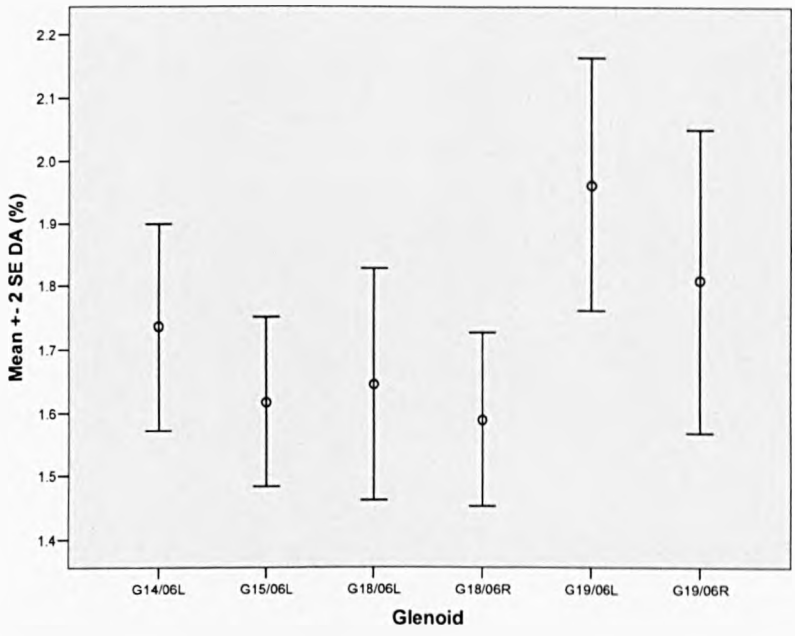

Figure 3.12 The DA values of the fresh bones.

3.2.5 Subchondral thickness results

To validate the uCT subchondral thickness measurements results were compared to those from the shadowgraph for a selection of three positions from three specimens. The measurements were obtained from both sides of three specimens, cut through zones 7, 3, and 9 only.

It is most unlikely that different methods will agree exactly, by giving the identical result for all specimens. To measure agreement between two different methods, a plot of the difference between the methods against their mean is more informative [211]. Figure 3.13 allows us to investigate any possible relationship between the measurements error and the true value. It's wrong to plot the differences against either value separately because the difference will be related to each value [212]. From the graph, the limits of agreement are small enough to be confident that the new method (uCT) can be used in place of the old (shadograph) for clinical purposes. The wide range between the standard deviation in the graph is because one

of the measurements drops out of the SD line. Since there was only 10% error in the measurement, the microCT is accurate and showed a marginal higher values.

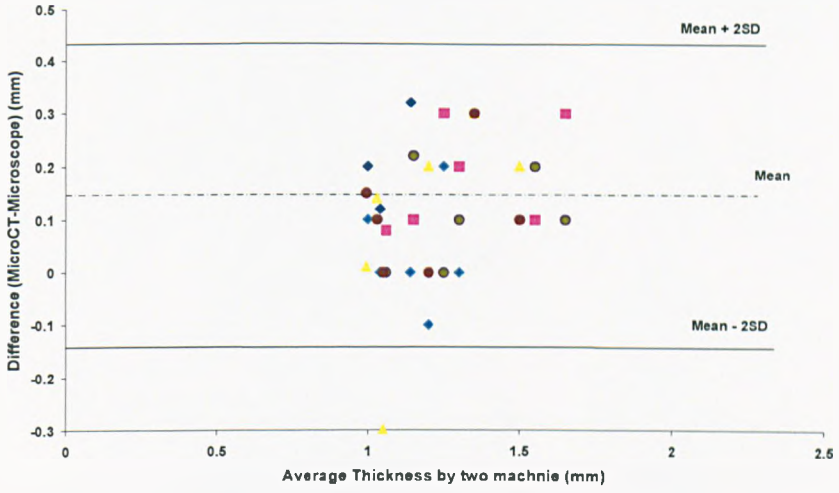

Figure 3.13 Difference against mean for subchondral thickness.

The mean subchondral thickness around each of the 11 indentation sites ranged from 0.88mm to 1.15mm for the embalmed specimens with an apparent pattern across the glenoid surface, although again analysis of variance demonstrated that the differences with position were significant. Table 3.8 shows the mean subchondral thickness values of the 11 zones of the embalmed bone. Figure 3.14 represents the subchondral thickness median values and higher of the glenoid surface across the 11 pre-selected areas.

Table 3.8 The subchondral thickness of 11 zones of the embalmed bone.

Zone	Subchondral Thickness	SD
1	0.95 ±	0.19
2	1.04 ±	0.18
3	1.12 ±	0.15
4	0.95 ±	0.19
5	0.88 ±	0.21
6	1.11 ±	0.23
7	1.15 ±	0.19
8	0.93 ±	0.18
9	1.11 ±	0.18
10	1.09 ±	0.19
11	1.01 ±	0.26

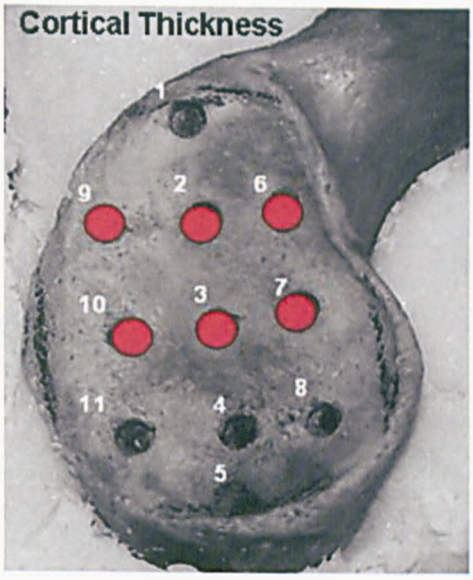

Figure 3.14 The median and higher values of the subchondral thickness of the 11 pre-selected regions of the embalmed bone.

The subchondral thickness values of the embalmed glenoids based on age range are provided in Figure 3.15. This ranged from 0.65mm to 1.2mm. The correlation in Table 3.9 shows that the association between subchondral thickness and the age of the specimens is very low 0%.

Table 3.9 The correlation of the subchondral thickness to the age of the embalmed bone.

	Glenoids age (y)	Subchondral Th. (mm)
Glenoids age (y) Pearson Correlation	1	-.004
Sig. (2-tailed)		.954
Subchondral Th. Pearson Correlation	-0.004	1
Sig. (2-tailed)	.954	

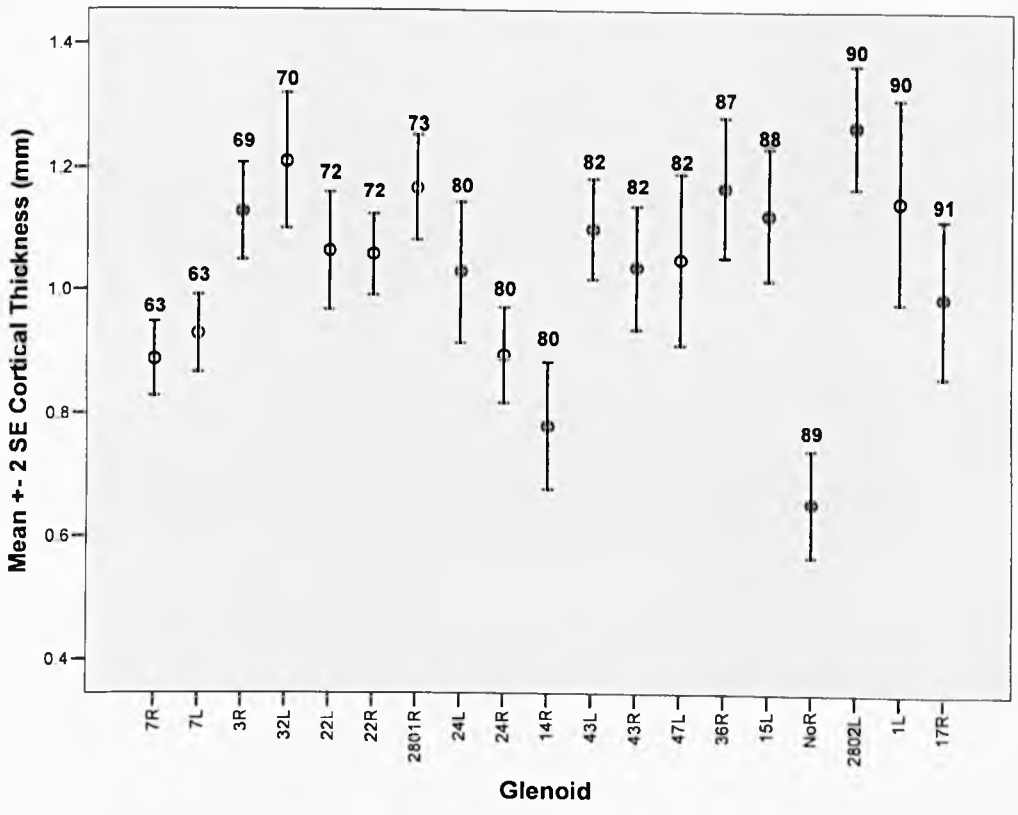

Figure 3.15 The subchondral thickness of the <u>embalmed</u> glenoid labelled with regards to their age.

The subchondral thickness values of the <u>fresh</u> bone post-cartilage removal for the 11 pre-selected regions are given in Table 3.10, and the values distribution is shown in Figure 3.16. The red dot represents the median and higher values. In general, there was a trend for larger values of subchondral thickness to be found at the superior-posterior margins of the glenoid whilst the thinner subchondral regions were near the inferior edge. The one way analysis for the subchondral thickness was $F=4.9$, $P<0.0000$.

Table 3.10 The subchondral thickness values of the fresh bone.

Zone	Subchondral Thickness	SD
1	1.30 ±	0.21
2	1.60 ±	0.48
3	1.26 ±	0.11
4	1.14 ±	0.12
5	1.00 ±	0.13
6	1.54 ±	0.51
7	1.31 ±	0.25
8	1.17 ±	0.22
9	1.76 ±	0.20
10	1.72 ±	0.34
11	1.11 ±	0.17

Figure 3.16 The subchondral thickness of the fresh bone, (median and higher values).

The subchondral thickness of the fresh glenoid values are given in Figure 3.17, which ranges from 1.13mm to 1.60mm. The subchondral thickness was higher in the fresh specimens.

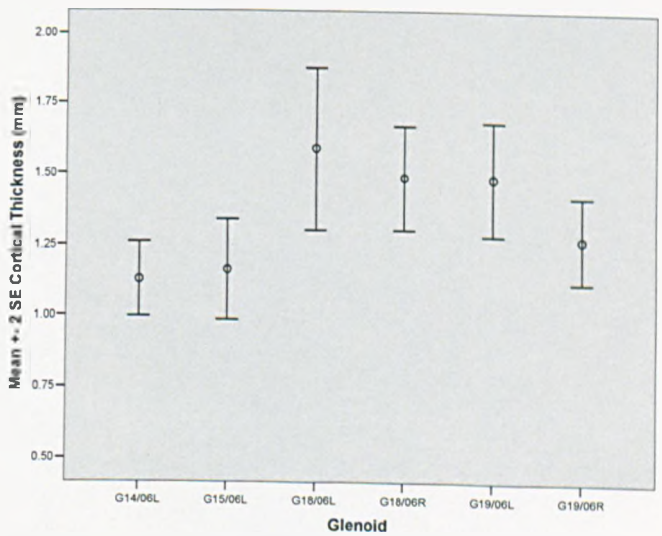

Figure 3.17 The subchondral thickness of the fresh glenoid

3.3 MECHANICAL PROPERTIES

3.3.1 Introduction

Measurement of the localised mechanical properties of the glenoid fossa is a necessary part of determining bone quality with respect to total shoulder arthroplasty. The mechanical properties assessed were the elastic modulus and the strength of the glenoid surface.

3.3.2 Stiffness and strength properties

Presented in Figure 3.18 is a typical load-displacement curve for an indentation test on the glenoid surface. All the plots were characterised by a small toe region that was followed by a relatively linear portion of the curve. The elastic modulus was determined from the maximum tangent gradient on this segment of the curve. The strength of the bone was taken to be the maximum load observed in the load-deformation curve divided by the cross-sectional area of the indentor. In those instances in which more than one peak was observed this maximum was defined to be the first maximum value followed by drop in load of 10 % or more.

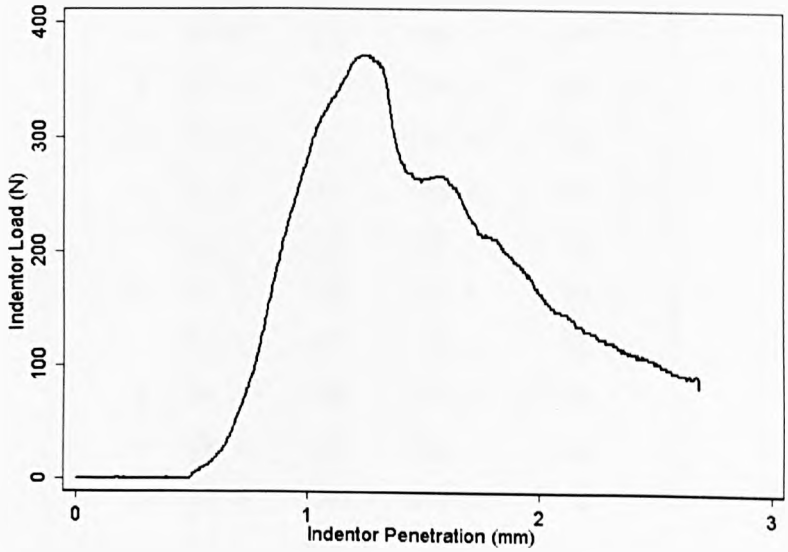

Figure 3.18 The load-deformation behaviour for a typical indentation test.

The average values of eleven pre-selected regions' mechanical properties for all scapulas are summarized in Table 3.11. The mean strength for each of the indentation sites ranged from 26 to 67 MPa (higher values at the superior and middle margins). One way of variance indicated that there were significant differences in the strength of the bone between positions on the glenoid (F = 14.0, P<0.001). Figure 3.19 showed the distribution of the strength of the bone across the glenoid surface, which displayed an apparent pattern across the regions. Similar results were observed for the elastic modulus in which the mean value ranged from 118 to 234 MPa, again, with a significant variation with position across the glenoid (F = 7.6, P<0.001). Figure 3.20 showed the distribution of the modulus of the bone across the glenoid surface, which displayed higher values at the superior and middle margins.

Table 3.11 Mean values for the strength, elastic modulus for each indented zone of the embalmed glenoids

Zone	Strength (MPa)		Elastic modulus (MPa)	
	Mean	SD	Mean	SD
1	39 ±	12	154 ±	49
2	57 ±	16	179 ±	42
3	56 ±	17	234 ±	66
4	34 ±	13	148 ±	61
5	26 ±	10	119 ±	38
6	67 ±	30	182 ±	73
7	44 ±	15	189 ±	81
8	28 ±	08	123 ±	41
9	48 ±	15	144 ±	44
10	58 ±	16	210 ±	52
11	33 ±	15	146 ±	59

Figure 3.19 and Figure 3.20 provides the median and higher strength and the elastic modulus values of the 11 pre-selected zones of the embalmed bones; respectively.

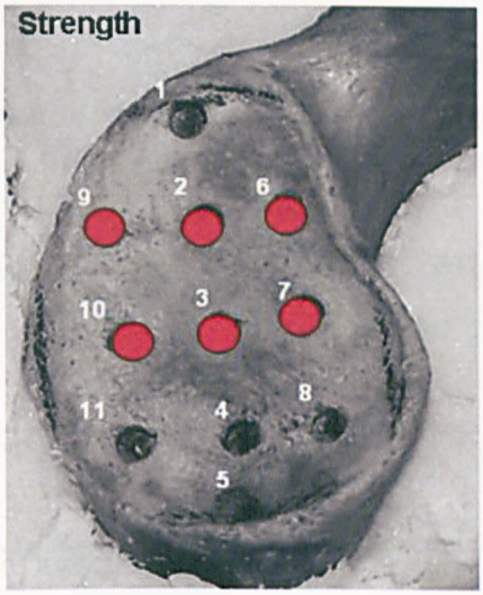

Figure 3.19 The median and higher values of the strength across the 11 zones in the embalmed glenoids.

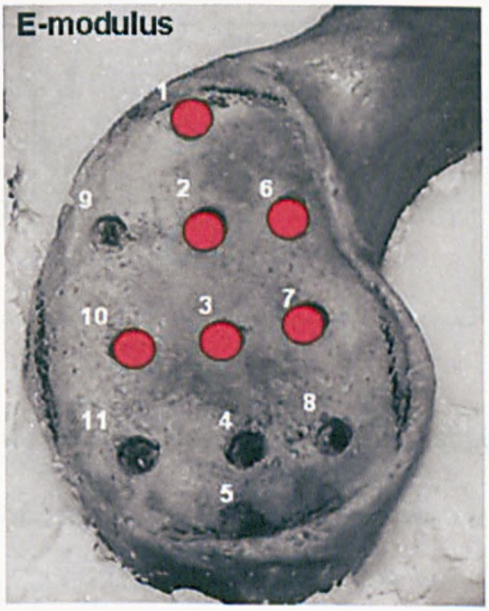

Figure 3.20 The median and higher values of the e-modulus across the 11 zones in the embalmed glenoids.

The correlations in Table 3.12 and Table 3.13 show the strength and the e-modulus association with the age of the embalmed glenoids are low, ~14% and ~1%; respectively. The strength had marginal correlation with the age of the specimens.

Table 3.12 The correlation of strength and the age of the specimens of the embalmed bone.

	Glenoids age (y)	Strength (MPa)
Glenoids age (y) Pearson Correlation	1	-.137*
Sig. (2-tailed)		.047
Strength (MPa) Pearson Correlation	-.137*	1
Sig. (2-tailed)	.047	

* Correlation is significant at 0.05 level (2-tailed)

Table 3.13 The correlation of the e-modulus and the age of the specimens of the embalmed bone.

	Glenoids age (y)	e-modulus (MPa)
Glenoids age (y) Pearson Correlation	1	-.079
Sig. (2-tailed)		.254
e-modulus(MPa) Pearson Correlation	-.079	1
Sig. (2-tailed)	.254	

Figure 3.21 shows the strength values of the 19 embalmed glenoids based on age, which ranges from 29.82 MPa to 60.6 MPa. A decrease in the strength can be seen as the age of the specimen's increases.

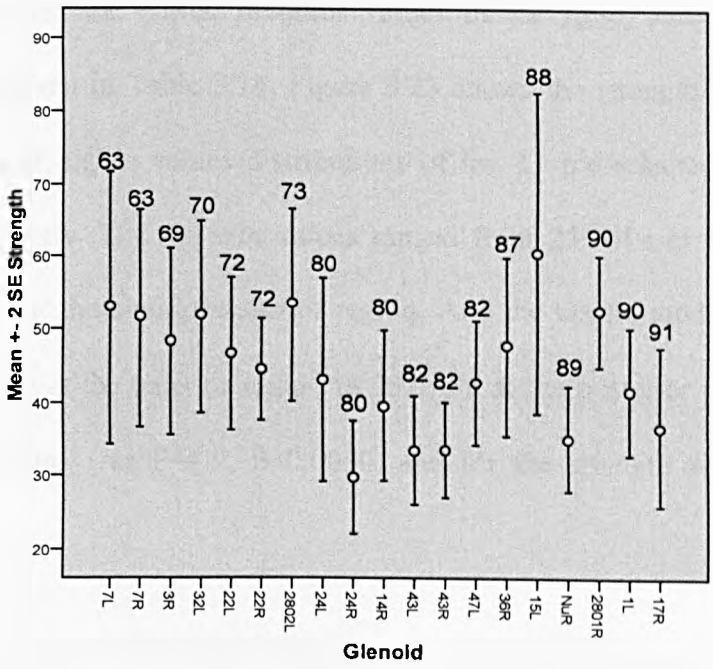

Figure 3.21 The strength distributions of the embalmed glenoids labelled with regards to their age.

Figure 3.22 shows the elastic modulus across the embalmed glenoids, which ranges from 138 MPa to 222 MPa.

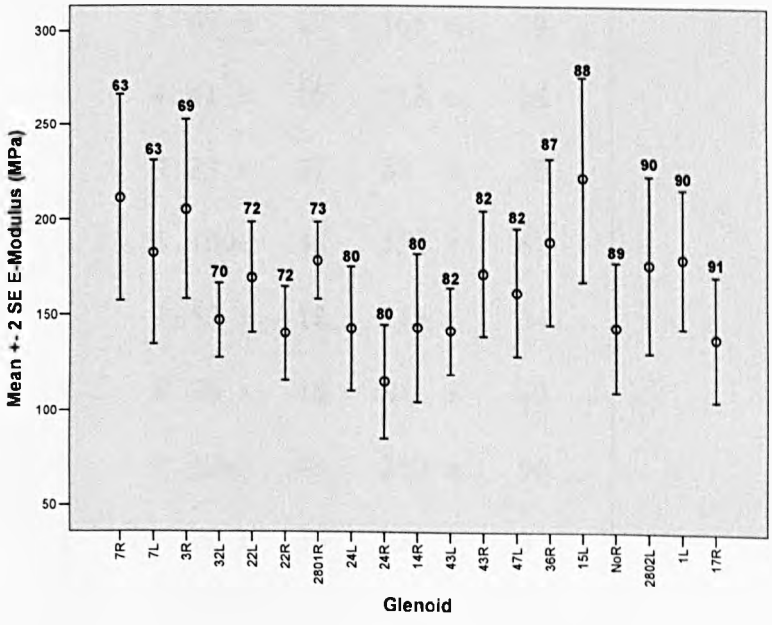

Figure 3.22 The e-modulus distributions of the embalmed glenoids labelled with regards to their age.

The strength and the elastic modulus values of the fresh bone were also measured and are given in Table 3.14. Figure 3.23 shows the strength and elastic modulus median and higher values distributions of the 11 pre-selected zones for fresh bone, respectively. The strength values ranged from 23 MPa at the inferior region to 109 MPa at the anterior-superior region. And the elastic modulus values ranged from 84 MPa at the anterior region to 231MPa at the posterior region. The one way of e-modulus was F=4.9, P<0.0000, and for the strength was F=6.34, P<0.0000.

Table 3.14 The strength and elastic modulus values of the 11 zones of the fresh bone.

Zone	Strength (MPa)		Elastic modulus (MPa)	
	Mean	SD	Mean	SD
1	66 ±	15	137 ±	25
2	88 ±	33	219 ±	72
3	63 ±	17	165 ±	59
4	41 ±	16	118 ±	36
5	23 ±	07	89 ±	29
6	109±	48	152 ±	61
7	57 ±	18	115 ±	34
8	36 ±	18	84 ±	42
9	106±	49	210 ±	96
10	96 ±	39	231 ±	81
11	45 ±	14	149 ±	23

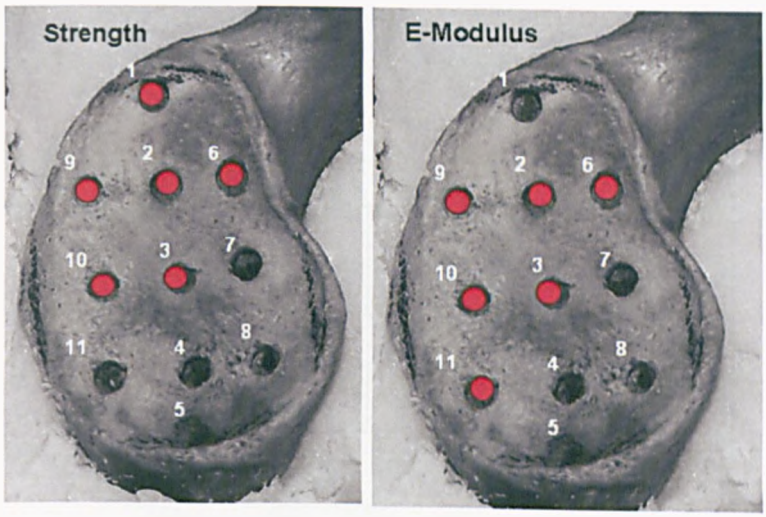

Figure 3.23 The median and the higher values regions of the strength and elastic modulus of the fresh bone.

Figure 3.24 shows the strength values and Figure 3.25 shows the elastic modulus of the six fresh glenoid. The strength ranged from 38 MPa to 93MPa and the elastic modulus from 125MPa to 212MPa.

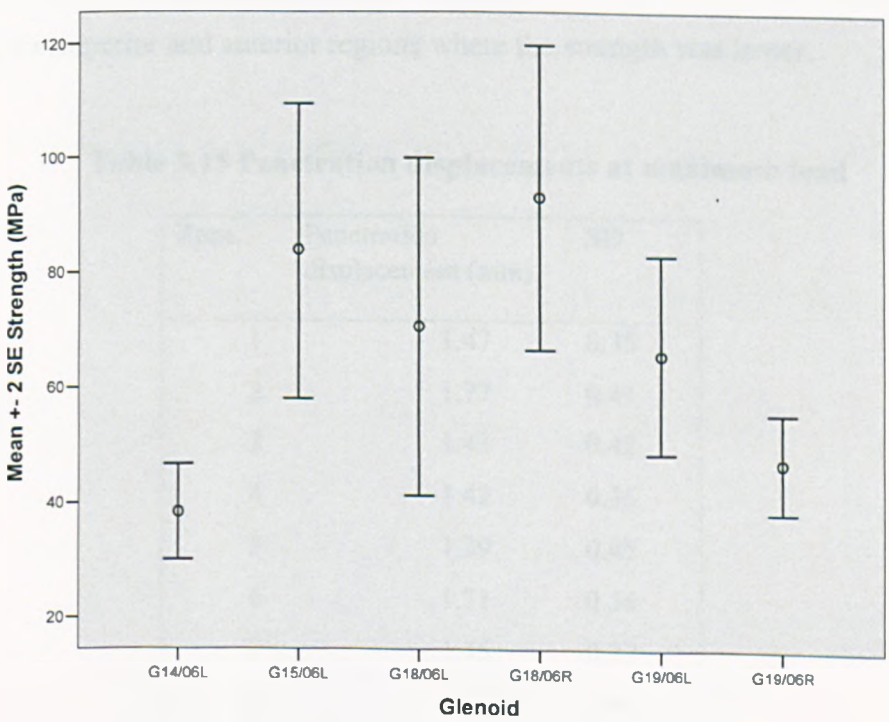

Figure 3.24 The strength of the six fresh bones.

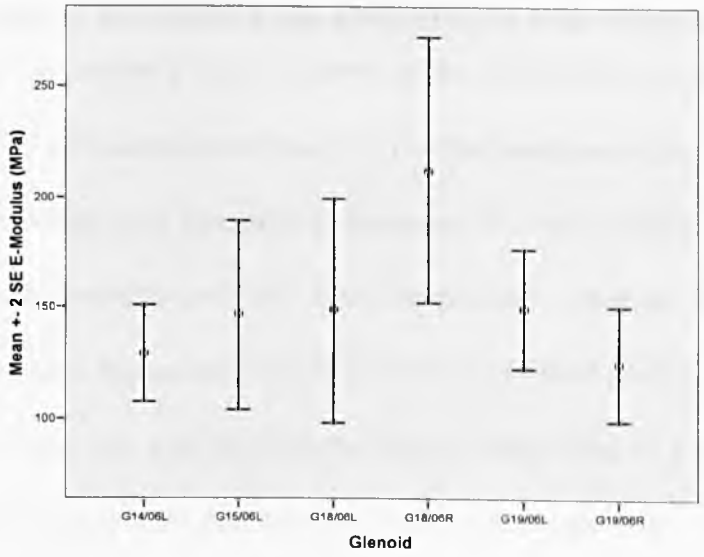

Figure 3.25 The elastic modulus of the <u>fresh</u> bone.

The maximum load applied in different regions, showed different penetration levels. Table 3.15 provides the values of penetration displacement at a maximum load, which showed small variation throughout the tests. The maximum load was obtained from different penetration in different regions and this penetration was higher at the superior and anterior regions where the strength was lower.

Table 3.15 Penetration displacements at maximum load

Zone	Penetration displacement (mm)	SD
1	1.47	0.35
2	1.77	0.41
3	1.43	0.42
4	1.42	0.35
5	1.39	0.45
6	1.71	0.36
7	1.45	0.37
8	1.47	0.41
9	1.58	0.40
10	1.41	0.37
11	1.46	0.39

3.3.3 Relationship of the mechanical properties to bone morphology

As outlined in chapter 2 little is known of the affect of the underlying bone morphology (BV/TV and subchondral thickness) on the mechanical properties of the glenoid surface (modulus and strength) as measured by the indentor. The direct association between strength and the two independent variables BV/TV and subchondral thickness is displayed in Figure 3.26 (more detailed graphs are provided in Appendix A). From this plot it can be seen that whilst there is a wide scatter, there is a possible linear relationship between both strength and both thickness and bone volume fraction. Multiple regression analysis was used to explore this possible relationship using the model:

$$S = b_0 + b_1B + b_2T$$

Where, S, is strength, B is BV/TV, and T the subchondral thickness. Account was taken of the lack of independence between data points as due to clustering of points taken from the same glenoid. This analysis indicated that both the bone volume fraction and the subchondral thickness have a significant effect on the strength (Table 3.16). It can be observed that the effect is strongest for the bone volume fracture, but the subchondral thickness, still has a significant effect.

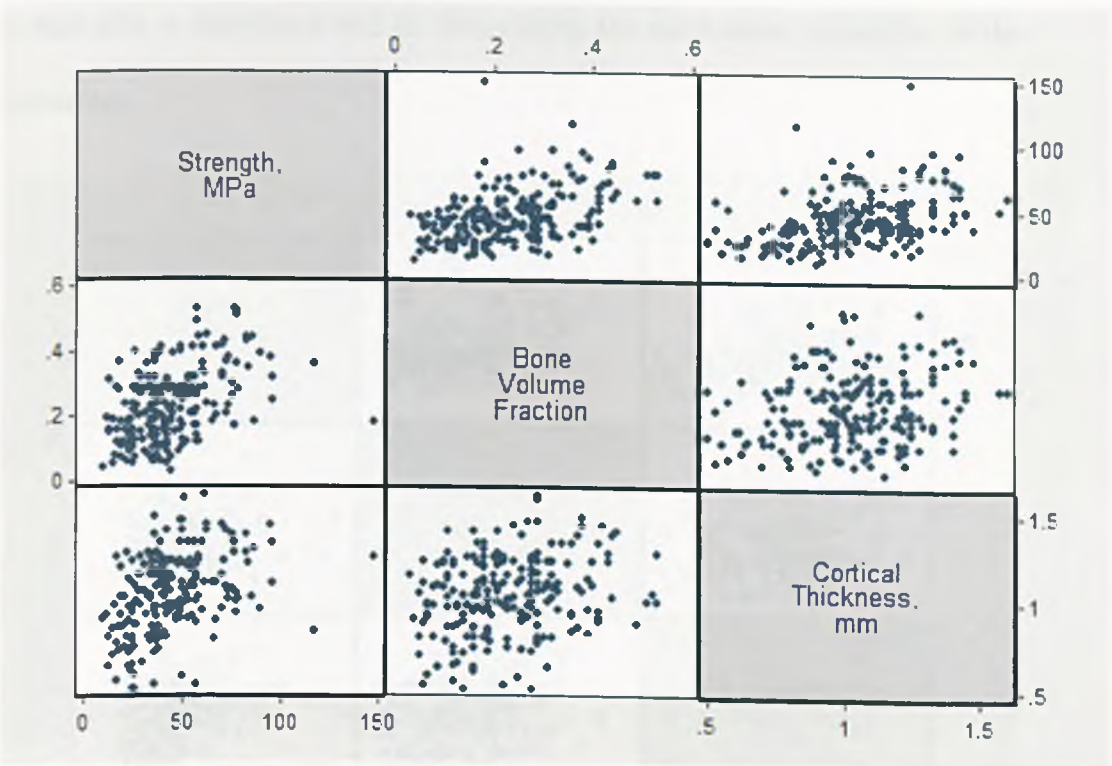

Figure 3.26 Direct associations between strength and BV/TV and the subchondral thickness.

Table 3.16 Regression of strength and BV/TV and subchondral thickness

Strength	Regression coefficients (b_i)	Standard Error in b_i	P value	Adjusted R^2: 0.31
BV/TV (b_1)	70	11	<0.001	
Thickness (b_2)	29	6	<0.001	
Constant (b_0)	-3	6	0.513	

Similar results were observed for the relationship for e-modulus versus bone volume fraction and subchondral thickness (Figure 3.27 and Table 3.17), (more detailed graphs are provided in Appendix A). As implied from Figure 3.26 and Figure 3.27, the R^2 values of 0.21 and 0.31 for the elastic modulus and strength analyses, respectively, indicate that these linear models are poor and that other

factors may play a significant role in determining the mechanical properties of the glenoid surface.

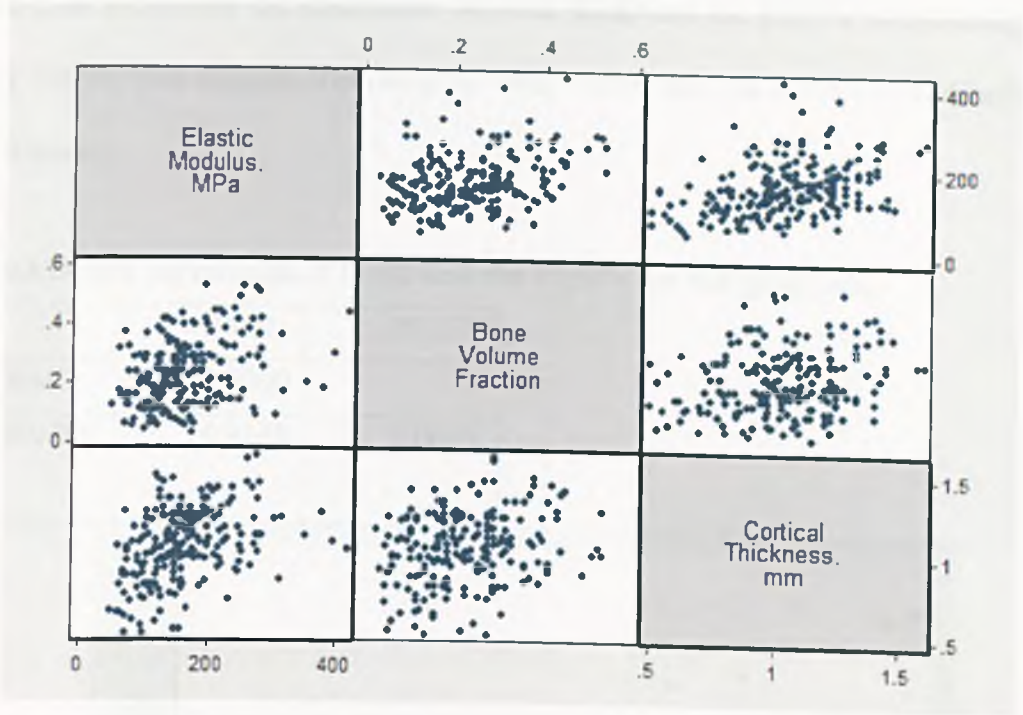

Figure 3.27 The relationship of e-modulus and the BV/TV and the subchondral thickness.

Table 3.17 Regression of e-modulus and BV/TV and subchondral thickness

E-modulus	Regression coefficients (b_i)	Standard Error in b_i	P value	Adjusted R^2: 0.21
BV/TV (b_1)	137	33	<0.001	
Thickness (b_2)	92	16	<0.001	
Constant (b_0)	34	17	0.0.47	

In each of the matrix plots a few outliers can be observed for which no experimental reason could be found for their position and, therefore, they were retained. Further, if they were removed from the analysis they made only a very marginal difference in the results.

The regression analysis in Table 3.18 is with BMD replacing bone volume to total volume ration (BV/TV) for the fresh bone. The correlation in Table 3.18 and Figure 3.28 shows that the association between BMD and the BV/TV is extremely strong ~ 92%. This suggests that using the BMD rather than the BV/TV would have no difference.

Table 3.18 The correlation of BMD and the BV/TV for the fresh bone.

	BMD	BV/TV
BMD	1.0000	
BV/TV	0.9148	1.0000

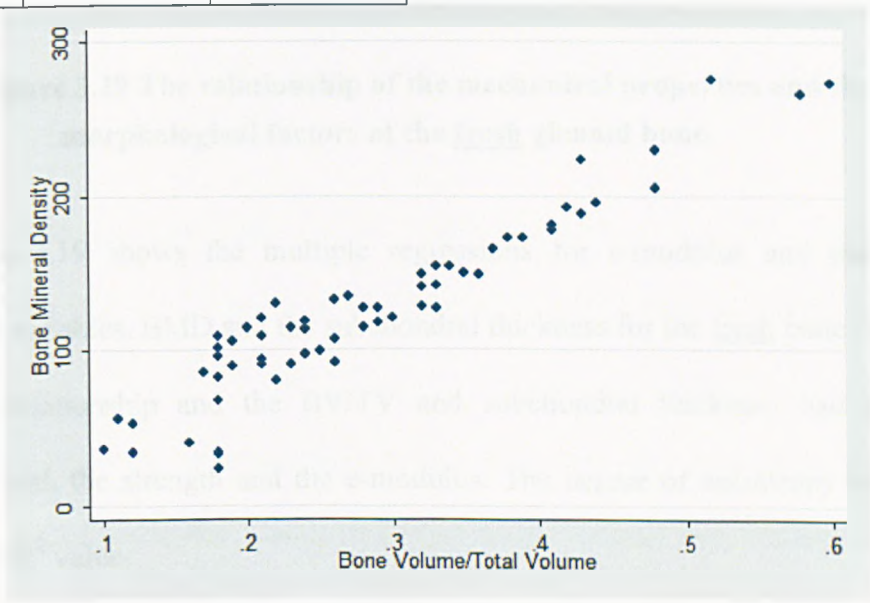

Figure 3.28 The BMD vs. BV/TV for the fresh glenoids

The direct association between strength and e-modulus and the two independent variables is displayed in Figure 3.29 (more detailed graphs are provided in Appendix A). As it was seen with the embalmed bone there was a linear relationship between strength and e-modulus, and the BV/TV and the subchondral thickness.

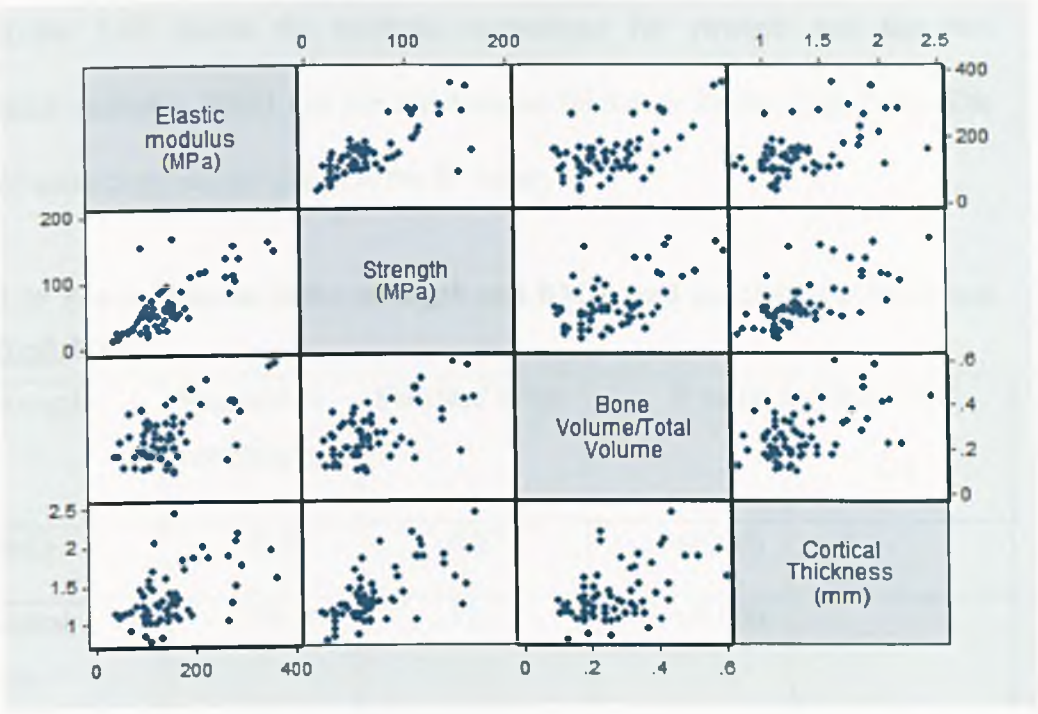

Figure 3.29 The relationship of the mechanical properties and the morphological factors of the fresh glenoid bone.

Table 3.19 shows the multiple regressions for e-modulus and the two independent variables, BMD and the subchondral thickness for the fresh bone. There was linear relationship and the BV/TV and subchondral thickness had direct association with the strength and the e-modulus. The degree of anisotropy had no effect on the R^2 value.

Table 3.19 The regression of the e-modulus and the BMD and the subchondral thickness of the fresh bone.

E-modulus	Regression coefficients	Standard Error	P value	Adjusted R^2: 0.35
BMD	0.42	0.15	<0.006	
Subchondral Th.	74	23	<0.002	
Constant	0.69	29	0.98	

Table 3.20 shows the multiple regressions for strength and the two independent variables, BMD and the subchondral thickness for the fresh bone. The degree of anisotropy had no effect on the R^2 value.

Table 3.20 The regression of the strength and BMD, and subchondral thickness of the fresh bone.

Strength	Regression coefficients	Standard Error	P value	Adjusted R^2: 0.5
BMD	0.20	0.07	<0.005	
Subchondral Thickness	56	11	<0.000	
Constant	-34	14	0.02	

The multiple regressions for the strength and the e-modulus using the independent variable BV/TV had marginal effect on the R^2 values. This explains that using BMD rather than BV/TV won't have any effect on the model. Addition of the anisotropy variable into the model has a mixed effect. For the e-modulus, it has no real effect on improving the model (not significant $P>0.05$), but it has marginal effect on the strength ($P\sim0.04$). Thus, high anisotropy may not reflect directionality in the indentation direction.

To compare the two groups a student's unpaired t-test was used to calculate the p-values (embalmed and fresh) and is provided in Table 3.21.

Table 3.21 The t-test for both groups of specimens.

Parameters	t-test	p-value	Fresh	Embalmed
			Mean SD	Mean SD
E-modulus	1.53	0.13	152 ± 71	166 ± 65
Strength	-5.94	0.00	66 ± 39	45 ± 21
BV/TV	-2.79	0.006	0.28 ±0.12	0.23 ± 0.11
Subchondral Thickness	-8.70	0.00	1.35 ±0.36	1.04 ± 0.22

From investigating the differences between the e-modulus in the two groups, no significant differences were found. Using the unpaired t-test the investigation of the differences between the strength revealed that the value was greater in the fresh specimens, and was significantly different. And the same test was carried out to compare the BV/TV for the two groups. The porosity was lower in the fresh specimens. This may explain the greater strength in this group, but not the equivalence of the e-modulus. For the subchondral thickness t-test investigation shows that the thickness was greater in the fresh specimens. And this may explain the greater the strength in the fresh bone, but some differences can be explained by a more consistent removal of cartilaginous material in the glenoid surface of the embalmed specimens. There was a significant difference between the two groups for the subchondral thickness.

To take into the account the differences in thickness and BV/TV, it can be looked by using regression analyses. Regress strength (and modulus) against the dependent variables (BV/TV, thickness and fresh/embalmed). Once these variables have been taken into account (BV/TV, thickness) then the results appear different

between fresh and embalmed. Strength shows no significant difference between the two groups (t=0.65, P = 0.52), however, now e-modulus shows a significant difference (t=-4.3, P = 0.00).

3.4 GLENOID COMPONENT FIXATION

3.4.1 Introduction

To obtain a better understanding of the dynamic behaviour of the glenoid component fixation, a bone substitute was used instead of a natural glenoid component due to the inherent variability in cadaveric materials. Further, the bone substitute was used because of its availability, relatively low cost and its similar properties to osteoporosis cancellous bone, which allow us to reduce the number of samples with which to compare important parameters. Although for purposes of validation that comparison with cadaveric glenoids would have been ideal these were not available. Previous tests had used Sawbone materials but these were of the closed pore nature, which do not allow the correct cement interdigitation. The type used here was of an open pore variety which has a porosity of approximately of 85 %, which is at the lower end of the range observed in the cadaveric samples. This value is particularly reflective of the more osteoporotic specimens of the age of 80 years and older.

3.4.2 BV/TV of trabecular bone and Sawbones

To compare the bone volume fraction of the sawbones and fresh trabecular bone, different regions of interest of both materials were measured from the microCT (Figure 3.30). Table 3.22 provides the BV/TV for both trabecular bone and Sawbones used in our simulation technique. The regions were chosen with regard to the 11 pre-selected regions on the glenoid. The result showed different regions of

sawbones showed slightly different values of bone volume fraction. This indicates that the Sawbones doesn't consist of a unique BV/TV values throughout its structure. The bone volume fraction of some of the glenoid bone had higher values than the Sawbones, when taking the minimum and maximum values. For some regions the values were lower for the Sawbones, but were significant for zones 4 and 7. These zones had lower BV/TV values in comparison to the posterior and superior regions of the glenoid.

Table 3.22 The bone volume fraction of glenoid trabecular bone and Sawbones

Regions	Glenoid Bone BV/TV		Sawbones BV/TV
	Mean	Range	Mean
Zone 2	0.24	0.16-0.38	0.13
Zone 4	0.21	0.14-0.27	0.16
Zone 7	0.28	0.13-0.34	0.19
Zone 10	0.44	0.29-0.60	0.15
Zone 5	0.23	0.13-0.37	0.14

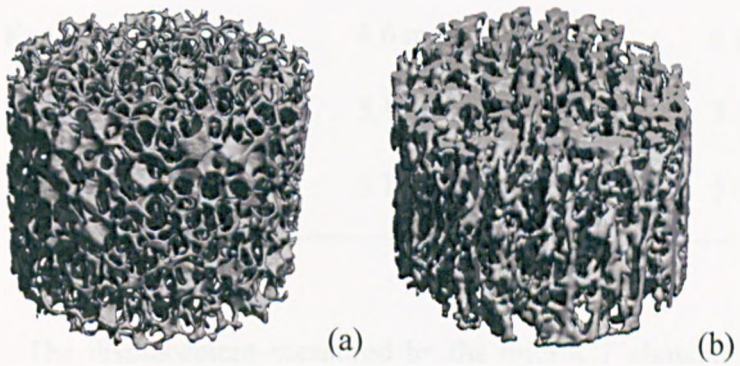

Figure 3.30 (a) Open cell Sawbones microCT image and (b) The glenoid trabecular bone image.

As outlined in the methods chapter two sets of tests were carried out both utilising 3 specimens for two types of glenoid components, keel and peg. Any subsidence was measured by both changes in displacement gained from the linear variable displacement transducer on the fatigue testing machine and the microCT scanner.

3.4.3 Components displacement

The results obtained from microCT images pre- and post-simulation provided the component displacement with regard to the sawbones destruction. Table 3.23 shows the displacement result for both 400-1000N and 800-1800N from the microCT images. These displacements were obtained using IDL software.

Table 3.23 MicroCT components displacement

Components (size 48)	400N-1000N Pre + Post simulation	800N-1800N Pre + Post simulation
Peg 1	5.4 mm	3 mm
Peg 2	5.9 mm	5.5 mm
Peg 3	3.5 mm	2 mm
Avg. ± SD	4.9 mm ± 1.3	4 mm ± 2.6
Keel 1	5.5 mm	6 mm
Keel 2	4.6 mm	6 mm
Keel 3	5.1 mm	3.5 mm
Avg. ± SD	5.1 mm ± 0.45	5.6 mm ± 1.84

The displacement measured by the microCT showed slightly higher values for the keel components in both sets of cyclic loads. There was a no significant correlation between the two types of components. The peg component had slightly

less subsidence rate and could show that this type of components can have better result in glenoid fixation.

Using the recordings from the LVDT the components displacement over time for keel and peg components at the two set of cyclic load was measured. The 100,000 cycles were completed in 28 hours time. The component displacement measured by subtracting the displacement with regards to the 2min from the simulator starting position for each of the keel and peg components. The measurement started from cycle number 100, to allow the machine's settlement. Figure 3.31 and Figure 3.32 provide the normalized displacement results verses cycles for the keel and peg components; respectively. The overall measurement showed that there was more displacement in the 400N-1000N through out the test, which can explain the earlier destruction of the Sawbones in the initial loading condition, in 800N-1800N. Greater component subsidence was observed in the higher loading condition. At the initial loading condition of 800N-1800N the Sawbones deformation could be seen visually, which in comparison to the lower loading condition this was different and deformation of the sawbones could occur in any stage of the test. However, there was no pattern between the low and high loading to be able to distinguish the difference of these two using the Sawbones.

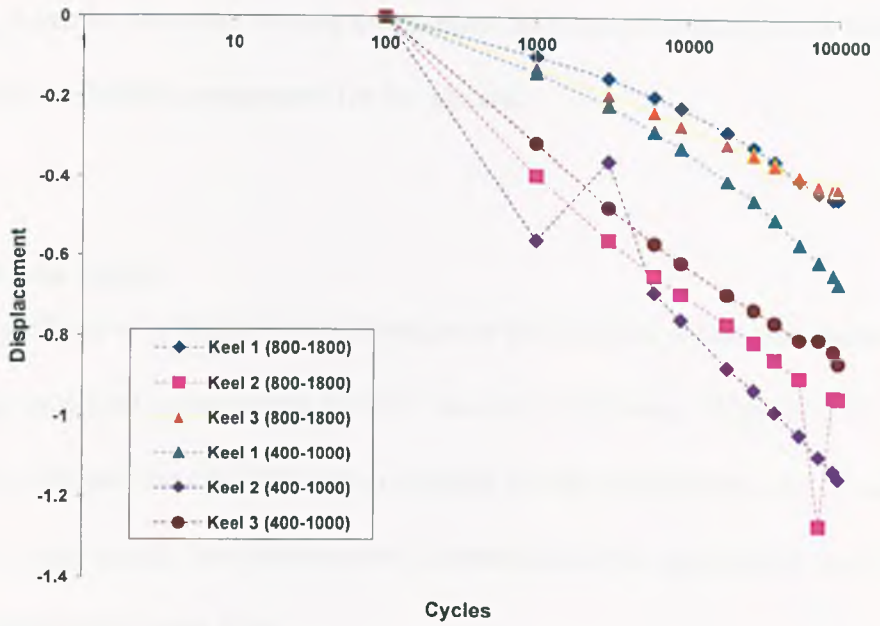

Figure 3.31 The relative displacement for two sets of cyclic loading for keel components.

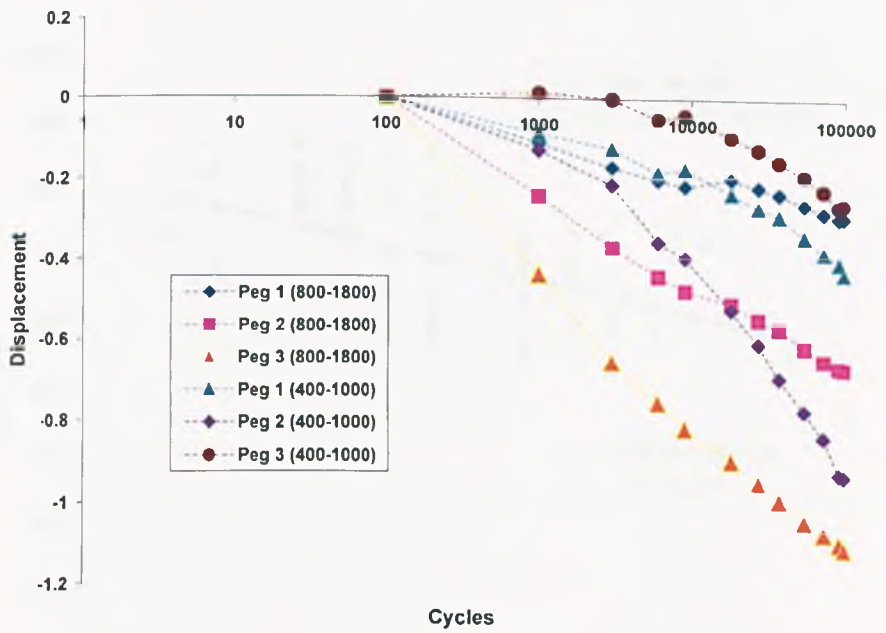

Figure 3.32 The relative displacement for two sets of cyclic loading for peg components.

The keel displacement was higher than the peg component in 800N-1800N cyclic loading and the keel displacement had higher subsided ratio with comparison to the peg component. By observing the displacement behaviour of the keel

component, it can be seen that the peg component had less movement and could be chosen as a better fixation component for the glenoid.

3.4.4 Stiffness results

The stiffness of different cycles throughout the simulation test was measured for both peg and keel components in both loading conditions. Figure 3.33 is a sample of the stiffness versus displacement graphs for the components. As it can be observed from the graph, the displacement increased and the gradient of the slope could be obtained from these plots.

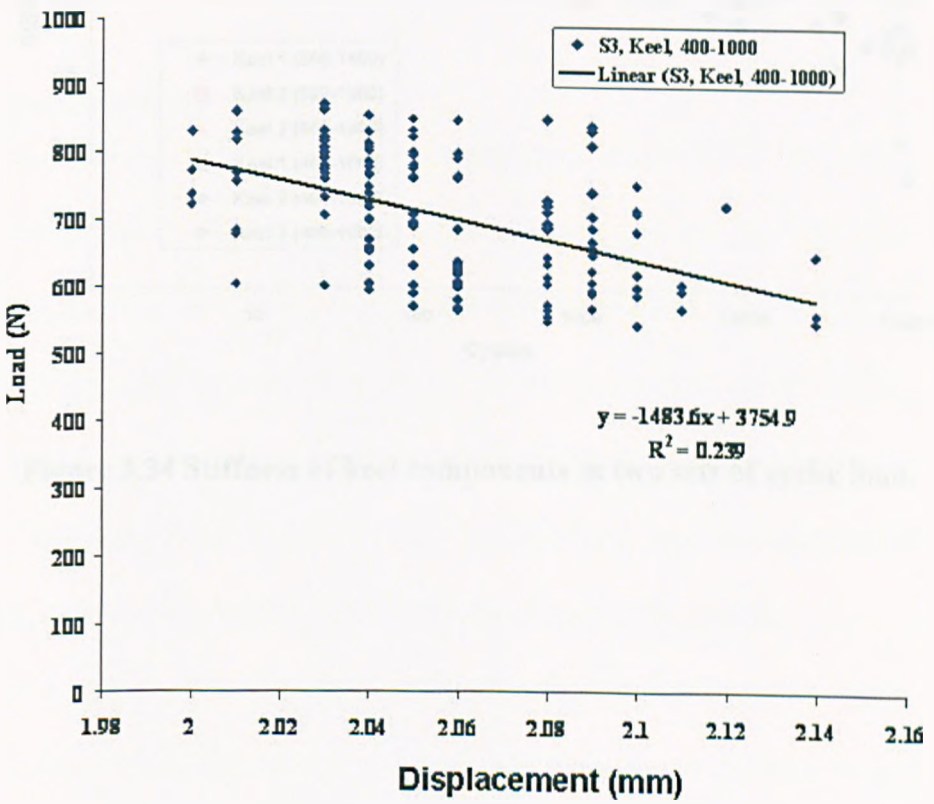

Figure 3.33 Load verses displacement, keel 400N-1000N.

Figure 3.34 and Figure 3.35 show the stiffness results of different cycles for keel and peg components, respectively. The deformation showed at 800N-1800N loading, was higher and the graph followed a more steady profile than the 400N-1000N cycles. Under initial cyclic loading the maximum deformation occurred, and could be seen visually. The stiffness was higher in 800N-1800N do to the fact that the Sawbones deformed in the initial stage of the test causing more stiffness and more steady profile throughout the test.

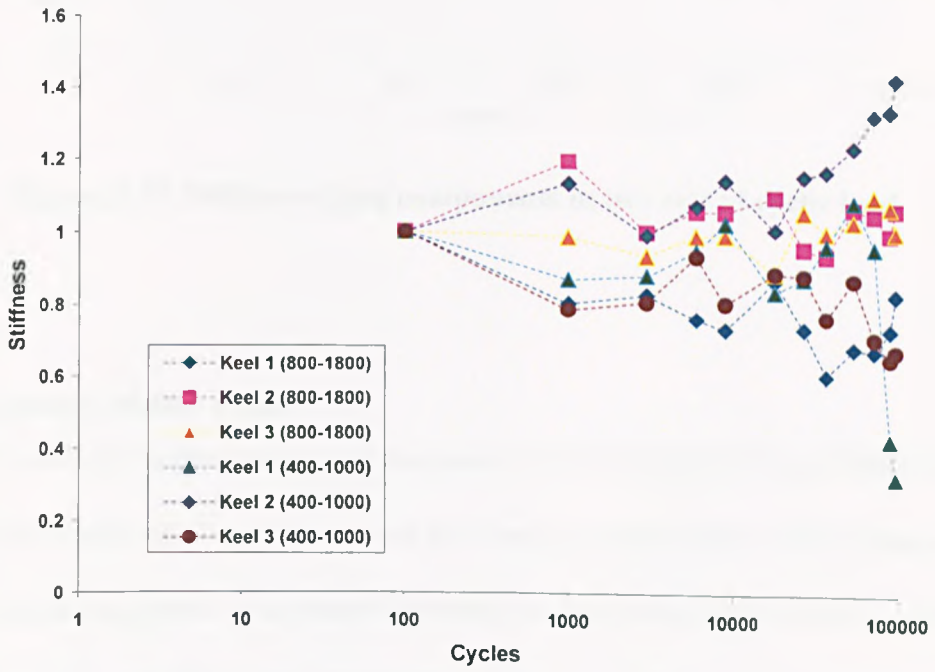

Figure 3.34 Stiffness of keel components in two sets of cyclic load.

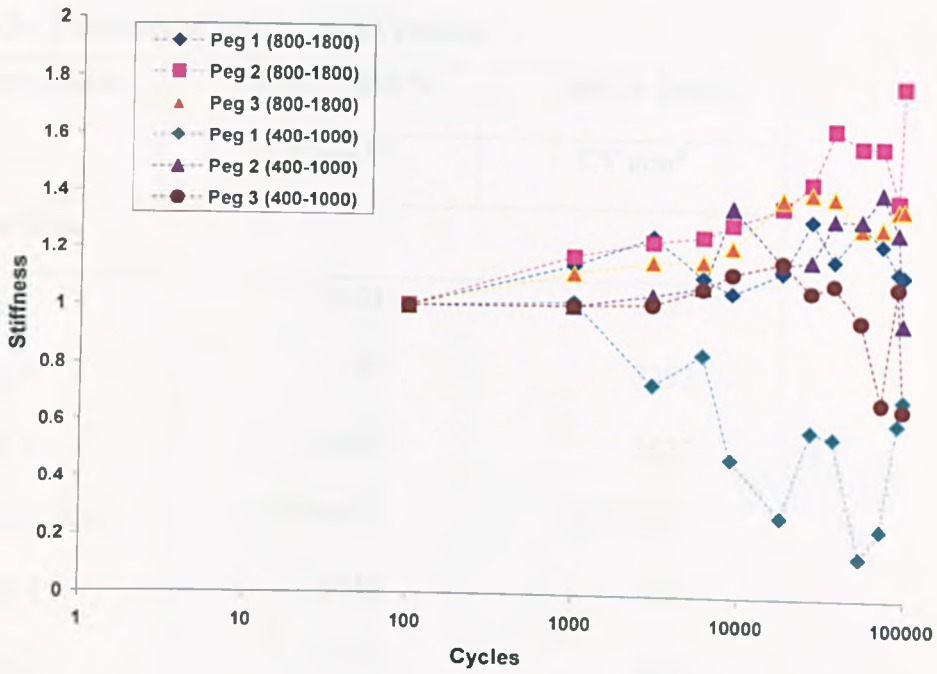

Figure 3.35 Stiffness of peg components in two sets of cyclic load.

3.4.5 Cement volume results

The volume of the cement was measured from the microCT data. Table 3.24 provides the results of CV of the cement pre- and post-simulation. The volume of cement used in the glenoid component fixation is an important factor in reducing the risk of loosening, and the surgeon technique is also a concern in this regard. Less cement volume was used in keel components in comparison to the peg components in 400N-1000N, and more in 800N-1800N. This explains that the surgeon technique can vary in choosing the volume of cement necessary for the operation and to reduce any risk of loosening a fixed amount can be prepared prior to insertion. There were slight changes in comparing the CV pre- and post-simulation, which can explain the volume of cement can change slightly over period of time. The microCT was used to show this comparison and the changes in the cement volume. This can explain that there will be slight changes in the cement volume post surgery.

Table 3.24 The cement volume (CV) results.

Component	400 N-1000 N	800 N-1800 N
	CV mm^3	CV mm^3
Pre-Sim.		
Peg 1	5054	3297
Peg 2	3687	3293
Peg 3	5470	3637
Avg. ± SD	4737±933	3409±197
Keel 1	5243	3690
Keel 2	4062	4695
Keel 3	3639	3617
Avg. ± SD	4315±831	4000±602
Post-Sim.		
Peg 1	5373	3270
Peg 2	3653	3261
Peg 3	5563	3628
Avg. ± SD	4863±1052	3386±209
Keel 1	5026	3642
Keel 2	4243	4553
Keel 3	3505	3558
Avg. ± SD	4258±761	3918±552

Figure 3.36 shows the cement volume values from pre-simulation and post-simulation for the two set of cyclic loading. This indicated that there was a slight

difference between the volume before and after simulation, and the volume of cement used in the 400 N – 1000 N was slightly higher.

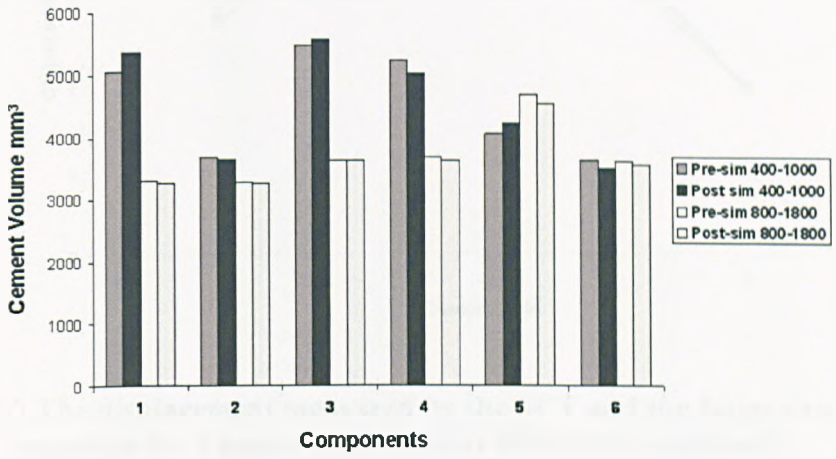

Figure 3.36 The cement volume of the six peg and keel components

An example of the displacements of the components measured by the microCT images and the fatigue machine are compared in Figure 3.37. The displacement in both measurements followed the same profile. It should be indicated that the Sawbones destruction occurred in the first few seconds of the test and could be seen visually.

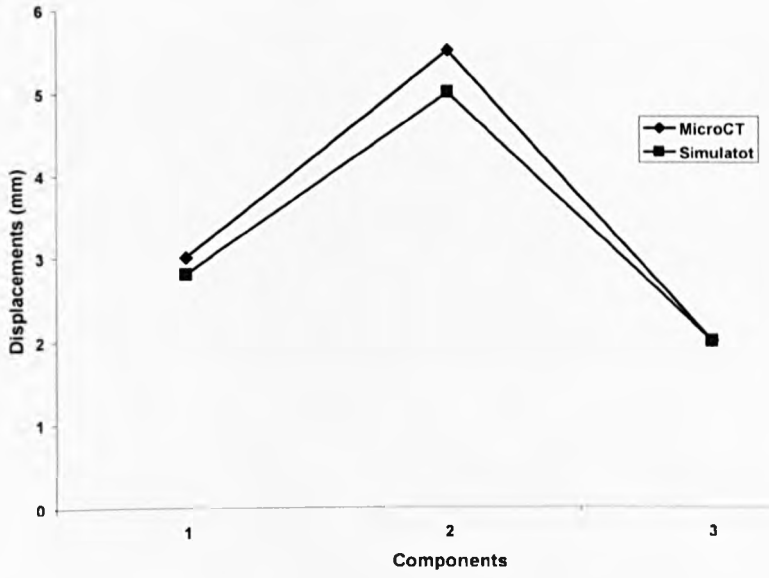

Figure 3.37 The displacement measured by the uCT and the fatigue testing machine for 3 pegs components at 800-1800 cyclic load.

3.4.6 The cement thickness

The average results of the cement thickness measured in seven different positions in X and Y direction of each keel and peg for 400N-1000N and 800N-18000N are given in Table 3.25.

Table 3.25 The average cement thickness surrounding each component

Component	400 N – 1000 N		800 N – 1800 N	
	Cement Thickness (mm)	SD	Cement Thickness (mm)	SD
Peg 1	2.56	±0.48	2.59	±0.80
Peg 2	2.11	±0.36	2.37	±0.40
Peg 3	2.45	±0.51	2.97	±0.75
Keel 1	3.12	±0.20	3.33	±0.43
Keel 2	3.17	±0.51	3.28	±0.60
Keel 3	2.61	±0.23	3.07	±0.52

Figure 3.38 shows the subsidence and the cement thickness for the keel and peg components.

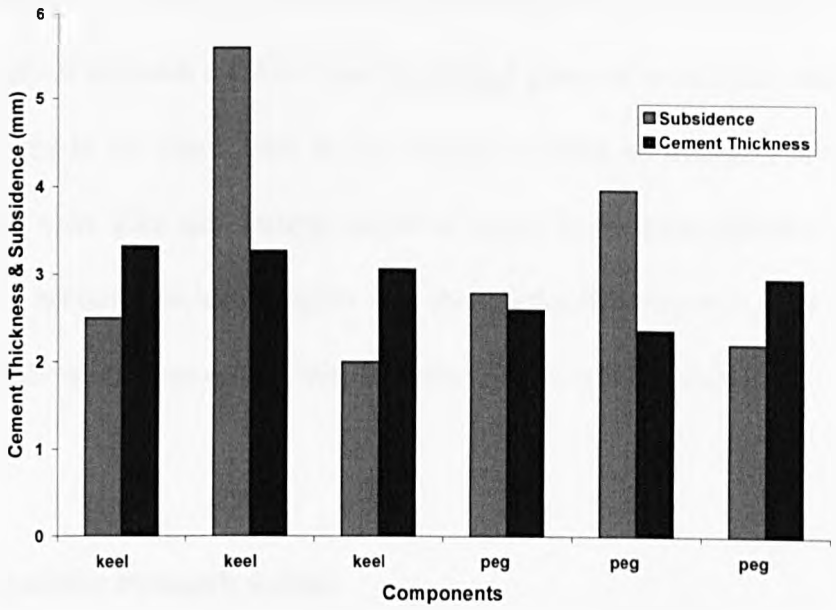

Figure 3.38 The cement thickness and the subsidence of peg and keel components.

In correlating the cement thickness and subsidence values, the $r_{pearson}$ was 0.021 and the p value 0.97. And in correlating cement thickness and the stiffness, $r_{pearson}$ was -0.33 and the p value 0.52. This can explain that there was no significant correlation between the cement thickness and the subsidence and the stiffness of the component, therefore, the volume of cement had no effect on the degree of subsidence. And this can explain that the subsidence occurred in the Sawbones rather than the components.

3.5 PULLOUT STRENGTH OF SUTURE ANCHORS

3.5.1 Introduction

A total of 32 tests were carried out, providing the glenoid BMD and the pullout strength of different regions. Nine embalmed glenoids were used, which only eight were listed in our result, due to the damage to bone on insertion. Two fresh frozen glenoid were also tested using Ethibond suture in the three anterior regions. The following section provides insights into the relationship between bone mineral density, the pullout strength and the displacement of the suture anchors.

3.5.2 The pullout strength values

While cycling at submaximal loads all anchors yielded initially by cutting through the cancellous bone until coming to rest against the cortex. The movement of the anchors and its positions were observed visually. Figure 3.39 shows the displacement of the anchor prior to apply cyclic loading. There was then no further movement until pullout. From the thirty two measurements of loading to failure in only six cases were suture breakage recorded. During two of the pullout tests the pc stopped and the load values were recorded from the analogue section of the machine. The highest load peak was chosen as the failure force, either for suture or anchors failure.

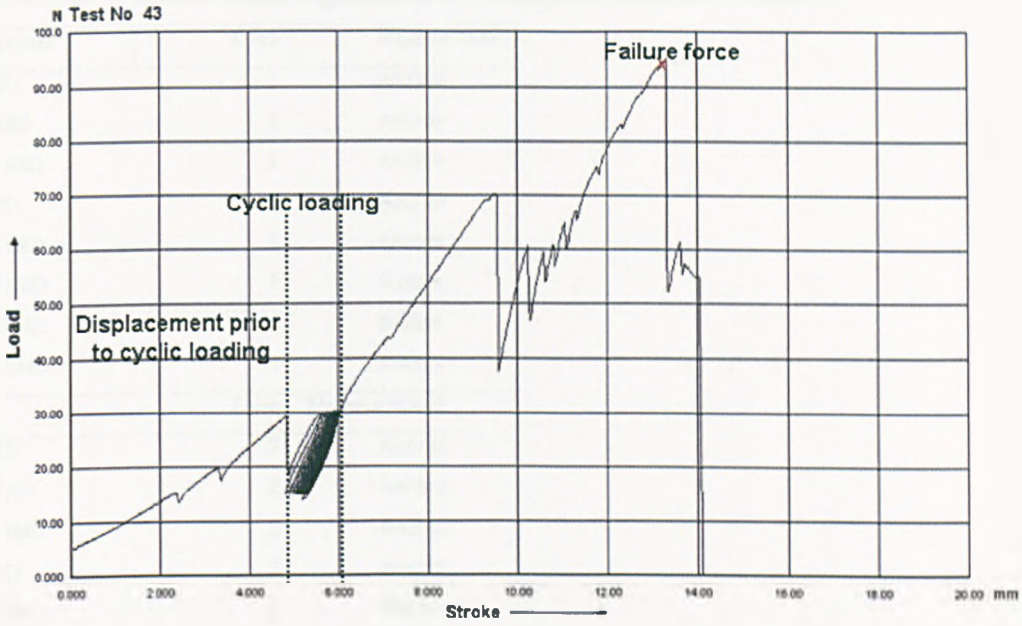

Figure 3.39 Initial migration of the anchor prior to pullout testing.

3.5.3 Relationship to bone morphology

While cycling at submaximal loads all anchors migrated. Six procedures failed within the suture materials (189±25N) whilst the remaining 25 failed by anchor pullout (126±40N), (Table 3.26). Figure 3.40 shows the relationship of the BMD to the pullout strength of the embalmed glenoids..

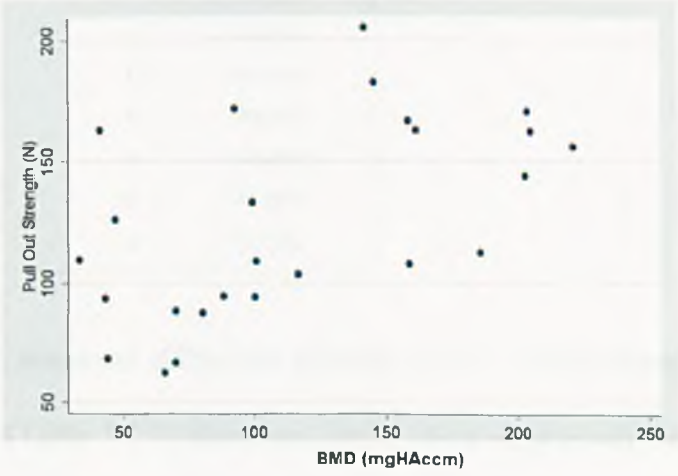

Figure 3.40 The relationship of the pullout strength to the BMD of the embalmed bone.

Table 3.26 The 4 zones of the 8 glenoids showing the material failure.

Glenoid	Zone	Material failure
G1/02 BMD	1	Anchor
G32/02 BMD	1	Anchor
G36/01L BMD	1	Anchor
G6/02 BMD	1	Anchor
GNoNuL BMD	1	Anchor
GuN/15L BMD	1	Suture
GuNM6L BMD	1	Suture
GuNM2R BMD	1	Anchor
	Zone	Material failure
G1/02 BMD	2	Anchor
G32/02 BMD	2	Anchor
G36/01L BMD	2	Anchor
G6/02 BMD	2	Anchor
GNoNuL BMD	2	Anchor
GuN/15L BMD	2	Suture
GuNM6L BMD	2	Anchor
GuNM2R BMD	2	Anchor
	Zone	Material failure
G1/02 BMD	3	Anchor
G32/02 BMD	3	Anchor
G36/01L BMD	3	Anchor
G6/02 BMD	3	Anchor
GNoNuL BMD	3	Anchor
GuN/15L BMD	3	Anchor
GuNM6L BMD	3	Suture
GuNM2R BMD	3	Anchor
	Zone	Material failure
G1/02 BMD	4	Anchor
G32/02 BMD	4	Suture
G36/01L BMD	4	Anchor
G6/02 BMD	4	Anchor
GNoNuL BMD	4	Anchor
GuN/15L BMD	4	Anchor
GuNM6L BMD	4	Anchor
GuNM2RBMD	4	Suture

There was no statistical difference between anchor failure strength and zone ($F=2.53$, $P=0.077$) (Table 3.27). However, there was a strong correlation between pullout strength and the local BMD, ($r_{pearson} = 0.56$, $P = 0.004$) for anchor failure. During pre-conditioning specimen mean slippage for each zone was between 3.9mm

to 5.7mm (Table 3.28). A significant correlation was observed between slippage and the BMD ($r_{pearson}$ = -0.38, P = 0.05). This can explain in regions of high BMD the slippage was lower and the pullout strength was higher.

Table 3.27 Pullout failure strength and the bone mineral density.

Zone	Pullout failure strength (N)			BMD (mg HA/cm^3)		
	Mean		SD	Mean		SD
1	162	±	51	156	±	82
2	113	±	35	101	±	64
3	118	±	36	111	±	67
4	160	±	47	125	±	65

Table 3.28 Initial displacement of the anchor

Zone	Displacement (mm)		
	Mean		SD
1	3.9	±	1.3
2	5.8	±	1.0
3	5.6	±	2.0
4	4.8	±	1.7

Figure 3.41 shows the median and higher values of the pullout force, the BMD, and the displacement, respectively. The highest pullout force value was obtained at the posterior and anterior-superior regions. The same distribution

obtained for the BMD values, but the displacement was higher at the anterior-inferior region. This explains that again the inferior-anterior region is the weakest area of the glenoid bone.

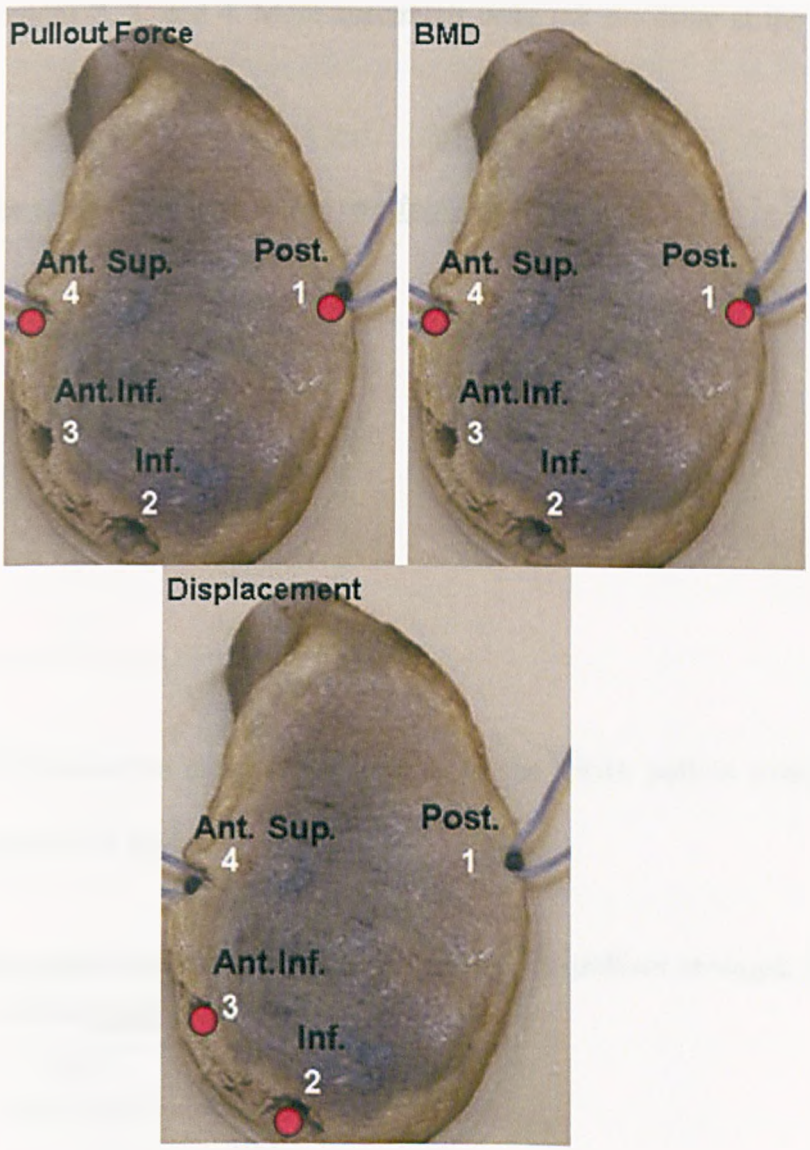

Figure 3.41 The pullout force, the BMD, and the displacement of the glenoid for the 4 anchored regions (red dot represent higher values).

The pullout force spatial values of the eight embalmed glenoid range from 69.3N to 184.1N. The values of the failure force for the suture ranged from 165.90N

to 225.10N, and the pullout failure force for the anchors ranged from 62.4N to 205.1N.

Table 3.29 shows the material failure of the two fresh frozen glenoids, anchored in regions 2, 3, and 4. More specimens were not available at the time of testing.

Table 3.29 The material failure of the two fresh cadavers.

Glenoid	Zone	Material failure
18/06 R	2	Suture
	3	Anchor
	4	Suture
15/06 L	2	Anchor
	3	Anchor
	4	Anchor

Table 3.30 shows the mean and SD values of the BMD, pullout strength and the displacement of the fresh glenoids.

Table 3.30 The mean and the SD values of the BMD, pullout strength and the displacement of the fresh glenoids.

Zone	BMD ($mgHAcm^3$)		Pullout strength (N)		Displacement (mm)	
	Mean	SD	Mean	SD	Mean	SD
2	116	± 24	110	± 43	3.1	± 0.42
3	135	± 11	102	± 52	4.7	± 2.40
4	139	± 38	113	± 4	4.1	± 0.80

An unpaired t-test was used to investigate the differences between the pullout strength in the two groups which showed no significant differences; t =1.55, P =0.13. An unpaired t-test to investigate the differences between the pullout strength

in the two groups, for those with anchor failure only showed no significant difference t=1.30 and P = 0.20 too. Again unpaired t-test was used to investigate the differences between the BMD in the two groups, and no significant difference t=-0.23 and P = 0.81 was obtained. Another t-test was used to investigate the differences between the displacements in the two groups showed that there is no significant differences; t=1.32 and P = 0.19. By looking at the regression of the two groups, effect looks marginally significant, with the higher strengths in the embalmed group; t = -1.94, P = 0.061.

3.5.4 Summary

This chapter has presented the result and the use of different methods in glenoid morphological and mechanical properties analysis. The BV/TV, subchondral thickness and the DA values showed to have impact on the mechanical properties (e-modulus and the strength) of the glenoid. The open cell sawbones was used to show the different component behaviour in glenoid fixation. This type of sawbones was useful in cement penetration, but not for modelling the shoulder arthroplasty. The pullout of Orthocord suture demonstrated that this type of suture is strong to be used in soft tissue reconstruction. And the statistic analysis of embalmed and fresh cadavers revealed that there were significant differences between the groups in indentation sites. However, more work is required to understand the shoulder arthroplasty properties.

4 Discussion

4.1 INTRODUCTION

This chapter presents the discussions of the analysis results obtained from the studies. The first part discusses both the results on bone morphology followed by the mechanical properties. The second section presents the glenoid fixation properties, and the final section discusses the pullout strength of suture anchors.

4.2 GLENOID BONE PROPERTIES.

In general, the regional variations in both the morphological and mechanical characteristics were in keeping with previous studies [30, 93]. However, there were disparities in the absolute values of both the elastic modulus and strength reported here and those accrued elsewhere which can result from a number of factors that include dissimilar specimens and significant variation in the experimental protocols and analyses [93] including the removal of the subchondral bone [82]. The choice of the indentor shape is also an important factor in achieving an accurate result. Grant et al [213] used hemispherical indentor for vertebra endplate analysis. They concluded that the shape of the indentor would tend to introduce error into the stiffness measurements, since the indentor area in contact with the bone changes as the indentation depth increase. However, in using flat indentor, this should be placed normal to the surface to prevent any edge creation in each indented area.

4.2.1 The morphological properties of the glenoid

The main purpose of this study was to provide valid information on bone volume fraction of different parts of the glenoid and its influence on the strength and the e-modulus. The significant differences in distribution of the BV/TV found in this study explain previous findings of the mechanical properties of the glenoid. The data provided from this study indicate that the glenoid consists of medium density cancellous bone.

This was the first study to combine indentation and microCT analyses to investigate the relationship between the glenoid's mechanical properties and bone morphology. The distribution of BV/TV and DA across the glenoid surface was found to be similar to that reported by Frich et al [82] and for BMD measurements by Lehtinen et al [167]. Significant differences were obtained with positions across the glenoid surface. A trend of BV/TV at the posterior edge of the glenoids was found in both embalmed and fresh specimens. There was also a significant correlation of the BV/TV to the age of the specimens. In particular in keeping these studies a band of bone across the glenoid that may provide superior mechanical properties for fixation of the glenoid component in terms of BV/TV was identified. This band runs from the base of the coracoid backwards through the central glenoid to the posterior margin. It is notable that the anteroinferior region has the poorest structural (lowest porosity) and biomechanical properties (lowest strength), fitting with the clinical observations of substantial bone loss secondary to instability [214]. This relationship also merits further study due to the fact that the biomechanics of instability and propensity for adverse impingements are also important as well as the mechanical properties of bone. The BMD of the fresh glenoid was also higher in the posterior margin and had similar trend to the BV/TV. The degree of anisotropy also was

higher at the mid-superior and the posterior edges and more isotropic at the superior and anterior edges. The DA was higher at the peripheral zones and more isotropic deep central. There was significant correlation of DA and the age of the specimens. However, the subchondral thickness measurements differ substantially from those previously reported [93]. Both the local bone volume fraction and the subchondral thickness influenced the strength at the glenoid surface as well as the elastic modulus of the bone. However, the explained variance was small and other factors not incorporated into this model may also have a significant impact on the strength and elastic modulus. The subchondral thickness is not correlated to the age of the specimens. The subchondral thickness was higher at the superior and the posterior edge and this can explain the higher strength in these regions.

In this particular set of experiments cadaveric tissue was used that had been embalmed and frozen fresh. Anglin et al [30] had previously suggested that embalmed preservation had minimal impact on the quality of the results for this type of experiment. In this respect the results in the study appeared contradictive in that simple comparison of the data showed a significant difference in the strength whilst a more robust analysis using regression, which takes account of the differences in the underlying porosity and subchondral thickness, showed a difference in elastic modulus. Overall the results suggest, however, that bone quality in terms of mechanical properties is altered following embalming and that this assertion by Anglin is incorrect. However, the general trends appear to be the same regardless of whether embalmed or fresh bone is used.

It has also reported that small changes in porosity or density of compact bone exert a more pronounced influence on its stiffness than would similar changes in trabecular bone [215, 216]. The strong correlations of compact bone elastic modulus with

bone volume fraction, a parameter for intracortical porosity, support this observation [79, 216]. McCalden et al. reported that changes in porosity accounted for 76% of the reduction in the strength of cortical bone [217]. In this study, linear relationship for μCT - porosity versus strength and elastic modulus were observed.

The advantages of microCT imaging are that it is a non-destructive, non-invasive, and precise procedure that allows measurement of trabecular and cortical bone of whole bones, as well as the repetitive 3D assessment and computation of microstructural properties of specimens. The structural indices determined from the micrographic images are dependent on the thresholding procedure used, which itself is dependent on the mineralisation of the bone and hence it's radiographic absorbency. To achieve a constant value for the measurements, a fixed threshold value was chosen for all measurements, making the segmentation efficient and fast, but which may lead to errors if differences in mineralisation varied across or between specimens. Changing the threshold value would alter the volume fraction values.

Significantly higher densities observed in the posterior superior region of the glenoid vault represent structural adaptation to functional stresses. Hayes et al [91] have mentioned that the cancellous bone is more dense in regions of higher stresses. The higher density area in the posterior part of the glenoid coincides with the direction of the trabeculae. Stresses are thought to be higher in the posterior glenoid vault.

The subchondral plate is not a completely solid structure. It contains vascular channels and occasionally small marrow spaces in fresh bone [94, 218]. It is, therefore, the embalmed glenoid thickness values found to be lower than values

found by Frich et al [93], Simikin et al [94] and the values from the fresh bone in this study. Although the calcified subchondral layer makes determination of cortical thickness difficult in fresh bone, this is not applicable to cadaveric bones prepared in papain, which have an easily defined surface plane.

4.2.2 The mechanical properties of the glenoid

The differences with respect to mechanical properties of the glenoid regions could, in part, be explained by the differences in trabecular microstructure. As expected the trends in the elastic modulus and strength data were extremely similar. This strong linear relationship between strength and modulus is supported in the literature [219, 220].

Since the radial direction is the strongest direction in the glenoid [82, 84, 93], the greatest differences being at the surface where the anisotropy is highest [30]. In this study the DA was higher in the mid-superior and posterior regions, where the strength was marginally higher. These directions play a role in the resistance to loading of glenoid prosthesis. At the surface, the trabeculae are oriented perpendicular to the surface [93, 221].

A more complete bone model for evaluating prosthesis performance should include the effect of age, sex and activity level which have dramatic effect on the bone properties [205, 222] . However, the result used here suits only the older population. Nevertheless, the small size of the indentor, spanning only a few trabecular spacing, caused even higher differences [223]. This study determined the strength and modulus throughout the cortical glenoid vault of nineteen glenoids by means of in situ indentation technique.

During surgery, parts of the central portion of the subchondral bone are usually removed and subsequently replaced by cement. It is this bone which appears to be the strongest and should be preserved to strengthen the glenoid structure.

The strength was higher in the superior and middle regions for both the embalmed and the fresh bones. The strength and the e-modulus had slight correlation with the age of the specimens.

The upper extremity is usually positioned anterior to the body during activity, adding a transverse contact pressure on the posterior part of the joint surface. The effect of increased stress to the posterior glenoid vault may be enhanced in cases of osteoporosis or muscle imbalance [2]. Apart from the compressive stresses of the arm movement, the pull exerted by numerous muscles and ligaments also applies some influence on the pattern of trabecular organization of the glenoid. This effect was remarkable at the inferior portion of the glenoid, which is affected by the pull from the long head of the triceps tendon and the intracapsular, inferior glenohumeral ligaments [224].

The stronger morphological factors had effect on the e-modulus, and there was a linear relationship (embalmed and fresh) between the e-modulus and the BV/TV, subchondral thickness and the DA. The DA did not show real effect on the e-modulus but marginal effect on the strength. Thus anisotropy may not reflect directionality in the indentation direction.

The e-modulus in the two groups showed no significant differences, but the strength was greater at the fresh specimens and significant differences were seen. The porosity was lower in fresh bone, which could explain the stronger strength in fresh bone too.

The cancellous bone within the glenoid exhibits a remarkable degree of organization suggesting the existence of a glenoid centre of pressure at the posterior cortex. The cancellous bone underneath the glenoid surface is shaped to absorb vertical loads. The regions around the dome area shaped to with stand shear stresses from translational movements of the humeral head on the joint surface.

4.3 GLENOID FIXATION

Although loosening of the glenoid component is a common complication of total shoulder arthroplasty, there is a limited basis for selecting a particular design of glenoid. Several studies have been undertaken on component fixation [111, 139, 169], but there are none that have investigated the relationship between the peg and keel design, the cement mantel and initial fixation strength. These previous studies have used synthetic glenoid models with consistent geometry and mechanical properties [169, 225, 226]. However, these Investigations have used polymeric foams with closed cells which do not allow the bone cement to flow and hence interdigitise as is the case with cancellous bone during insertion of the prosthesis were used [139, 169]. Experiments in this study were carried out with open cell foams that would enable the cement to flow within the surrogate bone structure and provide a more suitable morphological model.

The glenohumeral joint is subjected to a large range of loads and motions *in vivo* [227], but to undertake a realistic dynamics testing scenario then a simplified loading protocol needs to be utilised. In this case loads in keeping with those measured in clinical studies were chosen. In addition a loading protocol that included an eccentric load was utilised that would mimic the so-called rocking horse

phenomenon, which has been suggested to be the cause of glenoid component loosening.

From this study, it's clear that the Sawbones material is not applicable for mechanical testing of glenoid fixation. It may, however, be useful for looking at different cementing techniques and the interdigitation of cement for different cement formulations, designs of prostheses or surgical procedures. To test the shoulder arthroplasty a different foam may be used to look at different components performance.

4.4 PULLOUT STRENGTH OF SUTURE ANCHORS.

Many factors have been shown to affect the strength and durability of shoulder repairs for instability. Some of these are hardware dependent and may affect choice of implant or the way in which implants are used. For example anchor design and orientation [155, 157, 159] has an effect on initial and/or fatigue strength that is easy to demonstrate in the laboratory. Suture materials also have an obvious effect on the strength of repairs. Both the material properties and that gauge of sutures have a direct relationship to the strength of the construct.

Useful data has been derived on the pull out performance of suture anchors from other studies [153, 156, 164, 228, 229] and this allows some extrapolation on a qualitative if not quantitative level. Cadaveric human studies are now becoming available that have demonstrated some of the factors that can affect the strength of Bankart repairs. These include basic studies on pullout strength [154, 230, 231] and fatigue characteristics with cyclical loading, which might be relevant to the rehabilitation period [232]. The effect of biological parameters such as cortical thickness [164] has been observed and it is in this arena that the knowledge of this study is most rapidly

evolving. Unfortunately the cortical thickness at the glenoid rim varies substantially across distances of millimetres and this depends fundamentally on whether the measurements are made towards the articular surface or along the rim. The interplay between cortical thickness and underlying glenoid structure is simply not understood as yet. The other important parameter is the different location of the anchor in the glenoid. In this study the location of the anchors was specified by dividing each glenoid to 8 equal sections and locating the anchor in the same spot for each specimen. In this way, the repeatability of the measurement could be achieved.

This study has taken a cadaveric model and correlated the performance of a repair under initial cyclical loading followed by load to failure using a suture anchor that is in common clinical use. This has been combined with a newer suture material that is of sufficient strength that suture breakage was rarely responsible for loss of fixation - in almost all instances the system could be loaded until bone failure occurred. From this study it was observe that the effects of bone mineral density on the strength of fixation not only because of the variation in this parameter between specimens tested but also because of the variation that occurs around the rim of the glenoid. The strength of fixation that has been previously observed and related to cortical thickness [164], but not bone mineral density. Our measurements were made with quantitative microCT methods.

The study has shown that anchor pullout occurred due to bone failure at a value of between 101N and 156N in the embalmed bone. Those sutures that did fail did so at a mean (189N±25N). There was no significant difference between the two groups in pullout strength. The GII pullout strength was similar to that found by Roth et al. [164] and Barber et al.[228] finding. The weakest area for fixation is the anteroinferior glenoid rim, where suture anchors are most often used in the clinical

setting. The strongest area is the posterior glenoid rim, where anchors are least often used. The BMD of the tested regions and the displacement of anchors in those regions showed no significant differences between the two groups.

The relationship between fixation strength and bone structure is complex. This study now has data that show it to be dependant on cortical thickness and cancellous bone properties. Since the study could not predict these factors in any specimens with accuracy, steps should be taken to ensure that adequate fixation and that means a combination of suture and anchor that performs well in laboratory conditions, used in locations that provide adequate fixation. This study suggests that it may be unwise to rely on single anchors placed anteroinferior. Fixation would be improved significantly by augmenting the repair by anchors placed higher on the anterior rim. As yet this has not been quantified.

Finally it has been observed that during initial cyclical loading there is a degree of anchor displacement, measuring 3.9 to 5.7mm in this study. Again the greatest degree of displacement to settling occurred in the anteroinferior glenoid where cancellous bone density is least. It is common practice to pull on the sutures after inserting a tissue anchor to seat the device. To a degree this occurs automatically with commercial insertion systems, as the anchor has to be disengaged after introduction. The force required to properly settle an implant is not known. It is likely that in this study some of this settling could have been avoided by a firmer pull to seat the anchor after insertion. In rotator cuff repairs it has been shown, however, that cyclical loading leads to gap formation at the repair site [160]. This has been attributed to slippage of sutures through the material of the rotator cuff.

Displacement (Settling) of 5.7 +/- 0.98mm at the anteroinferior glenoid was observed, which could lead to significant separation of capsule from the prepared glenoid. From this observations it can only recommend that after insertion of this design of anchor that a number of firm tugs are applied to seat the anchor as firmly as possible and that attention is paid to knot tying such that tissues are covered as well as possible against the glenoid [233].

5 Conclusions and Future Works

5.1 INTRODUCTION

Through this thesis, an attempt was made to achieve the aims and objectives set out in the first chapter, which was to investigate the morphological and mechanical properties of the glenoid cavity and to qualify the influence of these factors on component fixation. A working plan was formulated in order to meet the different objectives that were set at the beginning of the thesis. While those objectives were achieved, new research and objectives emerged. This chapter outlines the main conclusions provides pointers to future work.

5.2 CONCLUSIONS AND FUTURE WORK RELATING TO THE INDIVIDUAL STUDIES

The first objective of this study was to use the uCT imaging technique to allow quantitative and qualitative measurement of the glenoid bone architecture. Further, the mechanical properties of the bone and its relationship to bone morphology were investigated. This enabled the confirmation that the inferior and inferior-anterior regions were the weakest zone in the glenoid cavity. The strength of the localised region of bone was found to be dependent on the thickness of the subchondral bone, the BV/TV and perhaps with the evidence from the fresh bones the BMD. Similar results were found for the relationship between elastic modulus and the bone parameters. Importantly there appeared to be a significant difference between the results from fresh and embalmed specimens, which contradicts the assertion made by Anglin et al [179]. Given that, only a small number of fresh specimens were

available for this study, it is advisable that future work builds up a large sample size and that an experiment is designed such that measurements can be undertaken on glenoids pre and post embalming. According to our findings, the anisotropy, BV/TV of the glenoid cancellous bone, details concerning the strength and modulus distribution, and the load-bearing function of the cortical shell should be considered in future finite element models of the glenoid. Moreover, the uCT images and parameters can be used to construct the FE model.

The second objective was to use a surrogate bone to simulate different glenoid component and obtain the effect of bone cement on fixation. Total joint arthroplasty provides an effective means for treating a variety of pathologies of the shoulder. However, several studies from within the literature suggest that the procedure has not been entirely optimised [5, 11, 19, 234] and that loosening of the glenoid component remains the most prevalent cause of patient dissatisfaction with the procedure [5, 234]. Generally, loosening is attributed either to mechanical failure in response to high tensile stress development in the fixation [13], or through osteolysis of the surrounding bone stock in response to particulate wear debris [116, 235]. Long-term issues arising from the component design may only become apparent after the design has been implemented in possibly thousands of patients. Pre-operative assessment of the proposed reconstruction can clarify the influence of design modifications upon the performance of the joint, and, in some cases, may indicate that certain prosthesis designs might provide a more favourable outcome for the patient in question. In this research project an investigation was undertaken of the newly developed open cell saw-bone as a model for glenoid fixation. Whilst this material maybe adequate in terms of cement interdigitation the current model did not provide a satisfactory mechanical base on which to do structural construct testing. A number of

improvements are required if the model is to replicate the loosening process observed *in vivo*. These include:

- Search for alternative open pore structures with the required mechanical as well as morphological properties
- Incorporation of a better representation of the cortical bone.
- In vitro experimentation on cadaveric tissue with which to validate the model.

New developments in rapid prototyping may provide a route to constructing these models as ceramic and ceramic-polymer composites can now be constructed that mimic both the geometry and to some extent the mechanical properties of bone, which can be fined tuned to suit the application.

The third objective was to determine the pullout strength of the new Orthocord ™ suture used with Mitek GII™ and its relationship to the BMD. Less suture failure in comparison to anchor failure can be concluded to be a satisfactory strong material to be used for different glenoid lesions, but younger specimens should be tested. Further study should conduct more fresh cadaveric bone including the soft tissue and more cyclic loading should be applied to study the influence of post-surgical rehabilitation on these types of suture anchors. According to our finding, the BMD correlated with the pullout forces in different regions, but more parameters should be study to validate this finding. Surface characteristics and suture construction affect the tendency for anchor slippage.

Recently, an advanced texture analysis tool was introduced by Langenberger et al [236]. In this study, the bone homogeneity factor (BHF) was introduced as an index for the quantitative measurement of bone structure.The homogeneity of the

bone means the structure and composition are uniform throughout. BHF is measured on HR-MR images of the calcaneus. Correlations of BHF with DXA measurements of the femoral neck were found to be significant ($r = 0.73$). The authors concluded that BHF is a potential index of skeletal status possible and could possibly be used to distinguish osteoporotic and non-osteoporotic bone. The BHF could be also measured in the future to look at the correlation of this factor on the mechanical properties of the glenoid.

6 Bibliography

1. Post, M., Jablon, M., Miller, H., Singh, M., Constrained total shoulder joint replacement: a critical review.; *Clinical Orthopaedic Related Research.*, 1979. **144**: p. 135-50.
2. Sarrafian, S.K., Gross and functional anatomy of the shoulder; *Clinical Orthopedics and Related Research*, 1983. **173**: p. 11-19.
3. Soslowsky, L.J., Bigliani, L.U., Flatow, E.L., Mow, V.C., Articular geometry of the glenohumeral joint.; *Clinical Orthopaedic and Related Research.*, 1992. **285**: p. 181-190.
4. Brems, J., The glenoid component in total shoulder arthroplasty.; *Journal of Shoulder and Elbow Surgery*, 1993. **2**: p. 47-54.
5. Franklin, J.L., Barrett, W.g., Jackins, S.E., Matsen, F.A., III, Glenoid loosening in total shoulder arthroplasty: association with rotator cuff deficiency.; *Journal of Arthroplasty*, 1988. **3**: p. 1-8.
6. Gartsman, G.M., Elkousy, H. A., Warnock, K. M., Edwards, T. B., O'Connor, D. P., Radiographic comparison of pegged and keeled glenoid components; *Journal of Shoulder and Elbow Surgery*, 2005. **14**(3): p. 252.
7. Benjamin, J.B., Lund, P. J., Radiologic guide to medical devices and foreign bodies.; *St Louis, Mo: Mosby-Year Book*, 1994: p. 348-385.
8. Hunter, T.B., Taljanovic, M., Overview of medical devices.; *Current Problems in Diagnostic Radiology*, 2001. **4**: p. 89-139.
9. Freiberg, A.A., The radiology of orthopedic implants: an atlas of techniques and assessment.; *Louis, Mo: Mosby*, 2001.
10. Berquist, T.H., Imaging atlas of orthopedic appliances and prostheses.; *New York, NY: Raven*, 1995.
11. Neer, C.S., Replacement arthroplasty for glenohumeral osteoarthritis.; *Journal of of Bone and Joint Surgery*, 1974. **56**: p. 1-13.
12. Levy, O., Copeland, S.A., Cementless surface replacement arthroplasty (Copeland CSRA) for osteoarthritis of the shoulder; *Journal of Shoulder and Elbow Surgery*, 2004. **13**(3): p. 266.

13. Gupta, S., van der Helm, F. C. T., van Keulen, F., Stress analysis of cemented glenoid prostheses in Total Shoulder Arthroplasty; *Journal of Biomechanics*, 2004. **37**(11): p. 1777.

14. Matsoukis, J., Tabib, W., Guiffault, P., Mandelbaum, A., Walch, G., Nemoz, C., Cortes, ZE., Edwards, TB., Primary Unconstrained Shoulder Arthroplasty in Patients with a Fixed Anterior Glenohumeral Dislocation; *Journal of Bone and Joint Surgery (Am).* 2006. **88**(3): p. 547-552.

15. Zhang, W., Mow, C. S., Wiedel, J. D., Unconstrained shoulder arthroplasty.; *Chinese Journal of Traumatology*, 2000. **15**(2): p. 72-75.

16. Pfahler, M., Jena, F., Neyton, L., Sirveaux, F., Mole, D., Hemiarthroplasty versus total shoulder prosthesis: Results of cemented glenoid components; *Journal of Shoulder and Elbow Surgery*, 2006. **15**(2): p. 154.

17. Lo, I.K.Y., Litchfield, R. B., Griffin, S., Faber, K., Patterson, S. D., Kirkley, A., Quality-of-Life Outcome Following Hemiarthroplasty or Total Shoulder Arthroplasty in Patients with Osteoarthritis. A Prospective, Randomized Trial; *The Journal of Bone and Joint Surgery*, 2005. **87**(10): p. 2178-2185.

18. Brems, J.J., Wilde, A. H., Borden, L. S., Boumphrey, F.R. S., Glenoid lucent lines.; *Paper presented at ASES 2nd Open Meeting, New Orleans*, 1986.

19. Boyd, A.D.J., Thomas, W. H., Scott, R. D., Sledge, C. B., Thornhill, T. S., Total shoulder arthroplasty versus hemiarthroplasty indications for glenoid resurfacing; *Journal of Arthroplasty*, 1990. **5**: p. 329-36.

20. Kelly, I.G., Foster, R. S., Fisher, W. D., Neer total shoulder replacement in rheumatoid arthritis.; *Journal of Bone and Joint Surgery (Br)*, 1987. **69-B**: p. 723-6.

21. Boyd, A.D., Aliabadi, P., Thornhill, T. S., Postoperative proximal migration in total shoulder arthroplasty. Incidence and significance.; *Journal of Arthroplasty*, 1991. **6**: p. 31-6.

22. Alexandre, T.e.a., Influence of glenohumeral conformity on glenoid stresses after total shoulder arthroplasty.; *Journal of shoulder and elbow surgery.*, 2006. **15**(4): p. 515-20.

23. Copeland, S., The continuing development of shoulder replacement: " reaching the surface"; *Journal of Bone and Joint Surgery (Am)*, 2006. **88-A**(4): p. 900-5.

24. Barrett, W.P., Franklin, J. L., Jackins, S. E., Wyss, C. R., et al., Total shoulder arthroplasty.; *Journal of bone and joint surgery*, 1987. **69A**: p. 865-872.

25. Haines, J.F., Trail, I. A., Nuttall, D., Birch, A., Barrow, A., The results of arthroplasty in osteoarthritis of the shoulder; *Journal of Bone and joint Surgery (Br)*. 2006. **88-B**(4): p. 496-501.

26. Chin, P.Y.K., Sperling, J.W., Cofield, R.H., Schleck, C., Complications of total shoulder arthroplasty: Are they fewer or different? *Journal of Shoulder and Elbow Surgery*, 2006. **15**(1): p. 19.

27. Matsen, F.A., Rockwood, C. A., Wirth, M. A., Lippitt, S. B., Glenohumeral arthritis and its management.; *In Rockwood CA, Matsen FA (eds): The shoulder, 2nd Edition. Philadelphia, WB, Saunders CO.*, 1998: p. 840-964.

28. Anglin, C., Wyss, U. P., Pichora, D. R., Glenohumeral Contact Forces; *Proceedings of the Mechanical Engineering [H]*, 2000. **214**: p. 637.

29. Doshi, R., Mahesh W., S., Singh, J., Review Article: MR Anatomy of normal shoulder.; *Indian Journal of Radiology and Imaging.*, 2002. **12**(2): p. 261-266.

30. Anglin, C., Tolhurst, P., Wyss, U. P., Pichora, D. R., Glenoid cancellous bone strength and modulus; *Journal of Biomechanics*, 1999. **32**(10): p. 1091-7.

31. Orr, T.E., Carter, D. R. and Schurman, D. J., Stress analysis critical for higher conformity designs.; *Clinical Orthopaedics and Related Research*, 1988. **212**: p. 217-224.

32. Friedman, R.J., An, Y., Chokeski, R., Kessler, L., Anatomic and Biomechanical Study of Glenohumeral Contact; *Journal of Shoulder and Elbow Surgery*, 1994. **3**: p. S35.

33. van der Helm, F.C.T., Veeger, H. E. J., Quasi-static analysis of muscle forces in the shoulder mechanism during wheelchair propulsion; *Journal of Biomechanics*, 1996. **29**(1): p. 39.

34. van der Helm, F., Analysis of the kinematic and dynamic behavior of the shoulder mechanism.; *Journal of Biomechanics*, 1994. **27**(5): p. 527-50.

35. Runciman, R.J., Biomechanical model of the shoulder joint.; *PhD thesis, Bioengineering Unit, University of Strathclyde.*, 1993.

36. Karlsson, D., Peterson, B., Towards a model for force predictions in the human shoulder.; *Journal of biomechanics.*, 1992. **25**(2): p. 189-99.

37. Karlsson, D., Force distriutions in the human shoulder.; *PhD thesis, Chalmers University of Technology, Goteborg, Sweden.*, 1992.

38. Dul, J., A biomechanical model to quantify shoulder load at the work place.; *Clinical biomechanics.*, 1988. **3**: p. 124-128.

39. Kessel, L., Bayley, I., Clinical Disorders of the Shoulder, 2nd edition; *Churchill Livingstone, Edinburgh*, 1986.

40. Buechel, F.F., Pappas, M. J., DePalma, A. F., Floating socket' total shoulder replacement: anatomical, biomechanical and surgical rationale.; *Journal of Biomedical Material Research.*, 1978. **12**: p. 89–114.

41. Poppen, N., Walker, P., Forces at the glenohumeral joint in abduction.; *Clinical Orthopaedics and Related Research.*, 1978. **135**: p. 165-70.

42. Inman, V.T., Saunders, J. B., Abbott, L. C., Observations on the function of the shoulder joint.; *Journal of Bone and Joint Surgery (Am).* 1944. **26**(1): p. 1-30.

43. McMinn, R.M.H., Lasts Anatomy - Regional and Applied 9 thed.; *New york, Churchill, Livengstone*, 1994.

44. Constant C. R., Historical background, anatomy and shoulder function; *Baillière's Clinical Rheumatology*, 1989. **3**: p. 429-435.

45. Saha, A.K., Theory of Shoulder Mechanism: Descriptive and Applied; *Charles C. Thomas Publishing Company, Springfield, Il*, 1961.

46. Harryman, D.T., Sidles, J. A., Harris, S. L., et al, The role of the rotator interval capsule in passive motion and stability of the shoulder; *Journal of Bone and Joint Surgery (Am)*, 1992. **74**: p. 53-66.

47. Pearl, M.L., Volk, A. G., Coronal plane geometry of proximal humerus relevant to prosthetic arthroplasty.; *Journal of shoulder and elbow surgery.*, 1996. **5**: p. 320-6.

48. Howell, S.M., Galinat, B. J., The glenoid-labral socket: A constrained articular surface; *Clinical Orthopaedic and Related Research.*, 1989. **243**: p. 122-125.

49. Iannotti, J.P., Gabriel, J. P., Schneck, S. L., et al, The normal glenohumeral relationships. An anatomical study of one hundred and forty shoulders.; *Journal of bone and joint surgery*, 1992. **74A**: p. 491-500.

50. Burkhart, S.S., DeBeer, J. F., Tehrany, A. M., Parten, P. M., Quantifying glenoid bone loss arthroscopically in shoulder instability; *Arthroscopy: The Journal of Arthroscopic & Related Surgery*, 2002. **18**(5): p. 488.

51. Warner, J.J., Bowen, M. K., Deng, X. H., Hannafin, J. A., Arnoczky, S. P., Warren, R. F., Articular contact patterns of the normal glenohumeral joint; *Journal of Shoulder and Elbow Surgery*, 1998. **7**: p. 381-388.

52. Basmajian, J.V., Bazant, F. J., Factors preventing downward dislocation of the adducted shoulder joint. An electromyographic and morphological study.; *Journal of Bone and Joint Surgery (Am)*, 1959. **41-A**: p. 1182-6.

53. Mallon, W.J., Brown, H. R., Vogler, J. B., Martinez, S., Radiographic and geometric anatomy of the scapula.; *Clinical Orthopaedics and Relatated Research*, 1992. **277**: p. 142-54.

54. Boileau, P., Walch, G., The three-dimentional geomtry of the proximal humerus: Implications for surgical technique and prosthetic design.; *Journal of Bone and joint Surgery (Br)*. 1997. **79-B**(5): p. 857-865.

55. McPherson E. J., F., R. J., An, Y. H., Chokesi, R., Dooley, R. L., Anthropometric study of normal glenohumeral relationships.; *Journal of shoulder and elbow surgery.*, 1997. **6**: p. 105-12.

56. Pearl, M.L., Volk, A. G., Retroversion of the proximal humerus in relationship to prosthetic replacement arthroplasty.; *Journal of shoulder and elbow surgery.*, 1995. **4**: p. 286-9.

57. Kronberg, M., Brostrom, L. A., Humeral head retroversion in patients with unstable humeroscapular joints.; *Clinical Orthopaedics*, 1990. **260**: p. 207-211.

58. Brown, T.D., Shaw, D.T., In vitro contact stress in the natural human hip.; *Journal of Biomechanics*, 1983. **16**: p. 373-84.

59. Karduna, A., Williams, G., Williams, J., Iannotti, J., Kinematics of the glenohumeral joint: influences of muscle forces, ligamentous constraints and articular geometry; *Journal of Orthopaedic Research*, 1996. **14**: p. 986-993.

60. Poppen, N.K., Walker, P. S., Normal and abnormal motion of the shoulder; *Journal of Bone and Joint Surgery (Am)*, 1976. **58**: p. 195-201.

61. Harryman, D.T., Sidles, J. A., Clark, J. M., McQuade, K. J., Gibb, T. D., Matsen, FA., Translation of the humeral head on the glenoid with passive glenohumeral motion.; *Journal of Bone and Joint Surgery (Am)*, 1990. **72**: p. 1334-43.

62. Kelkar, R., Wang, V.M., Flatow, E.L., Newton, P.M., Ateshian, G.A., Bigliani, L.U., Pawluk, R.J., Mow, V.C., Glenohumeral mechanics: a study of articular geometry, contact, and kinematics.; *Journal of Shoulder and Elbow Surgery*, 2001. **10**: p. 73-84.

63. Apreleva, M., Hasselman, C. T., Debski, R. E., Fu, F. H., Woo, S. L. Y., Warner, J. J. P., A dynamic Analysis of Glenohumeral Motion after Simulated Capsulolabral Injury. A Cadaver Model; *Journal of Bone and Joint Surgery (Am)*, 1998. **80**(4): p. 474-80.

64. Bigliani, L., Kelkar, R., E.,L., P, Roger G. M. D., Mow, Van C., Glenohumeral Stability: Biomechanical Properties of Passive and Active Stabilizers. [Miscellaneous Article]; *Clinical Orthopaedics and Related Research*, 1996. **330**: p. 13-30.

65. Boardman Iii, N.D., Debski, Richard E., Warner, Jan J. P., Taskiran, Emin, Maddox, Lisa, Imhoff, Andreas B., Fu, Freddie H., Woo, Savio L. Y., Tensile properties of the superior glenohumeral and coracohumeral ligaments; *Journal of Shoulder and Elbow Surgery*, 1996. **5**(4): p. 249.

66. Matsen, F.r., Lippitt, S. B., Sidles, J. A., Harryman, DT 2nd., Practical evaluation and management of the shoulder; *Philadelphia: Saunders*, 1994.

67. Novotny, J.E., Nichols, C. E., Beynnon, B. D., Normal kinematics of the unconstrained glenohumeral joint under coupled moment loads; *Journal of Shoulder and Elbow Surgery*, 1998. **7**(6): p. 629.

68. Tuoheti, Y., Itoi, E., Minagawa, H., Yamamoto, N., Saito, H., Seki, N., Okada, K., Shimada, Y., Abe, H., Attachment Types of the Long Head of the Biceps Tendon to the Glenoid Labrum and Their Relationships with the Glenohumeral Ligaments; *Arthroscopy: The Journal of Arthroscopic & Related Surgery*, 2005. **21**(10): p. 1242.

69. Turkel, S.J., Panio, M. W., Marshall, J. L., Stabilizing mechanisms preventing anterior dislocation of the glenohumeral joint.; *Journal of Bone and Joint Surgery (Am)*, 1981. **63**(8): p. 1208-17.

70. Levine, W.N., Flatow, E. L., Current concepts review: The pathophysiology of shoulder instabilty.; *The American Journal of Sports Medicine*, 2000. **28**: p. 910-917.

71. Warner, J., The gross anatomy of the joint surfaces, ligaments, labrum, and capsule.; *American Academy of Orthopaedic Surgeons, ed. Matsen FA, III, Fu FH, and Hawkins RJ. Rosemont, IL*, 1993: p. 7-28.

72. Norris, T.R., Fischer, J., Bigliani, L. U., The unfused acromial epiphysis and its relationship to impingement syndromes.; *Orthopaedics Transactions.*, 1983. **7**(3): p. 505.

73. Porcellini, G., Paladini, P., Campi, F., Paganelli, M., Shoulder Instability and Related Rotator Cuff Tears: Arthroscopic Findings and Treatment in Patients Aged 40 to 60 Years; *Arthroscopy: The Journal of Arthroscopic and Related Surgery*, 2006. **22**(3): p. 270.

74. Labriola, J.E., Lee, T. Q., Debski, R. E., McMahon, P. J., Stability and instability of the glenohumeral joint: The role of shoulder muscles; *Journal of Shoulder and Elbow Surgery*, 2005. **14**(1, Supplement 1): p. S32.

75. Iwashita, Y., Basic study of the measurement of bone mineral content of cortical and cancellous bone of the mandible by computed tomography; *Dentomaxillofac Radiology*, 2000. **29**(4): p. 209-215.

76. Miller, M.D., Miller's Review of Orthopedics 2nd ed.; *W.B. Saunders*, 1996.

77. Dee, R., et al., Principles of Orthopaedic Practice.; *2nd Ed. McGraw Hill.*, 1997.

78. Burstein, A.H., Reilly, D.T., Martens, M., Aging of bone tissue: mechanical properties.; *Journal of bone and joint surgery*, 1976. **58**(A): p. 82-86.

79. Carter, D.R., Hayes, W. C., The compressive behavior of bone as a two-phase porous structure; *Journal of Bone and Joint Surgery (Am)*, 1977. **59**(7): p. 954-962.

80. Nordin, M., Frankel, V., Biomechanics of the Skeletal System.; *Lea & Febiger.*, 1980.

81. Haddock, S.M., Yeh, O. C., Mummaneni, P. V., Rosenberg, W. S., Keaveny, T. M., Fatigue behavior of human vertebral trabecular bone.; *Transactions of the Orthopaedic Research Society*, 2000. **25**: p. 733.

82. Frich, L.H., Jensen, N.C., Odgaard, A., Pedersen, C.M., Sojbjerg, J.O., Dalstra, M., Bone strength and material properties of the glenoid; *Journal of Shoulder and Elbow Surgery*, 1997. **6**(2): p. 97.

83. Oxland, T.R., Grant, J. P., Dvorak, M. F., Fisher, C. G., Effects of endplate removal on the structural properties of the lower lumbar vertebral bodies; *Spine*, 2003. **28**(8): p. 771-7.

84. Mansat, P., Barea, C., Hobatho, M., Darmana, R., Mansat, M., Anatomical variation of the mechanical properties of the glenoid.; *Journal of shoulder and elbow surgery.*, 1998. 7(2): p. 109-115.

85. Martin, R., Determinants of the mechanical properties of bone.; *Journal of biomechanics.*, 1991. **(suppl)**: p. 79-88.

86. Hvid, I., Cancellous bone at the knee a comparison of two methods of bone strength measurements.; *Archeive of Orthopaedic Surgery.*, 1985. **104**: p. 211-7.

87. Hobatho, M., Rho, J. Y., Ashman, R. B., Atlas of mechanical properties of human cortical and cancellous bone.; *In Van Der Perre G, Lowet G, Borgwardt A, editors. In VIVO assessment of bone aualitv bv vibration and wave propagation techniques ' Pa;t iI. Leuven: ACCO*, 1991: p. 7-38.

88. Bergmann, G., Biomechanics and pathomechanics of the shoulder joint with reference to; *In: Koebel R, Helbig 6, Blauth W, editors. Shoulder replacement. Berlin: Springer-Verlag*, 1987: p. 33.

89. De Luca, C., Forrest, W., Force analysis of individual muscles acting simultaneously on the shoulder joint during isometric abduction.; *Journal of Biomechanics*, 1973. **6**: p. 385-93.

90. Lang, S., Ultrasonic method for measuring elastic coefficient of bone and results on fresh and dried bovines bones.; *IEEE Trans Biomedical Engneering.*, 1970: p. 17.

91. Hayes, W.C., Snvder, B., Levine, B. M., Ramaswanv, S., Stress-morphology relationships in trabecular bone of the patella.; *In: Gallaaher RH. Simon BR, lohnson PC, Gross IF, editors. Finite elements in biomechanics. John Wile; & Sons*, 1982.

92. Keating, J.F., Waterworth, P., Shaw-Dunn, J., Crossan, J., The relative strength of the rotator cuff muscles. A cadaver study.; *Journal of Bone and joint Surgery (Br).* 1993. **75B**: p. 137-140.

93. Frich, L.H., Odgaard, A., Dalstra, M., Glenoid bone architecture; *Journal of Shoulder and Elbow Surgery*, 1998. 7(4): p. 356.

94. Simkin, P.A., Heston, R. F., Downey, D. J., Benedict, R. S., Soo Chai, H., Subchondral architecture in bone of the canine shoulder.; *Journal of Anatomy.*, 1991. **175**(2): p. 13-27.

95. Nagels, J., Valstar, E. R., Stokdijk, M., Rozing, P. M., Patterns of loosening of the glenoid component; *Journal of Bone and joint Surgery (Br).* 2002. **84-B**(1): p. 83-87.

96. Torchia, M.E., Cofield, R. H., Settergren, C. R., Total shoulder arthroplasty with the neer prosthesis: Long-term results; *Journal of Shoulder and Elbow Surgery*, 1997. **6**(6): p. 495.

97. Barrett, W.P., Franklin, J. L., Jackins, S. E., Wyss, C. R., Matsen, F. A., Total shoulder arthroplasty; *Journal of Bone and Joint Surgery (Am)*, 1987. **69**(6): p. 865-872.

98. Amstutz, H.C., Thomas, B. J., Kabo, J. M., Jinnah, R. H., Dorey, F. J., The Dana total shoulder arthroplasty; *Journal of Bone and Joint Surgery (Am)*, 1988. **70**(8): p. 1174-1182.

99. Charles, A., Rockwood, Jr., Shoulder Arthroplasty - Indications and technique- ; *17th Annual San Diego Meeting, Arthroscopy & Arthroplasty of the shoulder.*, 2000.

100. Blevins, F.T., Pollo, F. E., Torzilli, P. A., Warren, R. F., Effect of humeral head component size on hemiarthroplasty translations and rotations; *Journal of Shoulder and Elbow Surgery*, 1998. **7**(6): p. 591.

101. Büchler, P., Farron, A., Rakotomanana, L., Humeral head reconstruction: Neer versus anatomically based prothesis.; *Proceedings of the 68th annual meeting of the American Academy of Orthopedic Surgeons (AAOS), San Francisco.*, 2001.

102. Wirth, M.A., Shoulder Arthroplasty. Edited by Gilles Walch and Pascal Boileau. New York, Springer, 1999. $185.00, 444 pp; *Journal of Bone and Joint Surgery (Am)*, 2000. **82**(10): p. 1526-.

103. Harryman, D.T., Sidles, J. A., Harris, S. L., Lippitt, S. B., Matsen, FA, 3rd, The effect of articular conformity and the size of the humeral head component on laxity and motion after glenohumeral arthroplasty. A study in cadavera.; *Journal of Bone and Joint Surgery (Am).* 1995. **77**: p. 555-63.

104. Williams, J.G.R., Wong, K. L., Pepe, M. D., Tan, V., Silverberg, D., Ramsey, M. L., Karduna, A., Iannotti, J. P., The effect of articular malposition after total shoulder arthroplasty on glenohumeral translations, range of motion, and subacromial impingement; *Journal of Shoulder and Elbow Surgery*, 2001. **10**(5): p. 399.

105. Neer, C.S., II, Anterior Acromioplasty for the Chronic Impingement Syndrome in the Shoulder; *Journal of Bone and Joint Surgery (Am)*, 2005. **87**(6): p. 1399-.

106. Dee, D.T., Yang, B. Y., McMahon, P. J., Lee, T. Q., Effect of malaligning posterior offset of the humerus: a cadaveric study of shoulder hemiarthroplasty.; *Proceeding of the 68th annual meeting of the American Academy of Orthopedic Surgeons (AAOS), San Francisco.*, 2001.

107. Pearl, M.L., Kurutz, S. A. M., Geometric Analysis of Commonly Used Prosthetic Systems for Proximal Humeral Replacement; *Journal of Bone and Joint Surgery (Am).* 1999. **81**(5): p. 660-71.

108. Friedman R. J., Humeral technique in total shoulder arthroplasty.; *Orthopaedics Clinical of North America.*, 1998. **29**: p. 393-402.

109. Gupta, S., van der Helm, F. C. T., van Keulen, F., Stress analysis of cemented and uncemented glenoid prostheses.; *In:Proc 12th Conf. Euro. Soc. Biomech. Royal Academy of Medicine in Ireland: Dublin*, 2001: p. 161.

110. Rockwood, C.A., Matsen, FA III., Glenohumeral arthritis and its management. In: Rockwood CA, Matsen FA III, editors. The shoulder.; *Philadelphia: Saunders*, 1998. **2**: p. 840-964.

111. Anglin, C., Wyss, U. P., Nyffeler, R. W., Gerber, C., Loosening performance of cemented glenoid prosthesis design pairs; *Clinical Biomechanics*, 2001. **16**(2): p. 144.

112. Roper, B.A., Paterson, J. M., Day, W. H., The Roper-Day total shoulder replacement; *The Journal Of Bone And Joint Surgery (Br)*, 1990. **72**(4): p. 694.

113. Lacroix, D., Murphy, L. A., Prendergast, P. J., Three-dimensional finite element analysis of glenoid replacement prostheses: a comparison of keeled and pegged anchorage systems; *Journal Of Biomechanical Engineering*, 2000. **122**(4): p. 430.

114. Wirth, M.A., Rockwood, Jr, C.A., Complications of shoulder arthroplasty.; *Clinical Orthopaedics and Related Research*, 1994. **307**: p. 47-69.

115. Bauer, G.S., Murthi, A. M., Bigliani, L. U., Fixation for the millennium: The shoulder; *The Journal of Arthroplasty*, 2002. **17**(4, Supplement 1): p. 9.

116. Wallace, A.L., Phillips, R. L., MacDougal, G. A., Walsh, W. R., Sonnabend, D. H., Resurfacing of the glenoid in total shoulder arthroplasty. A comparison, at a mean of five years, of prostheses inserted with and without cement; *The Journal Of Bone And Joint Surgery (Am)*, 1999. **81**(4): p. 510.

117. Prendergast, P.J., Murphy, L. A., Selection of glenoid prosthesis-type based on an assessment of glenoid bone quality.; *Third meeting of the International Shoulder Group.*, 2000.

118. Murphy, L.A., Prendergast, P. J., Resch, H., Structural analysis of an offset-keel design glenoid component compared with a center-keel design; *Journal of Shoulder and Elbow Surgery*, 2001. **10**(6): p. 568.

119. Trail, I.A., Nuttall, D., The results of shoulder arthroplasty in patients with rheumatoid arthritis; *Journal of Bone and joint Surgery (Br).* 2002. **84-B**(8): p. 1121-1125.

120. Archibeck, M.J., Berger, R. A., Jacobs, J. J., Quigley, L. R., Gitelis, S., Rosenberg, A. G., Galante, J. O., Second-generation cementless total hip arthroplasty. Eight to eleven-year results; *The Journal Of Bone And Joint Surgery (Am)*, 2001. **83-A**(11): p. 1666.

121. Levy, O., Funk, L., Sforza, G., Copeland, S. A., Copeland Surface Replacement Arthroplasty of the Shoulder in Rheumatoid Arthritis; *Journal of Bone and Joint Surgery (Am).* 2004. **86**(3): p. 512-518.

122. Lazarus, M.D., Jensen, K. L., Southworth, C., Matsen, FA., 3rd, The radiographic evaluation of keeled and pegged glenoid component insertion; *The Journal Of Bone And Joint Surgery (Am)*, 2002. **84-A**(7): p. 1174.

123. Wirth, M.A., Korvick, D. L., Basamania, C. J., Toro, F., Aufdemorte, T. B., Rockwood, Jr C. A., Radiologic, mechanical, and histologic evaluation of 2 glenoid prosthesis designs in a canine model; *Journal of Shoulder and Elbow Surgery*, 2001. **10**(2): p. 140.

124. Giori, N.J., Beaupre, G. S., Carter, D. R., The influence of fixation peg design on the shear stability of prosthetic implants; *Journal Of Orthopaedic*

Research: Official Publication Of The Orthopaedic Research Society, 1990. **8**(6): p. 892.

125. Matsen, F.A., Rockwood, C.A., Wirth, M.A., Lippitt, S.B., Glenohumeral arthritis and its management.; *In: C.A. Rockwood and F.A. Matsen, Editors, The shoulder, Saunders, Philadelphia.*, 1999: p. 233-276.

126. Oosterom, R., Rozing, P. M., Verdonschot, N., Bersee, H. E., Effect of joint conformity on glenoid component fixation in total shoulder arthroplasty.; *Proceeding of the Institution of Mechanical Engineering [H].* 2004. **218**(5): p. 339-47.

127. Sneppen, O., Fruensgaard, S., Johannsen, H. V., Olsen, B. S., Sojbjerg, J. O., Andersen, N. H., Total shoulder replacement in rheumatoid arthritis: proximal migration and loosening.; *Journal of shoulder and elbow surgery.*, 1996. **5**(1): p. 47-52.

128. Couteau, B., Mansat, P., Estivalezes, E., Darmana, R., Mansat, M., Egan, J., Finite element analysis of the mechanical behavior of a scapula implanted with a glenoid prosthesis; *Clinical Biomechanics*, 2001. **16**(7): p. 566.

129. Swieszkowski, W., Bednarz, P., Prendergast, P. J., Contact stresses in the glenoid component in total shoulder arthroplasty.; *Proceeding of the Institution of Mechanical Engineering [H].* 2003. **217**(1): p. 49-57.

130. Walch, G., Edwards, T. B., Boulahia, A., Boileau, P., Mole, D., Adeleine, P., The Influence of Glenohumeral Prosthetic Mismatch on Glenoid Radiolucent Lines: Results of a Multicenter Study; *Journal of Bone and Joint Surgery (Am)*, 2002. **84**(12): p. 2186-2191.

131. Wirth, M.A., Basamania, C., Rockwood, Jr C.A., Fixation of glenoid component: Keel versus pegs; *Operative Techniques in Orthopaedics*, 1994. **4**(4): p. 218.

132. Collins, D., Tencer, A., Sidles, J., Matsen, F., Edge displacement and deformation of glenoid components in response to eccentric loading. The effect of preparation of the glenoid bone; *Journal of Bone and Joint Surg (Am)*, 1992. **74**(4): p. 501-507.

133. Pearl, M.L., Volk, A. G., Coronal plane geometry of the proximal humerus relevant to prosthetic arthroplasty.; *Journal of Shoulder and Elbow Surgery*, 1996. **5**(4): p. 320-6.

134. Cofield, R.H., Daly, P. J., Total shoulder arthroplasty with a tissue-ingrowth glenoid component.; *Journal of Shoulder and Elbow Surgery*, 1992. **1**: p. 77-85.

135. Walker, P.S., Some bioengineering considerations of prosthetic replacement for the glenohumeral joint.; *In: Inglis AE, editor. Symposium on total joint replacement of the upper extremity. St Louis: CV Mosby Company*, 1982: p. 25-32.

136. Sneppen, O., Fruensgaard, S., Johannsen, H. V., Olsen, B. S., Sojbjerg, J. O., Andersen, N. H., Total shoulder replacement in rheumatoid arthritis: Proximal migration and loosening; *Journal of Shoulder and Elbow Surgery*, 1996. **5**(1): p. 47.

137. Friedman, R.J., Biomechanics and design of shoulder Arthroplasties.; *In: Friedman RJ (ed) Arthroplasty on the shoulder. Thieme, New York.*, 1994: p. 27-40.

138. Boileau, P., Walch, G., Liotard, J. P., Kinematics of shoulder replacement.; *In: Walch G, Boileau P (eds) Shoulder Arthroplasty. Springer, Heidelberg Berlin New York*, 1999: p. 29-39.

139. Harman, M., Frankle, M., Vasey, M., Banks, S., Initial glenoid component fixation in "reverse" total shoulder arthroplasty: A biomechanical evaluation; *Journal of Shoulder and Elbow Surgery*, 2005. **14**(1, Supplement 1): p. S162.

140. Davy, L., Hsiao-Li, M., Shih-Chieh, H., Tain-Hsiung, C., Jiunn-Jer, W., Open Bankart repair with suture anchors for traumatic recurrent anterior shoulder instability: comparison of results between small and large Bankart lesions.; *Knee Surgery Sports Traumatol Arthroscopy*, 2006. **14**: p. 82-87.

141. Warner, J.J.P., Bowen, MK., Deng, X., Torzilli, PA., Warren, RF., Effect of joint compression on inferior stability of the glenohumeral joint; *Journal of Shoulder and Elbow Surgery*, 1999. **8**(1): p. 31.

142. O'Connel, P.W., Nuber, G.W., Mileski, R.A., Lautenschlager, E., The contribution of the glenohumeral ligaments to anterior stability of the shoulder joint.; *American Journal of Sport Medicine.*, 1990. **18**: p. 449.

143. Fabbriciani, C., Milano, G., Demontis, A., Fadda, S., Ziranu, F., Mulas, P. D., Arthroscopic versus open treatment of Bankart lesion of the shoulder: a

prospective randomized study.[see comment]; *Arthroscopy*, 2004. **20**(5): p. 456-62.

144. Bigliani, L.U., Newton, P. M., Steinmann, S. P., Connor, P. M., McIlveen, S. J., Glenoid Rim Lesions Associated with Recurrent Anterior Dislocation of the Shoulder; *American Journal of Sports Medicine.*, 1998. **26**(1): p. 41-45.

145. Maffet, M.W., Gartsman, G. M., Moseley, B., Superior labrum-biceps tendon complex lesions of the shoulder; *American Journal of Sports Medicine.*, 1995. **23**(1): p. 93-98.

146. Snyder, S.J., Karzel, R. P., Del Pizzo, W., Ferkel, R. D., Friedman, M. J., SLAP lesions of the shoulder.; *Arthroscopy*, 1990. **6**(4): p. 274-9.

147. Woertler, K., Simone, W., MR imaging in sports-related glenohumeral instability.; *European Radiology.*, 2006. **16**(12): p. 2622-2636.

148. Strobel, K., Treumann, T. C., Allgayer, B., Posterior Entrapment of the Long Biceps Tendon After Traumatic Shoulder Dislocation: Findings on MR Imaging; *American journal of Roentgenology.*, 2002. **178**(1): p. 238-239.

149. Weiland, D.E., MacGillivray, J. D., Isolated Supraspinatus Muscle Paralysis after Shoulder Dislocation: A Case Report; *American Journal of Sports Medicine.*, 2003. **31**(3): p. 462-464.

150. Habermeyer, P., Gleyze, P., Rickert, M., Evolution of lesions of the labrum-ligament complex in posttraumatic anterior shoulder instability: a prospective study.; *Journal of shoulder and elbow surgery.*, 1999. **8**: p. 66.

151. Langford, J., Bishop, J., Lee, E., Flatow, E., Outcomes Following Open Repair of Bankart Lesions for Recurrent, Traumatic Anterior Glenohumeral Dislocations.; *Orthopedics.*, 2006. **29**: p. 1008.

152. Fujii, Y., Yoneda, M., Wakitani, S., Hayashida, K., Histologic analysis of bony Bankart lesions in recurrent anterior instability of the shoulder; *Journal of Shoulder and Elbow Surgery*, 2006. **15**(2): p. 218.

153. Barber, F.A., Cawley, P., Prudich, J. F., Suture anchor failure strength-an *in vivo* study.; *Arthroscopy.*, 1993. **9**: p. 647-52.

154. Leedle, B.P., Miller, M. D., Pullout strength of knotless suture anchors; *Arthroscopy: The Journal of Arthroscopic & Related Surgery*, 2005. **21**(1): p. 81.

155. Tingart, M.J., Apreleva, M., Lehtinen, J., Zurakowski, D., Warner, Jon J. P., Anchor Design and Bone Mineral Density Affect the Pull-out Strength of Suture Anchors in Rotator Cuff Repair: Which Anchors Are Best to Use in Patients With Low Bone Quality? *American Journal of Sports Medicine.*, 2004. **32**(6): p. 1466-1473.

156. Barber, F.A., Snyder, S. J., Abrams, J. S., Fanelli, G. C., Savoie, I. I. I. Felix, H., Arthroscopic bankart reconstruction with a bioabsorbable anchor; *Journal of Shoulder and Elbow Surgery*, 2003. **12**(6): p. 535.

157. Bardana, D.D., Burks, R. T., West, J. R., Greis, P. E., The effect of suture anchor design and orientation on suture abrasion: An in vitro study; *Arthroscopy: The Journal of Arthroscopic & Related Surgery*, 2003. **19**(3): p. 274.

158. Ilahi, O.A., Al-Fahl, T., Bahrani, H., Luo, Z., Glenoid suture anchor fixation strength: effect of insertion angle; *Arthroscopy: The Journal of Arthroscopic & Related Surgery*, 2004. **20**(6): p. 609.

159. Meyer, D.C., Fucentese, S. F., Ruffieux, K., Jacob, H. A. C., Gerber, C., Mechanical testing of absorbable suture anchors.; *Arthroscopy: The Journal of Arthroscopic & Related Surgery*, 2003. **19**: p. 188-193.

160. Rupp, S., Georg, T., Gauss, C., Kohn, D., Seil, R., Fatigue Testing of Suture Anchors; *American Journal of Sports Medicine.*, 2002. **30**(2): p. 239-247.

161. DiRaimondo, C.A., Alexander, J. W., Noble, P. C., Lowe, W. R., Lintner, D. M., A Biomechanical Comparison of Repair Techniques for Type II SLAP Lesions; *American Journal of Sports Medicine.*, 2004. **32**(3): p. 727-733.

162. Richmond, J.C., Donaldson, W. R., Fu, F., Harner, C. D., Modification of the Bankart reconstruction with a suture anchor. Report of a new technique; *American Journal of Sports Medicine.*, 1991. **19**(4): p. 343-346.

163. Wolf, E.M., Wilk, R.M., Richmond, J.C., Arthroscopic Bankart repair using suture anchors.; *Operative Techniques in Orthopaedics.*, 1991. **1**: p. 184-191.

164. Roth, C.A., Bartolozzi, A. R., Ciccotti, M. G., Wetzler, M. J., Gillespie, M. J., Snyder-Mackler, L., Santare, M. H., Failure properties of suture anchors in the glenoid and the effects of cortical thickness; *Arthroscopy: The Journal of Arthroscopic and Related Surgery*, 1998. **14**(2): p. 186.

165. Shall, L.M., Cawley, P. W., Soft tissue reconstruction in the shoulder. Comparison of suture anchors, absorbable staples, and absorbable tacks; *American Journal of Sports Medicine*, 1994. **22**(5): p. 715-8.

166. Carpenter, J.E., Fish, D. N., Huston, L. J., Goldstein, S. A., Pull-out strength of five suture anchors; *Arthroscopy*, 1993. **9**(1): p. 109-13.

167. Lehtinen, J.T., Tingart, M.J., Apreleva, M., Warner, J.J.P., Total, trabecular, and cortical bone mineral density in different regions of the glenoid; *Journal of Shoulder and Elbow Surgery*, 2004. **13**(3): p. 344.

168. Harman, M., M. Frankle, M. VaseyS. Banks, Initial glenoid component fixation in "reverse" total shoulder arthroplasty: A biomechanical evaluation; *Journal of Shoulder and Elbow Surgery*, 2005. **14**(1, Supplement 1): p. S162.

169. Anglin, C., Wyss, U. P., Pichora, D. R., Mechanical testing of shoulder prostheses and recommendations for glenoid design; *Journal of Shoulder and Elbow Surgery*, 2000. **9**(4): p. 323.

170. Oosterom, R., Rozing, P. M., Bersee, H. E. N., Effect of glenoid component inclination on its fixation and humeral head subluxation in total shoulder arthroplasty; *Clinical Biomechanics*, 2004. **19**(10): p. 1000.

171. ASTM F1839-97: Standard specification for rigid polyurethane foam for use as a standard material for testing orthopaedic devices and materials.

172. Hasan, S.S., J.M. Leith, B. Campbell, R. Kapil, K.L. SmithF.A. Matsen, 3rd, Characteristics of unsatisfactory shoulder arthroplasties; *Journal of Shoulder & Elbow Surgery*, 2002. **11**(5): p. 431-41.

173. Ibarra, C., D.M. DinesJ.A. McLaughlin, Glenoid replacement in total shoulder arthroplasty; *Orthopedic Clinics of North America*, 1998. **29**(3): p. 403-13.

174. Lacroix, D., L.A. MurphyP.J. Prendergast, Three-dimensional finite element analysis of glenoid replacement prostheses: a comparison of keeled and pegged anchorage systems; *Journal of Biomechanical Engineering*, 2000. **122**(4): p. 430-6.

175. Nyffeler, R.W., Anglin, C., Sheikh, R., Gerber, C., Influence of peg design and cement mantle thickness on pull-out strength of glenoid component pegs; *Journal of Bone and Joint Surgery (Br)*, 2003. **85-B**(5): p. 748-752.

176. Churchill, R.S., Boorman, R. S., Fehringer, E. V., Matsen, F. A., 3rd, Glenoid cementing may generate sufficient heat to endanger the surrounding bone; *Clinical Orthopaedics and Related Research*, 2004(419): p. 76-9.

177. Buchler, P., Ramaniraka, N. A., Rakotomanana, L. R., Iannotti, J. P., Farron, A., A finite element model of the shoulder: application to the comparison of normal and osteoarthritic joints; *Clinical Biomechanics*, 2002. **17**(9-10): p. 630-9.

178. Terrier, A., Buchler, P., Farron, A., Bone-cement interface of the glenoid component: stress analysis for varying cement thickness; *Clinical Biomechanics*, 2005. **20**(7): p. 710-7.

179. Anglin, C., Tolhurst, P., Wyss, U. P., Pichora, D. R., Glenoid cancellous bone strength and modulus; *Journal of Biomechanics*, 1999. **32**(10): p. 1091.

180. Linde, F., Pongsoipetch, B., Frich, L. H., Hvid, I., Three-axial strain controlled testing applied to bone specimens from the proximal tibial epiphysis; *Journal of Biomechanics*, 1990. **23**(11): p. 1167-72.

181. Hvid, I., Rasmussen, O., Jensen, N. C., Nielsen, S., Trabecular bone strength profiles at the ankle joint; *Clinical Orthopaedics and Related Research*, 1985(199): p. 306-12.

182. Goldstein, S.A., The mechanical properties of trabecular bone: dependence on anatomic location and function; *Journal of Biomechanics*, 1987. **20**(11-12): p. 1055-61.

183. Müller, R., Hahn, M., Vogel, M., Delling, G., Rüegsegger, P., Morphometric analysis of noninvasively asessed bone biopsies: Comparison of high-resolution CT and histologic sections; *Bone*, 1996. **18**: p. 215-220.

184. Boyd, S.K., Muller, R., Matyas, J. R., Wohl, G. R., Zernicke, R. F., Early morphometric and anisotropic change in periarticular cancellous bone in a model of experimental knee osteoarthritis quantified using microcomputed tomography; *Clinical Biomechanics*, 2000. **15**(8): p. 624-31.

185. Linde, F., Elastic and viscoelastic properties of trabecular bone by a compression testing approach; *Danish Medical Bulletin*, 1994. **41**(2): p. 119-38.

186. Hara, T., Tanck, E., Homminga, J., Huiskes, R., The influence of microcomputed tomography threshold variations on the assessment of

structural and mechanical trabecular bone properties; *Bone*, 2002. **31**(1): p. 107.

187. Ding, M., Odgaard, A., Hvid, I., Accuracy of cancellous bone volume fraction measured by micro-CT scanning; *Journal of Biomechanics*, 1999. **32**(3): p. 323.

188. Lorensen, W.E., Cline, H. E., Marching cubes: a high resolution 3d surface construction algorithm.; *Computer graphics*, 1987. **21**(4): p. 163-169.

189. Andresen, R., Werner, H. J., Schober, H. C., Contribution of the cortical shell of vertebrae to mechanical behaviour of the lumbar vertebrae with implications for predicting fracture risk; *British Journal of Radiology*, 1998. **71**(847): p. 759-765.

190. Grant, J.P., Oxland, T. R., Dvorak, M. F., Mapping the structural properties of the lumbosacral vertebral endplates; *Spine*, 2001. **26**(8): p. 889-96.

191. Grampp, S., Steiner, E., Imhof, H., Radiological diagnosis of osteoporosis.; *European Radiology*, 1997. **7**(2): p. S11-S19.

192. Kuhn, J.L., Goldstein, S. A., Feldkamp, L. A., Goulet, R. W., Jesion, G., Evaluation of a microcomputed tomography system to study trabecular bone structure; *Journal of Orthopaedic Research*, 1990. **8**(6): p. 833-42.

193. Ruegsegger, P., Koller, B., Muller, R., A microtomographic system for the nondestructive evaluation of bone architecture; *Calcified Tissue International*, 1996. **58**(1): p. 24-9.

194. Odgaard, A., Gundersen, H. J., Quantification of connectivity in cancellous bone, with special emphasis on 3-D reconstructions; *Bone*, 1993. **14**(2): p. 173-82.

195. Currey, J.D., The mechanical consequences of variation in the mineral content of bone; *Journal of Biomechanics*, 1969. **2**(1): p. 1-11.

196. Schaffler, M.B., Burr, D. B., Stiffness of compact bone: effects of porosity and density; *Journal of Biomechanics*, 1988. **21**(1): p. 13-6.

197. Scanco Medical, A.G., MicroCT 20 User's Guide, software revision 2.1; 1997: p. 54-55.

198. Mittra, E., Rubin, C., Qin, Y., Interrelationship of trabecular mechanical and microstructural properties in sheep trabecular bone; *Journal of Biomechanics*, 2005. **38**(6): p. 1229.

199. Sone, T., Tamada, T., Jo, Y., Miyoshi, H., Fukunaga, M., Analysis of three-dimensional microarchitecture and degree of mineralization in bone metastases from prostate cancer using synchrotron microcomputed tomography; *Bone*, 2004. **35**(2): p. 432.

200. Tomomitsu, T., Mimura, H., Murase, K., Tamada, T., Sone, T., Fukunaga, M., Fractal analysis of trabecular architecture: with special reference to slice thickness and pixel size of the image; *Nippon Hoshasen Gijutsu Gakkai Zasshi*, 2005. **61**(6): p. 819-25.

201. Kim, D.G., Christopherson, G. T., Dong, X. N., Fyhrie, D. P., Yeni, Y. N., The effect of microcomputed tomography scanning and reconstruction voxel size on the accuracy of stereological measurements in human cancellous bone; *Bone*, 2004. **35**(6): p. 1375-82.

202. Batte, S.W.P., Cordy, M.E., Lee, T.Y., King, G.J.W., Johnson, J.A., Chess, D.G., Cancellous bone of the glenoid: correlation of quantitative CT and mechanical strength.; *Transactions of the Orthopaedic Research Society*, 1996. **21**: p. 707.

203. Barea, C., Mansat, P., Hobatho, M.C., Darmana, R., Mansat, M., Mechanical properties of the glenoid cancellous bone; *Transactions of the Orthopaedic Research Society*, 1997. **22**: p. 877.

204. Timoshenko, S.P., Goodier, J.N., Theory of Elasticity; *3rd Edition. McGraw-Hill, New York*, 1970: p. 408.

205. Keaveny, T.M., Hayes, W. C., A 20-year perspective on the mechanical properties of trabecular bone; *Journal Of Biomechanical Engineering*, 1993. **115**(4B): p. 534-42.

206. van Drongelen, S., van der Woude, L. H., Janssen, T. W., Angenot, E. L., Chadwick, E. K., Veeger, D. H., Glenohumeral contact forces and muscle forces evaluated in wheelchair-related activities of daily living in able-bodied subjects versus subjects with paraplegia and tetraplegia; *Archives of Physical Medicine and Rehabilitation*, 2005. **86**(7): p. 1434-40.

207. Veeger, H.E., Rozendaal, L. A., van der Helm, F. C., Load on the shoulder in low intensity wheelchair propulsion; *Clinical Biomechanics*, 2002. **17**(3): p. 211-8.

208. Bankart, A.S.B., The pathology and treatment of recurrent dislocation of the shoulder.; *British Journal of surgery*, 1938. **26**: p. 23-29.

209. Rowe, C.R., Patel, D., Southmayd, W. W., The Bankart procedure: a long-term end-result study; *Journal of Bone and Joint Surgery (Am)*, 1978. **60**(1): p. 1-16.

210. Wolf, E.M., Wilk, R. M., Richmond, J. C., Arthroscopic Bankart repair using suture anchors.; *Operative Techniques in Orthopaedics*, 1991. **1**: p. 184-191.

211. Bland, J.M., Altman, D.G., Statistical methods for assessing agreement between two methods of clinical measurement.; *Lancet.*, 1986. **i**: p. 307-310.

212. Gill, J.S., Zezulka, A.V., Beevers, D.G., Davies, P., Relationship between initial blood pressure and its fall with treatment.; *Lancet.*, 1985. **i**: p. 567-69.

213. Grant, J.P., Oxland, T. R., Dvorak, M. F., Fisher, C. G., The effects of bone density and disc degeneration on the structural property distributions in the lower lumbar vertebral endplates.; *Journal of Orthopaedic Research*, 2002. **20**(5): p. 1115-20.

214. Boileau, P., Villalba, M., Hery, J.Y., Balg, F., Ahrens, P., Neyton, L., Risk Factors for Recurrence of Shoulder Instability After Arthroscopic Bankart Repair; *Journal of Bone and Joint Surgery (Am)*, 2006. **88**(8): p. 1755-1763.

215. Snyder, S.M., Schneider, E., Estimation of mechanical properties of cortical bone by computed tomography.; *Journal of Orthopaedics Research*, 1991. **9**: p. 422-31.

216. Schaffler, M.B., Burr, D. B., Stiffness of compact bone: effects of porosity and density.; *Journal of Biomechanics*, 1988. **21**: p. 13-6.

217. McCalden, R.W., McGeough, J. A., Barker, M. B., Court, C. M., Age related changes in the tensile properties of cortical bone. The relative importance of changes in porosity, mineralization, and microstructure.; *Journal of Bone and Joint Surgery (Am)*, 1993. **75**: p. 1193-205.

218. Post, M., Constrained arthroplasty of the shoulder; *Orthopedic Clinics of North America*, 1987. **18**(3): p. 455-62.

219. Linde, F., Hvid, I., Madsen, F., The effect of specimen geometry on the mechanical behaviour of trabecular bone specimns.; *Journal of Biomechanics*, 1992. **25**(4): p. 359-368.

220. Martens, M., Van Audekercke, R., Delport, P., De Meester, P., Mulier, J.C., The mechanical characteristics of cancellous bone at the upper femoral region.; *Journal of Biomechanics*, 1983. **16**(12): p. 971-983.

221. Gibson, L.J., The mechanical behaviour of cancellous bone.; *Journal of Biomechanics*, 1985. **18**(5): p. 317-328.

222. McCalden, R.W., McGeough, J. A., Court, C. M., Age-related changes in the compressive strength of cancellous bone.; *Journal of Bone and Joint Surgery (Am)*, 1997. **79A**(3): p. 421-427.

223. Hvid, I., Trabecular bone strength at the knee.; *Clinical Orthopaedics.*, 1988. **227**: p. 210-221.

224. Beltran, J., Bencardino, J., Padron, M., Shankman, S., Beltran, L., Ozkarahan, G., The middle glenohumeral ligament: normal anatomy, variants and pathology; *Skeletal Radiology*, 2002. **31**(5): p. 253-62.

225. Fukuda, K., Chen, C. M., Cofield, R. H., Chao, E. Y., Biomechanical analysis of stability and fixation strength of total shoulder prostheses.; *Orthopaedics.*, 1988. **11**(1): p. 141-9.

226. Boileau, P., Sinnerton, R. J., Chuinard, C., Walch, G., Arthroplasty of the shoulder; *Journal of Bone and Joint Surgery (Br)*, 2006. **88-B**(5): p. 562-575.

227. Anglin, C., Wyss, U.P., Pichora D.R., Glenohumeral contact forces; *Proceedings of the Institution of Mechanical Engineers.*, 2000. **214 part H**: p. 637-644(8).

228. Barber, F.A., Herbert, M. A., Click, J. N., The ultimate strength of suture anchors; *Arthroscopy*, 1995. **11**: p. 21-28.

229. Barber, F.A., Feder, S. M., Burkhart, S. S., Ahrens, J., The relationship of suture anchor failure and bone density to proximal humerus location: a cadaveric study; *Arthroscopy.*, 1997. **13**: p. 340-5.

230. Zumstein, M., Jacob, H. A. C., Schneeberger, A. G., In vitro comparison of standard and knotless metal suture anchors; *Arthroscopy: The Journal of Arthroscopic & Related Surgery*, 2004. **20**(5): p. 517.

231. Mohammed, K.D., Sonnabend, D. H., Goldberg, J. A., Hutabarat, S., Walker, P., Walsh, W. R., Biomechanical Performance of Bankart Repairs in a Human Cadaveric Shoulder Model; *American Journal of Sports Medicine*, 1998. **26**(6): p. 831-835.

232. Wetzler, M.J., Bartolozzi, A. R., Gillespie, M. J., Roth, C. A., Ciccotti, M. G., Snyder-Mackler, L., Santare, M. H., Fatigue properties of suture anchors in anterior shoulder reconstructions: Mittek GII; *Arthroscopy: The Journal of Arthroscopic & Related Surgery*, 1996. **12**(6): p. 687-93.

233. De Beer, J.F., Arthroscopic Bankart repair: some aspects of suture and knot management.; *Arthroscopy.*, 1999. **15**: p. 660-2.

234. Brems, J., The glenoid component in total shoulder arthroplasty.; *Journal of shoulder and elbow surgery.*, 1993. **2** (47-54).

235. Gunther, S.B., Graham, J., Norris, T. R., Ries, M. D., Pruitt, L., Retrieved glenoid components: A classification system for surface damage analysis; *The Journal of Arthroplasty*, 2002. **17**(1): p. 95.

236. Langenberger H, Shimizu Y, Windischberger C, et al. Bone homogeneity factor: an advanced tool for the assessment of osteoporotic bone structure in high-resolution magnetic resonance images; *Invest Radiology* 2003; **38**: 467-472.

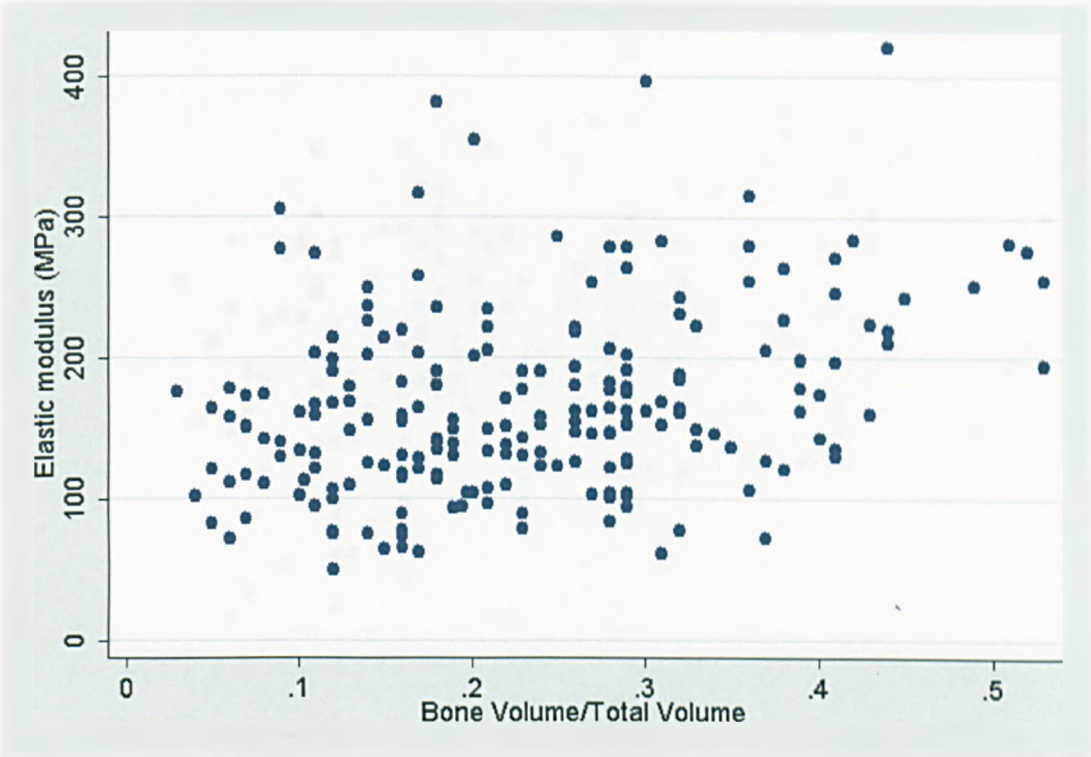

Figure A.1 The relationship of elastic modulus vs. bone volume fraction of the embalmed glenoids.

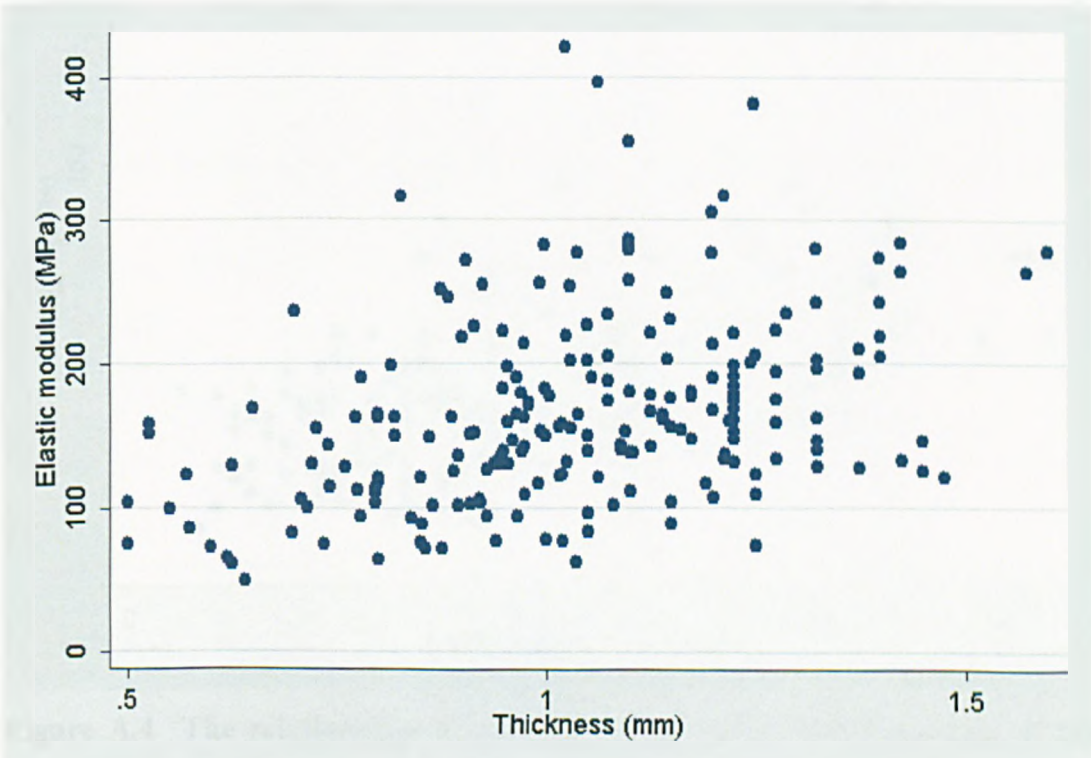

Figure A.2 The relationship of elastic modulus vs. subchondral thickness of the embalmed glenoids.

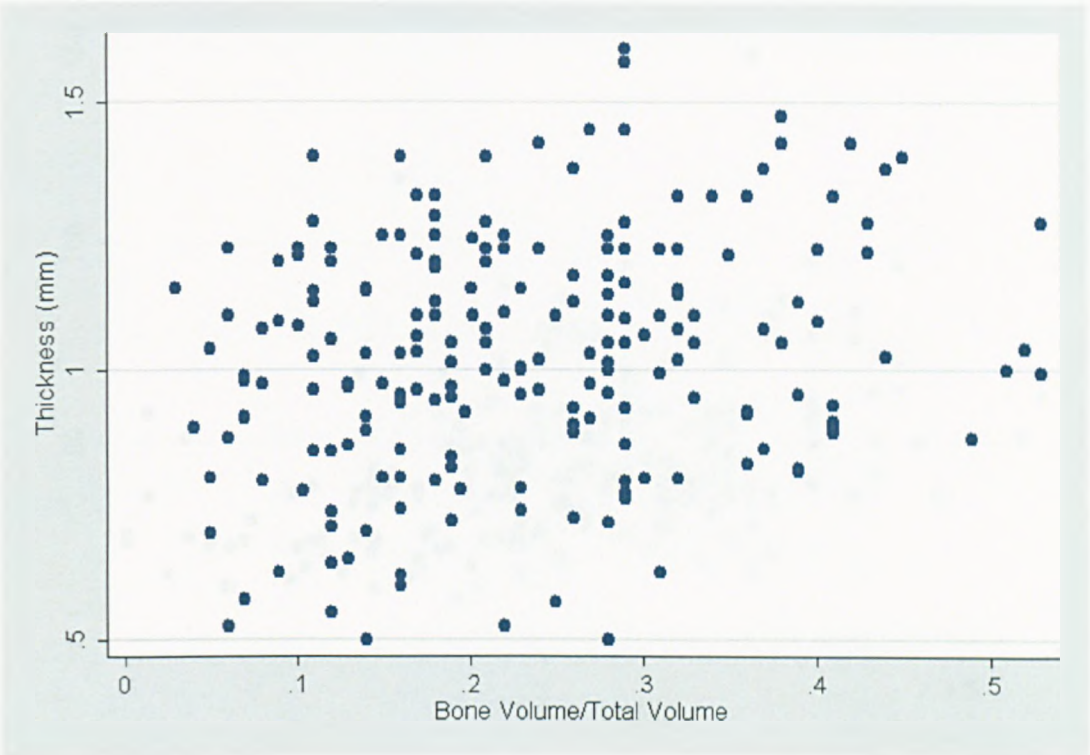

Figure A.3 The relationship of subchondral thickness vs. bone volume fraction of the embalmed glenoids.

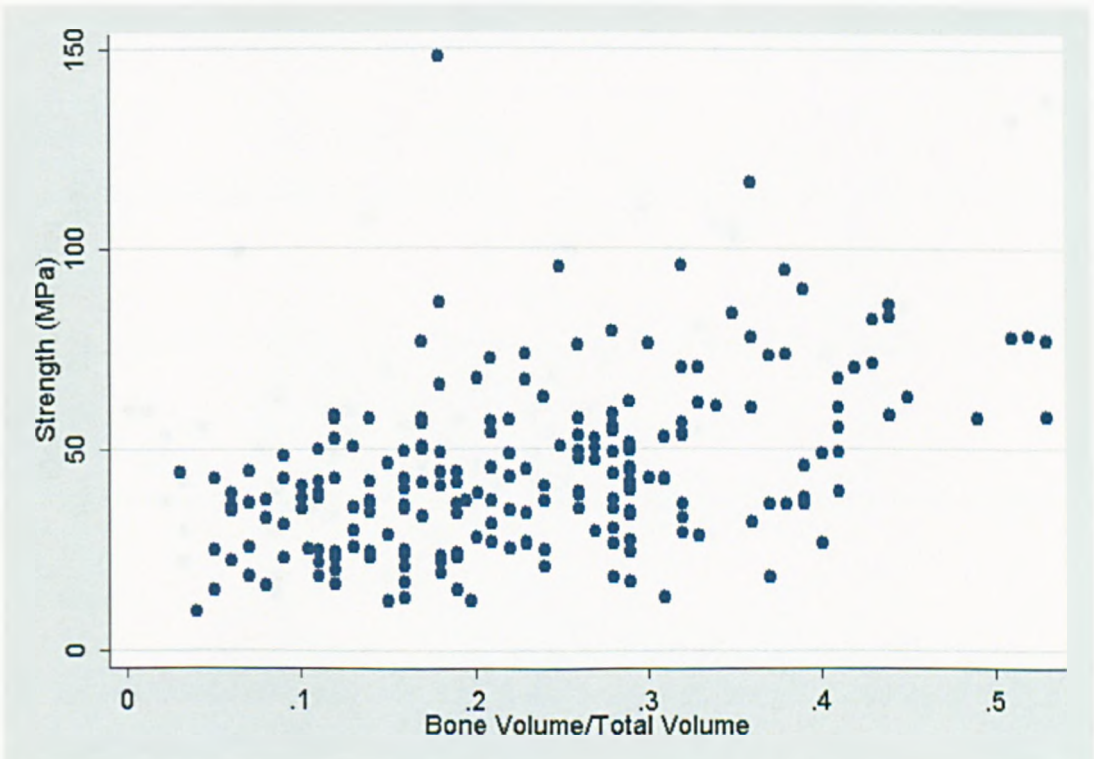

Figure A.4 The relationship of strength vs. the bone volume fraction of the embalmed glenoids.

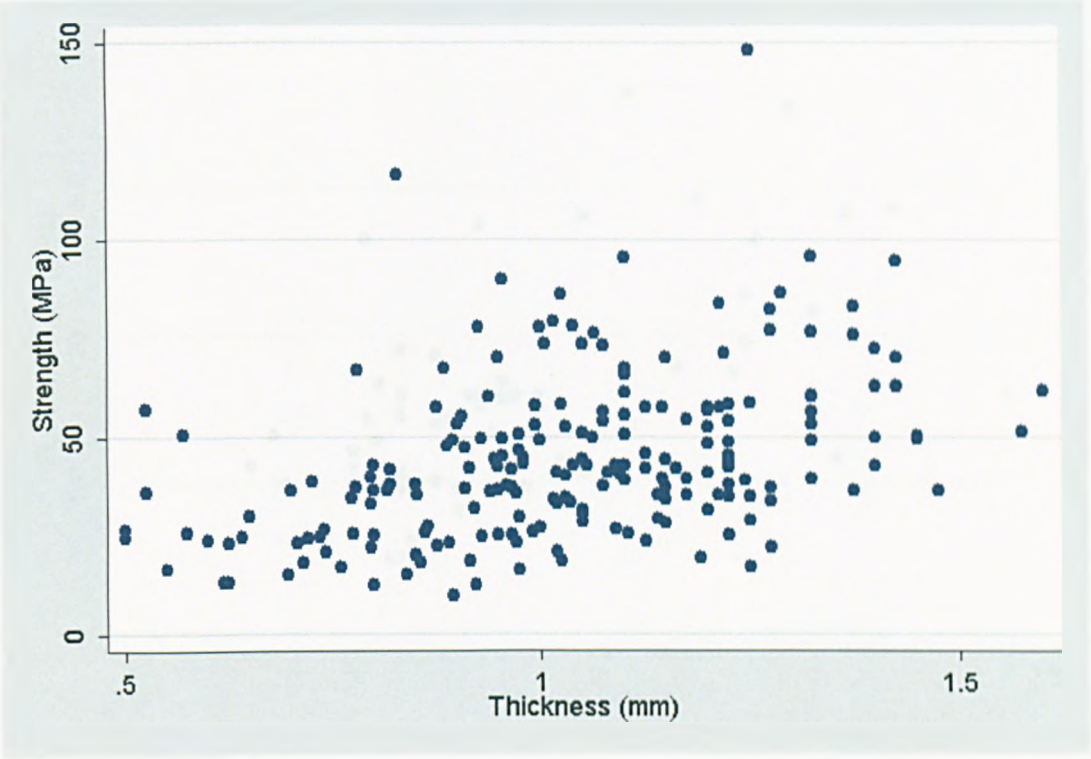

Figure A.5 The relationship of strength vs. subchondral thickness of embalmed glenoids.

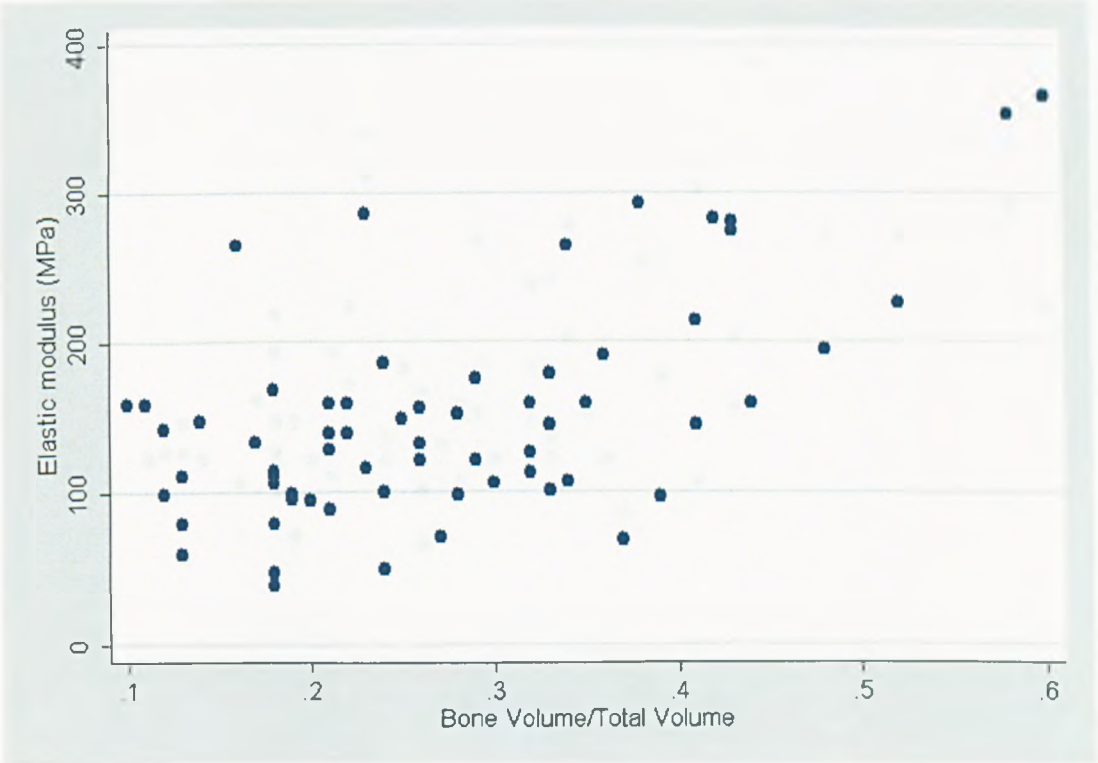

Figure A.6 The relationship of elastic modulus vs. bone volume fraction of the fresh glenoids.

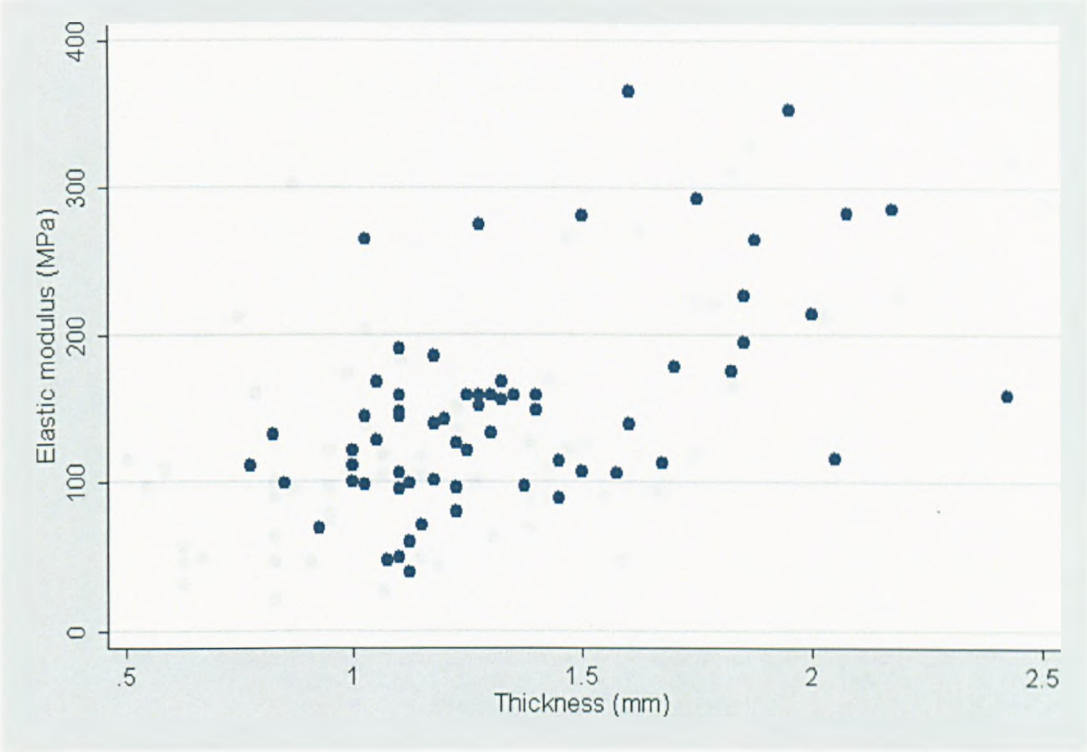

Figure A.7 The relationship of elastic modulus vs. subchondral thickness of the fresh glenoids.

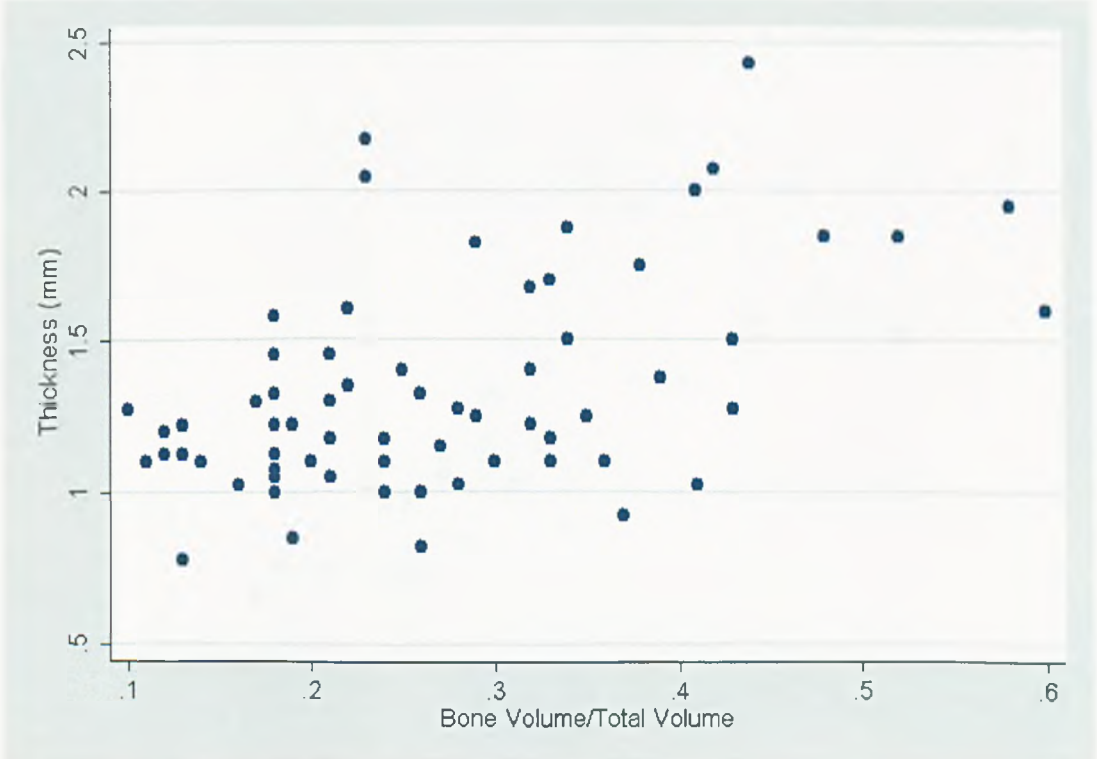

Figure A.8 The relationship of subchondral thickness vs. the bone volume fraction of the fresh glenoids.

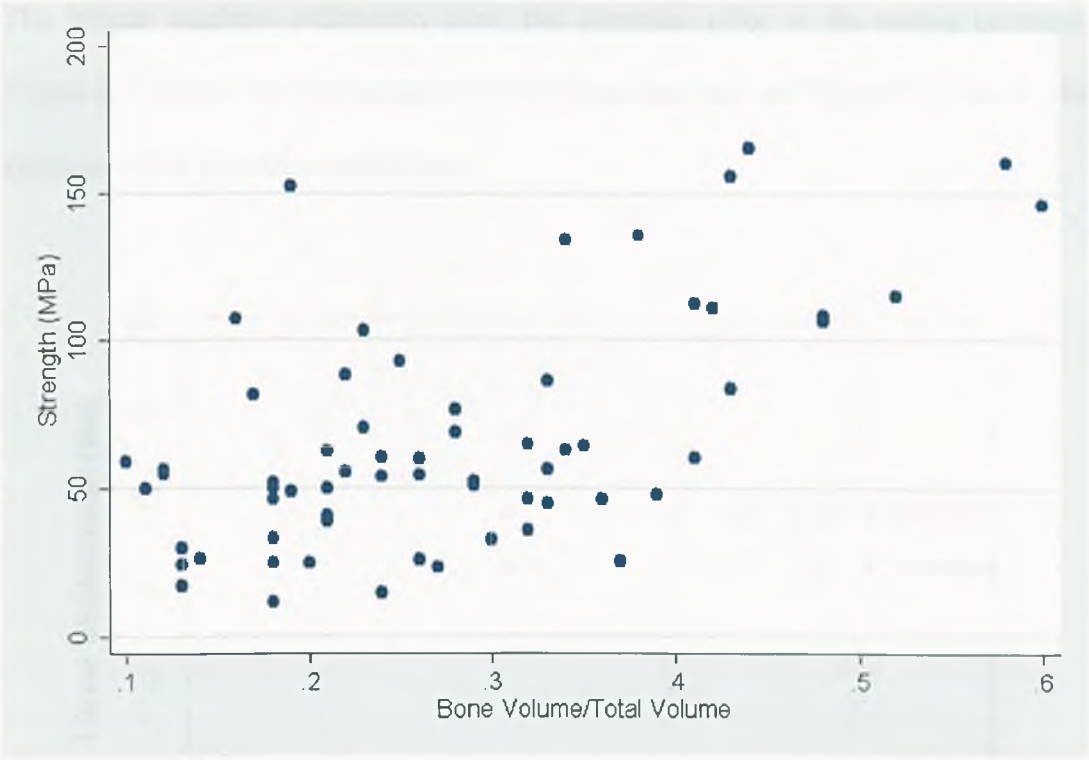

Figure A.9 The relationship of the strength vs. the bone volume fraction of the fresh glenoids.

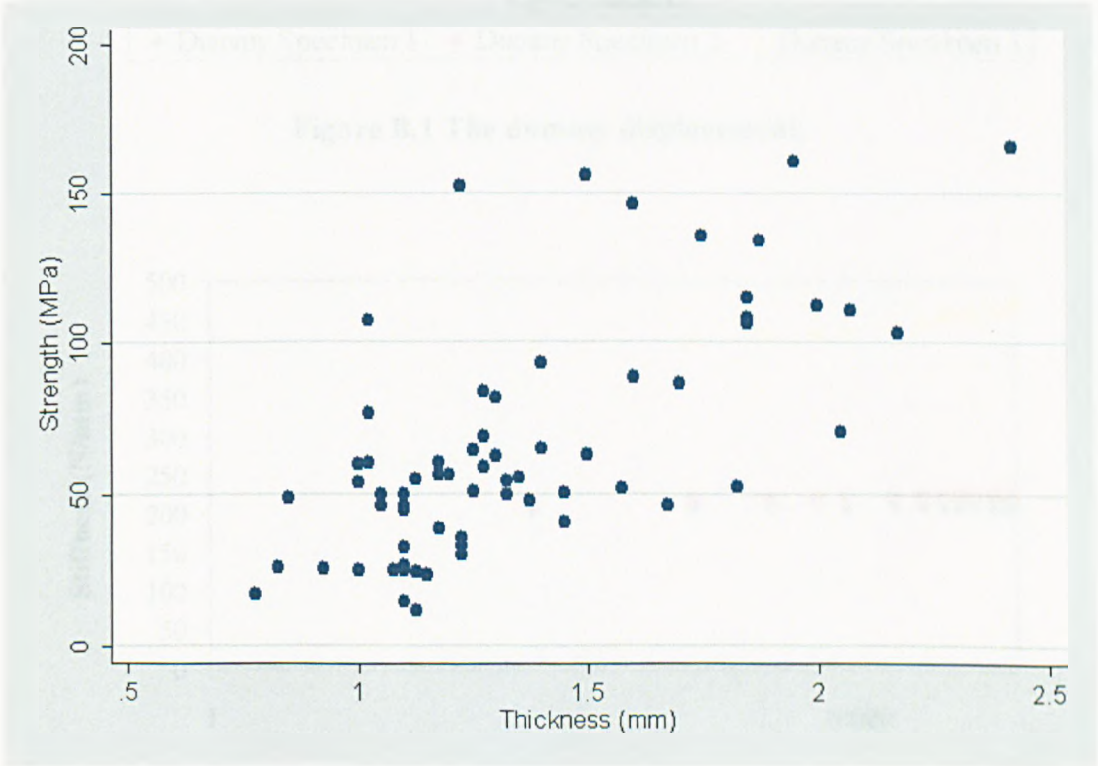

Figure A.10 The relationship of the strength vs. the subchondral thickness of the fresh glenoids.

The fatigue machine calibration using the dummies prior to the testing protocol. Figure B.1 shows the displacement of the three stations and Figure B.2 shows the stiffness of the dummies, respectively.

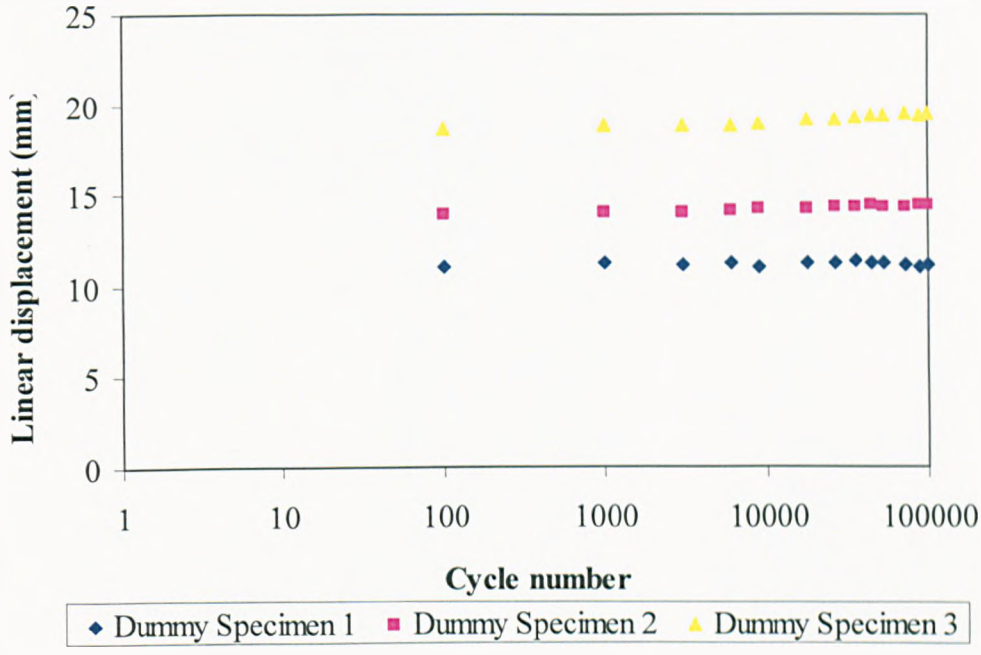

Figure B.1 The dummy displacement.

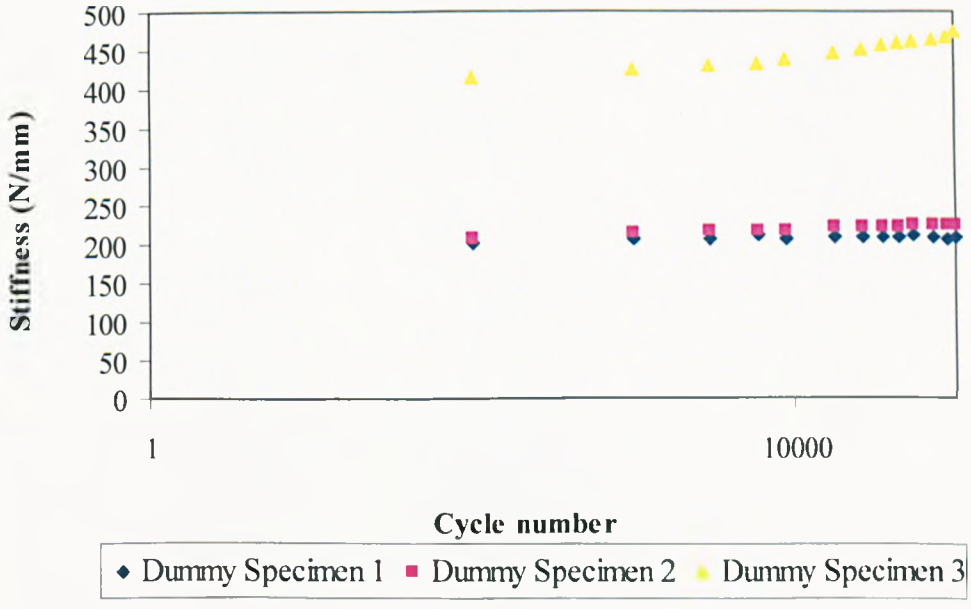

Figure B.2 The dummy stiffness.